HEAD AUGMENTATION IN HYDRAULIC TURBINES BY MEANS OF DRAFT TUBE EJECTORS

by

Robert P. Siegel

Thesis Submitted to the Faculty of the

Virginia Polytechnic Institute and State University

in partial fulfillment of the requirements for the degree of

Master of Science

in

Mechanical Engineering

APPROVED:

H. L. Moses, Chairman

F. J. Pierce

T. E. Diller

May, 1982

Blacksburg, Virginia

ACKNOWLEDGEMENTS

I would like to express my gratitude to the following people for their contributions to my personal and professional growth during the last fifteen months.

To my wife, Janet, for her unflinching sacrifices, her unconditional support and love.

To my son, Noah, for putting up with "I'm busy now", so many times, and for teaching me to walk slower.

To Dr. H. L. Moses, for his encouragement, patience and guidance as my major professor.

To Dr. F. J. Pierce and Dr. T. E. Diller for their interest in serving on my committee.

To Dr. J. Moore for his interest and his helpful suggestions.

To Johnny Cox, "Jack" Gray, and all of the guys down in the shop for their time, effort, and down to earth advice.

To Lenny Myatt and Will Haines for their friendship and encouragement in the early stages.

And finally to Neta Byerly, for turning a mess of blue pen tracks into what you're reading now.

This work was supported in part by Department of Energy contract DE-FC07-80ID12208. Thanks also to the College of Engineering for their financial support through the Pratt Supplemental Fellowship.

TABLE OF CONTENTS

	Page
ACKNOWLEDGEMENTS	ii
TABLE OF CONTENTS	iii
LIST OF FIGURES	iv
LIST OF TABLES	viii
NOMENCLATURE	ix
1. INTRODUCTION	1
1.1 Background	1
1.2 Draft Tubes and Diffusers	5
1.3 Overview of VPI&SU Draft Tube Project	8
2. LITERATURE REVIEW	11
2.1 Draft Tubes	11
2.2 Diffusers	15
3. DRAFT TUBE PROJECT DEVELOPMENT	21
3.1 One-Dimensional Analysis	21
3.2 Two-Dimensional Diffuser Model	24
3.3 Phase Two - Performance Maps	25
3.4 Revised System Model	35
3.5 Experimental Model Design	37
4. EXPERIMENTAL STUDY	42
4.1 Construction of Apparatus	42
4.1.1 Draft Tubes	42
4.1.2 Turbine/Bypass Assembly	44

TABLE OF CONTENTS (continued)

	Page
4.1.3 Mixing Tube Construction	47
4.1.4 Shaft, Bearing, and Seals	52
4.2 Test Facility and Layout	52
4.3 Instrumentation	54
4.4 Experimental Procedure	60
4.5 Experimental Uncertainty	63
5. EXPERIMENTAL RESULTS	65
5.1 Pressure Recovery	65
5.2 Turbine Performance	75
6. ANALYSIS	79
6.1 Comparison of Experiment with Numerical Model	79
6.2 Revised Performance Maps	88
6.3 Full Scale System Performance	91
6.4 Economic Analysis	94
6.5 Cavitation Considerations	104
7. CONCLUSIONS AND RECOMMENDATIONS	109
BIBLIOGRAPHY	111
APPENDIX A - Listing of System Program	117
VITA	122
ABSTRACT	

LIST OF FIGURES

Figure	Title	Page
1	Cost Distribution for Low-Head Projects	3
2	Cost Distribution for Ultra Low Head Projects	5
3	Effect of Draft Tube on System Performance	6
4	Mitchell Dam Plant with Thurlow Backwater Suppressor	13
5	Hodenpyl Plant with Tefft Tube and White Hydraucone Regainer	14
6	Model for One-Dimensional Analysis	22
7	Results of One-Dimensional Analysis	23
8	Flow Chart of the Numerical Analysis	26
9	Results of the Numerical Analysis	27
10	Schematic Diagram of the Experimental Apparatus . . .	28
11	Comparison of Prediction with Experiments: Pressure Recovery, Phase One	29
12	Idealized Inlet Velocity Profile	31
13	Diffuser Performance with BLC	33
14	Ejector-Diffuser Performance	34
15	Ejector-Diffuser System Performance	38
16	Photograph of Model Turbine Runner	40
17	Photograph of Experimental Draft Tube	45
18	Turbine/By-Pass Assembly	46
19	Exploded View of Turbine/Bypass Assembly	48
20	IGV Construction	49
21	Photograph of Stator Assembly	50

LIST OF FIGURES (continued)

Figure	Title	Page
22	Photograph of Rotor and Stator	51
23	Schematic of Shaft Support Assembly	53
24	Water Supply Line with Venturi Flowmeter	55
25	Cantilever Beam Arrangement Used for Torque Measurement	57
26	Yaw Probe	59
27	Location of Pressure Taps	61
28	Experimental Apparatus	62
29	Experimental Results: Pressure Recovery	67
30	Experimental Results: Head Augmentation	68
31	Experimental Results: Exit Swirl Angle	69
32	Experimental Results: C_p for Various Swirl Angles	70
33	Experimental Results: Effect of Bypass	71
34	Experimental Results: System Characteristic	72
35	Experimental Results: Power Output	73
36	Experimental Results: Variation of Bypass	74
37	Experimental Results: Turbine Efficiency	77
38	Velocity Profiles Showing Core Stall	80
39	Revised Model Inlet Velocity Profile	83
40	Schematic of Revised Mixing Length Model	85
41	Comparison of Experiment with Model	87
42	Effect of Reynolds Number on Pressure Recovery	89
43	Revised Performance Maps	90

LIST OF FIGURES (continued)

Figure	Title	Page
44	Full Scale System: Cost Ratio	99
45	Full Scale System: Power Output	101
46	Full Scale System: Cost	102
47	Turbine Elevation Parameters	106
48	Full Scale System: Turbine Elevation	107

LIST OF TABLES

Table	Title	Page
1	BLC System Performance	36
2	Experimental Design Performance Specifications	41
3	Experimental Model Specifications	43
4	Experimental Uncertainties	64
5	Experimental Results: Pressure	66
6	Performance Data: 200 kW System	95
7	Performance Data: 300 kW System	96
8	Performance Data: 400 kW System	97
9	Performance Data: 500 kW System	98

NOMENCLATURE

A	Area
AR	Diffuser Area Ratio
BYP	Bypass Fraction
C	Absolute Velocity
C_p	Pressure Recovery Coefficient
D or d	Diameter
F	Force
g	Gravitational Acceleration
H or h	Head
IGV	Inlet Guide Vanes
K	Loss Coefficient
ℓ	Mixing Length
N	Rotational Speed
p	Pressure
P	Power
Q	Volumetric Flow Rate
r	Radius
RA	Bypass Area Ratio
Re	Reynolds Number
RV	Velocity Ratio
SG	Specific Gravity
T	Torque
TVR	Turbine Velocity Ratio

NOMENCLATURE (continued)

U	Axial Velocity
V	Average Velocity
WKD	Wake Depth
X	Axial Position
Y	Laternal Position
Z	Elevation
α	Angle of Incidence
β	Angle of Departure
δ	Shear Layer Thickness
κ	Constant
λ	Constant
η	Efficiency
ρ	Mass Density
σ	Thoma Cavitation Factor
θ	Diffuser Cone Half-Angle
μ	Dynamic Viscosity
ω	Rotational Speed (Radians)

Subscripts

0	Headwater
1	Turbine Inlet
2	Turbine Discharge
3	Diffuser Inlet
4	Tailwater

NOMENCLATURE (continued)

c	Core
D	Dynamometer
diff	Diffuser
d.t.	Draft Tube
eff	Effective
G	Generator
i	Inner
j	Jet
ℓ	Loss
m	Mean
max	Maximum
n	Nozzle
o	Outer
oa	Overall
p	Pressure Tap
ref	Reference
s	Free Surface
t	Turbine
tot	Total
w	Wake

1. INTRODUCTION

A major hindrance in the development of ultra low-head and small scale hydropower systems is the high capital cost of the associated mechanical equipment. This thesis describes the development, construction and testing of a small, ultra low-head system in which the effective head across a turbine is increased by means of a high velocity annular bypass flow which acts as a jet pump in conjunction with a conical draft tube. The result is that, in a situation where sufficient flow exists, a small turbine can be used to produce as much power as would ordinarily require a larger, more expensive turbine. It is suggested that a system such as this could serve to open previously unfeasible sites for development.

1.1 Background

The term hydropower can be taken literally to mean the instantaneous rate at which energy is made available by the spontaneous migration of significant quantities of water toward a more stable state of mechanical equilibrium. The amount of energy made available in this process is proportional to the product of the gross head, or total pressure difference and the flow rate of the given stream or river. The amount of energy that can be extracted by a turbine, however, is proportional to the flow through the turbine and the pressure difference which can be effected across the turbine, i.e., the effective head.

The simple proportionality between the power, head, and flow tends

to imply that either the head or the flow are equally valuable in the assessment of a potential hydropower site, as long as both are present to some appreciable degree. This is not the case, however, since not only must a low-head turbine handle more flow, but the flow will generally be at a lower velocity, making its size and therefore its cost requirements substantially greater for the same power output. This relationship is given by:

$$P \alpha D^2 H_{eff}^{3/2} \tag{1.1}$$

The result is that low-head sites cost substantially more to develop since in general mechanical equipment comprises between 20-50 per cent of the total project cost depending upon civil requirements [1].

Figure 1 shows the relative costs of the various aspects of low-head projects which were reported in response to the DOE Program Research and Development Announcement in 1978 [2]. The costs are in 1979 dollars. Figure 2 gives the same information for projects in the ultra-low-head range. Equipment costs are given by

$$\text{cost (\$/KW)} = 200\ (10.9 - 1.017\ H) \qquad 1 < H < 6 \tag{1.2}$$

where the head is in meters.

This relation helps to explain why more than half of the roughly 5400 untapped dams which have been identified by the U.S. Army Corps of Engineers [3] as having power production capability have heads less than 26 ft. (8m). It has simply not been economically feasible to develop these sites with large expensive turbines. It is only as the reality of

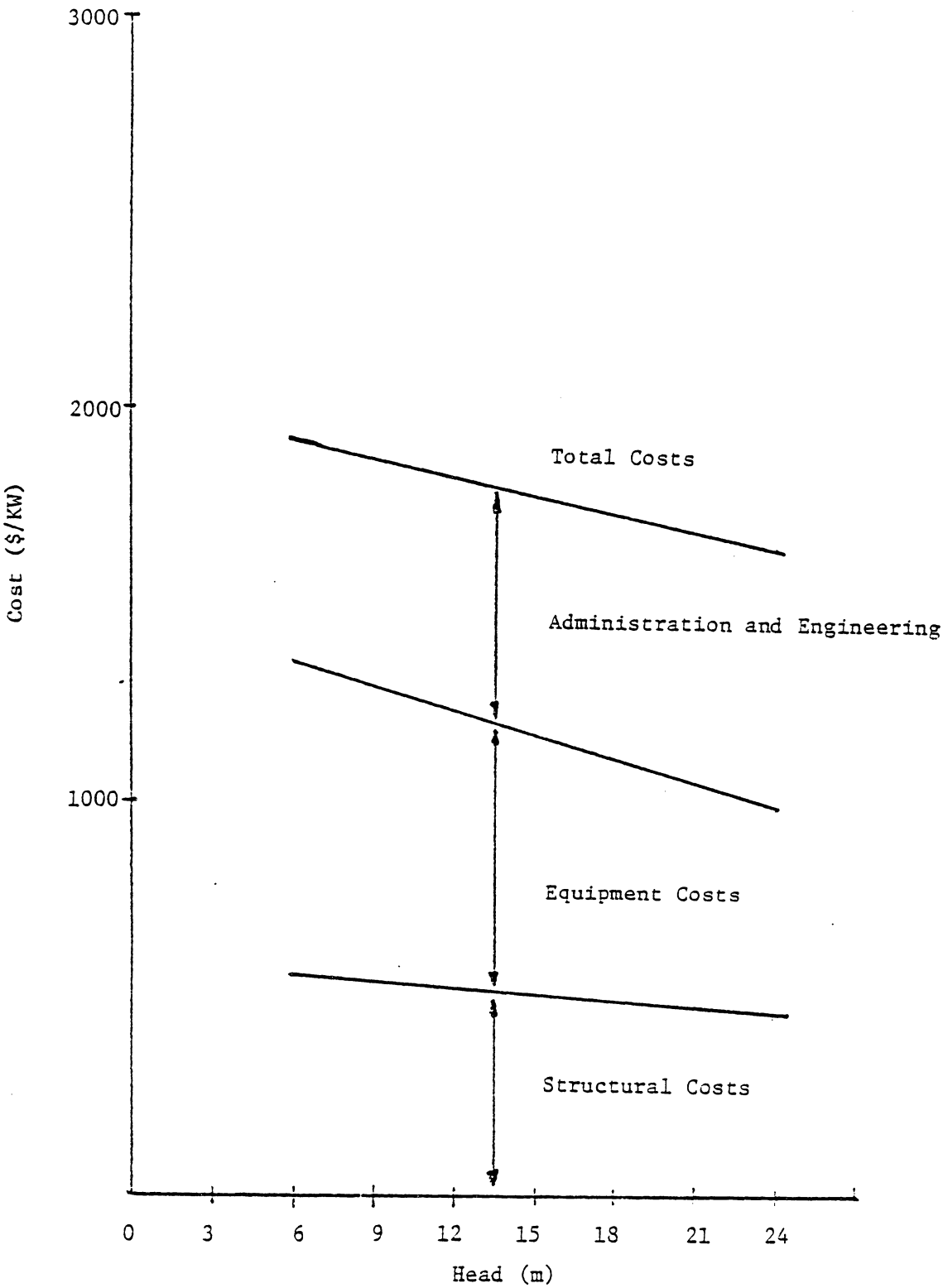

Figure 1. Cost Distribution for Low-Head Projects [2]

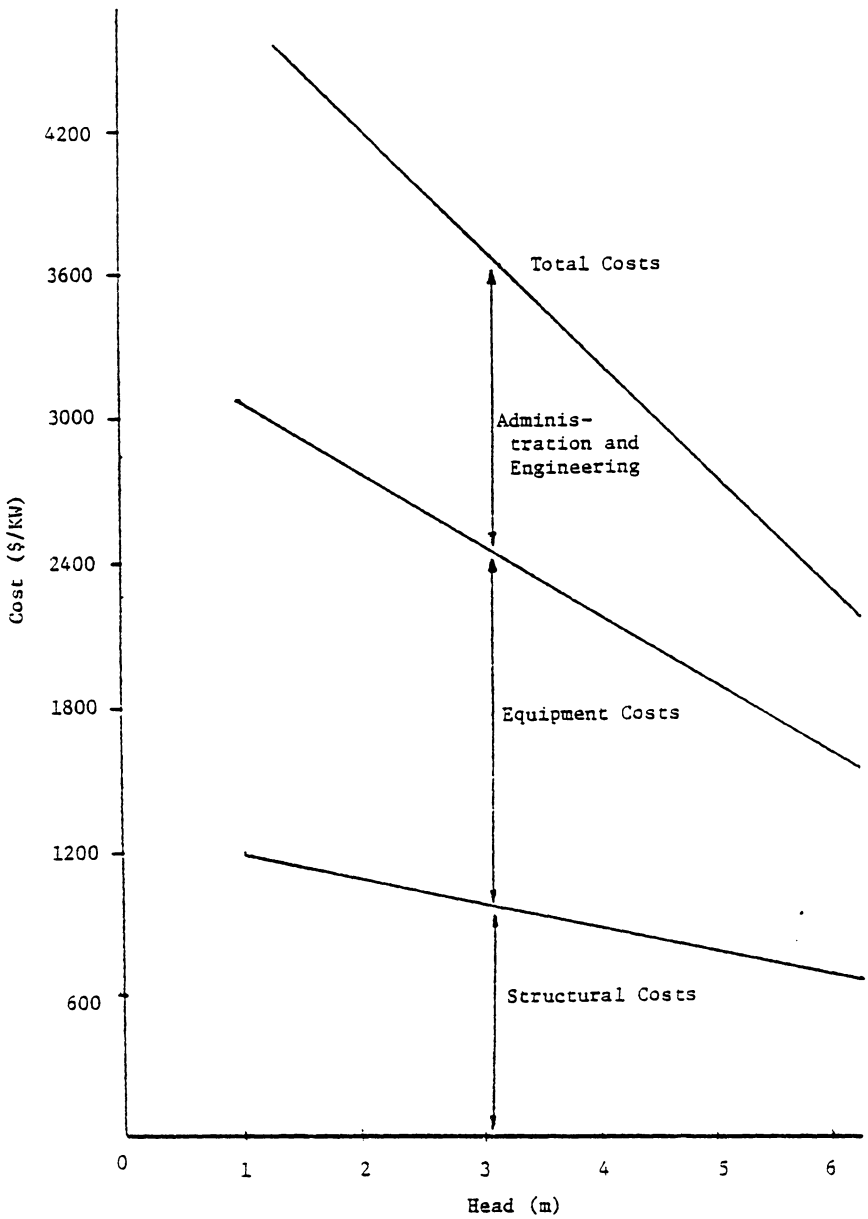

Figure 2. Cost Distribution for Ultra Low-Head Projects [2]

dwindling fossil fuels has become clear that interest in these low-head sites, as in all untapped energy sources, has been renewed. It has been estimated that 30,000 MW of capacity or 95 billion KW-hours/year are available from existing non-hydropower dams [4]. In 1981 hydropower produced 238.7 x 10^3 GW-hr or 10.2 per cent of the total U.S. demand [5]. In North America a 7241 MW hydropower capacity increase is projected for the period 1981-90 [6]. The question now becomes, "How can we harness this energy most cost effectively and enable previously unfeasible projects to become feasible?" The remainder of this thesis is an attempt to provide a fragment of the answer to this question.

1.2 Draft Tubes and Diffusers

Perhaps the most significant distinction between low- and high-head systems from a mechanical point of view is the large portion of the available energy which is kinetic in the low-head system. Kinetic energy in the discharge of a low-head turbine can represent as much as 50-60 per cent of the total energy available in the flow field [7]. Unless this energy is recovered by means of an effective draft tube, it is entirely lost. Figure 3 shows the importance of a good draft tube in a low-head system. As kinetic energy is recoverd by deceleration, the effective head across the turbine must be increased as illustrated by Bernoulli's Equation,

$$p + \rho g z + h_\ell + \tfrac{1}{2}\rho V^2 = \text{const.} \qquad (1.3)$$

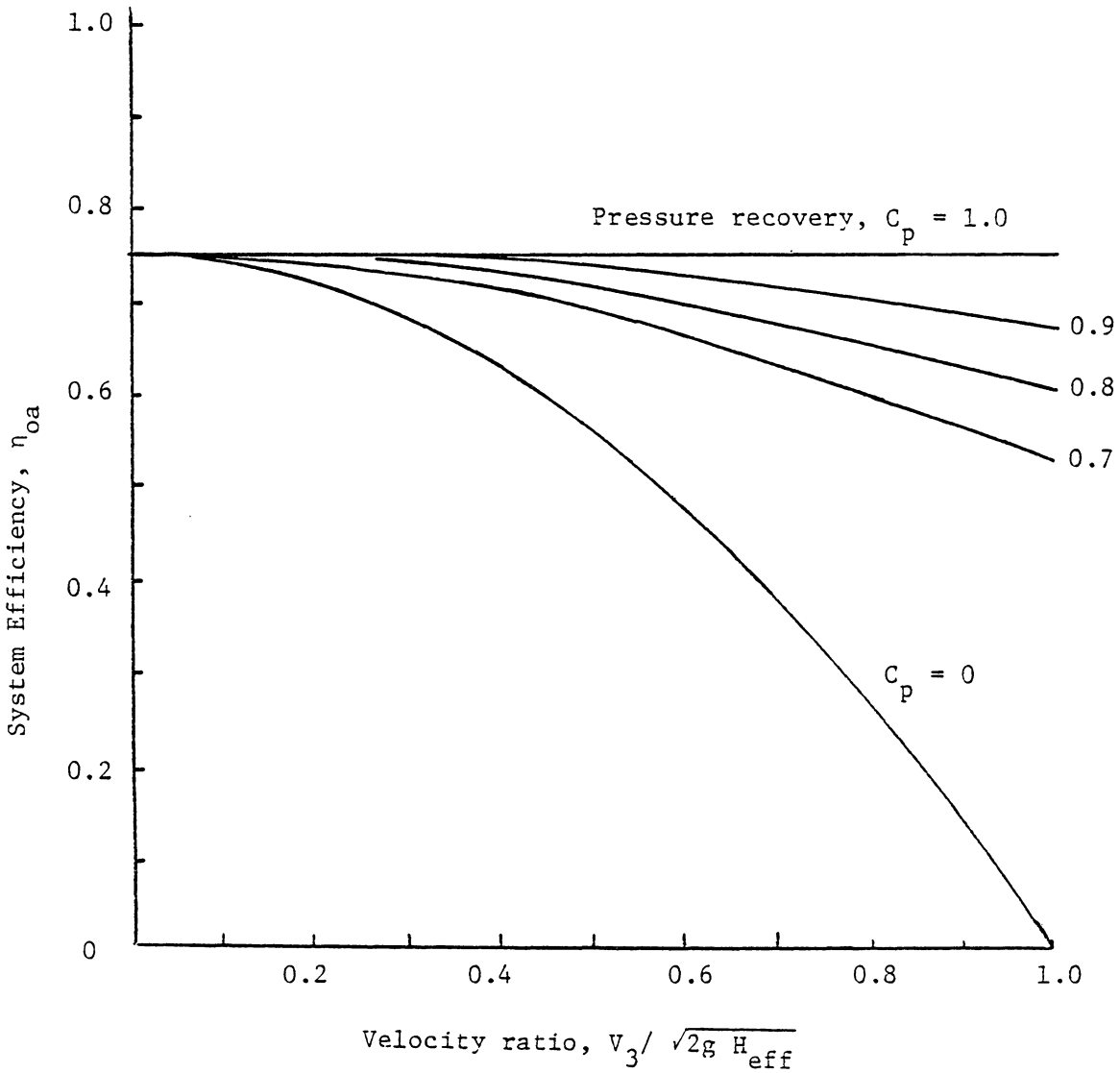

Figure 3. Effect of Draft Tube on System Performance

where

$$H_{eff} = p + \rho g z + h_{\ell} \tag{1.4}$$

Equation (1.1) shows that this increase in effective head can produce an increased power output, or the power output can be maintained with a smaller turbine. In either case the cost per kilowatt of the system will be reduced, since the cost is a strong function of turbine diameter.

A draft tube is basically a straightforward application of a flow diffuser to a hydraulic turbine insofar as flow deceleration and static pressure recovery are its primary objectives. An important distinction lies in the fact that not all flow diffusers are used in applications where the kinetic energy at the exit is considered a loss. This is reflected in the definition of the respective efficiencies. Generally for a diffuser [8]:

$$\eta_{diff} = \frac{V_3^2 - V_4^2 - 2g\,\Delta h}{V_3^2 - V_4^2} \tag{1.5}$$

whereas for a draft tube:

$$\eta_{d.t.} = \frac{V_3^2 - V_4^2 - 2g\,\Delta h}{V_3^2} \tag{1.6}$$

where the subscripts are consistent with Fig. 6.

Both the diffuser and the draft tube are examples of adverse pressure gradient flow which to this day is not completely understood. Empirical correlations and rules of thumb still serve to a large extent

as primary design tools along with testing of laboratory models and, more recently, computer models.

1.3 Overview of VPI&SU Draft Tube Project

The draft tube project at VPI&SU originated with the intention of investigating the principle of tangential injection, which has been demonstrated to enhance diffuser performance, in a hydraulic draft tube application. In this application, a portion of the flow in the penstock which bypasses the turbine will serve as a high pressure jet that can be used for boundary layer control or serve as a jet pump in the turbine discharge. The result is an enhanced pressure recovery which is accomplished at the expense of a portion of the penstock flow. The projected impact of this design lies in the reduction of turbine size which is made possible through head augmentation, thus bringing ultra low-head systems into the economic feasibility range.

Development of the VPI&SU draft tube project took place in three distinct phases; an analytical phase, a design phase, and an experimental phase.

During the analytical phase, first a simplified one-dimensional model and later an improved two-dimensional finite-difference program were developed to predict the pressure recovery in a conical diffuser with annular injection in the axial direction. The accuracy of the computer model was then confirmed with a laboratory model test with several different injection rates using air as the working fluid.

In the second phase of the project, performance maps of diffusers with various geometries and injection rates were developed using the finite difference program. These performance maps were then input into a system modeling program for the complete hydropower system.

In the system program, the benefit of head augmentation was weighed against the cost of sacrificing available flow, so that the net effect of the diffuser-bypass component on the overall performance of the system could be determined. The results of this investigation revealed that annular injection could be used to improve system performance through two independent mechanisms. With moderate amounts of injection, the bypass flow would energize the wall boundary layer, delaying the onset of separation and making possible the use of shorter, wider angled diffusers. With higher injection rates, a jet pumping effect was observed, producing lower pressures at the turbine exit and resulting in improved system performance through increased effective head. The optimum design for experimental study was chosen to be a jet pumping system with a 9 degree total angle conical diffuser and a bypass area ratio of 0.45. The design was scaled to a 10-cm fixed blade propeller turbine runner which was available at the VPI&SU facility. Fixed inlet guide vanes were designed to produce a nearly free vortex flow which would be swirl free under design conditions.

The final phase of the project, which is the subject of this report, involved the construction of the test model system, instrumentation and layout of the experimental facility, experimental testing and data reduction, and economic analysis. The actual system performance

was compared with the predictions of the numerical analysis and the program was modified so as to better simulate the highly turbulent flow in the turbine discharge. The improved performance maps were then used in the system program so that the experimental results could be extended to include the full range of bypass rates applied to full scale turbines. The overall concept was then subjected to economic evaluation and the final results are presented.

2. LITERATURE REVIEW

2.1 Draft Tubes

There are a number of excellent references available which elaborate the principles of traditional draft tube design [8,9,10,11,]. These books generally include qualitative descriptions of flow requirements, basic equations, rules of thumb for simplification and a substantial list of realistic constraints which generally must be met. Draft tubes in general are quite large and are therefore subject to many structural and cost considerations. For example many draft tubes are elbow shaped to help minimize excavation. Concerns such as this, as well as cavitation considerations, often take precedence over optimum flow geometry, especially in larger systems.

Numerous attempts have been made to improve the efficiency of hydropower systems through better draft tube design. The first U.S. patent for a draft tube was granted in June of 1840 [12]. Since that time have come the White hydraucone regainer [9], a horizontal baffle plate which spreads the turbine discharge, and the Moody draft tube [8], which contained a solid core to help reduce cavitation and recover a portion of any swirl component which might be present in the flow. Both of these designs were eventually discarded because of excessive excavation requirements and difficulty in construction. Experiments with multiple baffles and flow splitters [13] have also been tried but basically the horizontal and vertical flared draft tubes and the cast concrete elbow have endured beyond their more elaborate alternatives.

The basic draft tube references which have been mentioned all include some discussion of the problem of cavitation. This is a serious problem which can occur if the absolute pressure at the turbine discharge should be allowed to fall below the saturation pressure. The resulting flash vaporization which occurs can cause significant damage to the equipment and reduce performance considerably.

Another problem which has received more recent attention is that of draft tube surge. This is a serious vibration problem generally associated with excessive swirl in the turbine discharge. A comprehensive review of the subject is presented by Falvey [14]. The low pressures in the core which are caused by large amounts of swirl are generally considered to be responsible for gross instabilities in the diffuser flow field.

One of the most important concerns in hydropower practice is the variability of the available water supply, both above and below the design condition. In an effort to counteract the loss of effective head due to rising tailwater during flood periods, several head increasers have been developed which utilize excess flow. One of these is the Thurlow Backwater Suppressor [15] which produces a standing wave beneath the draft tube, effectively reducing the tailwater elevation during high water periods, see Fig. 4. Users of this device have reported effective heads during these periods in excess of the normal operating head. The Moody Ejector Turbine [16] and the Tefft Tube [15] are equipped with a gate to allow excess flow to enter the low pressure draft tube throat during flood periods, Fig. 5. The resulting high velocity jet produces

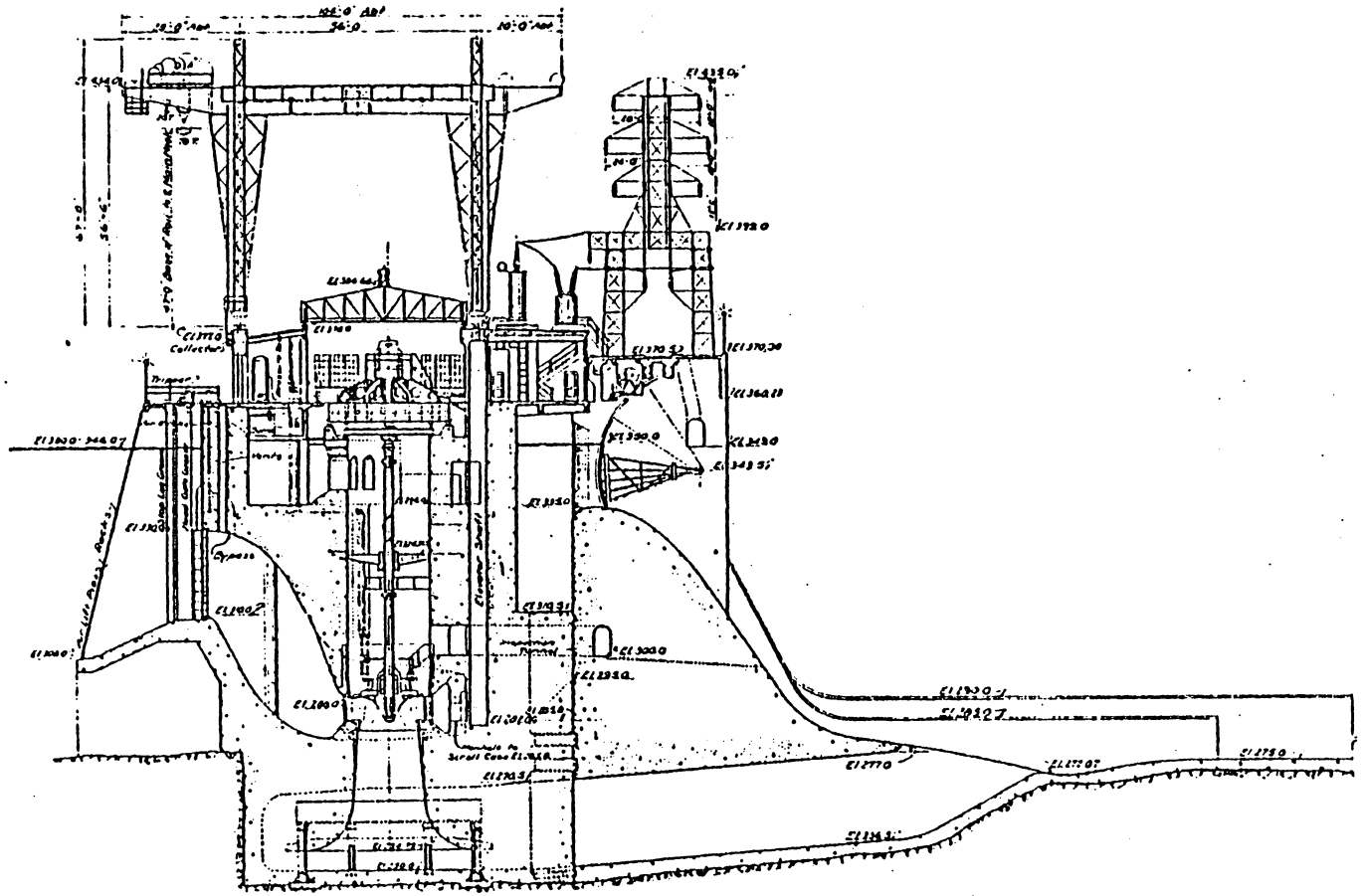

Figure 4. Mitchell Dam Plant with Thurlow Backwater Suppressor [15]

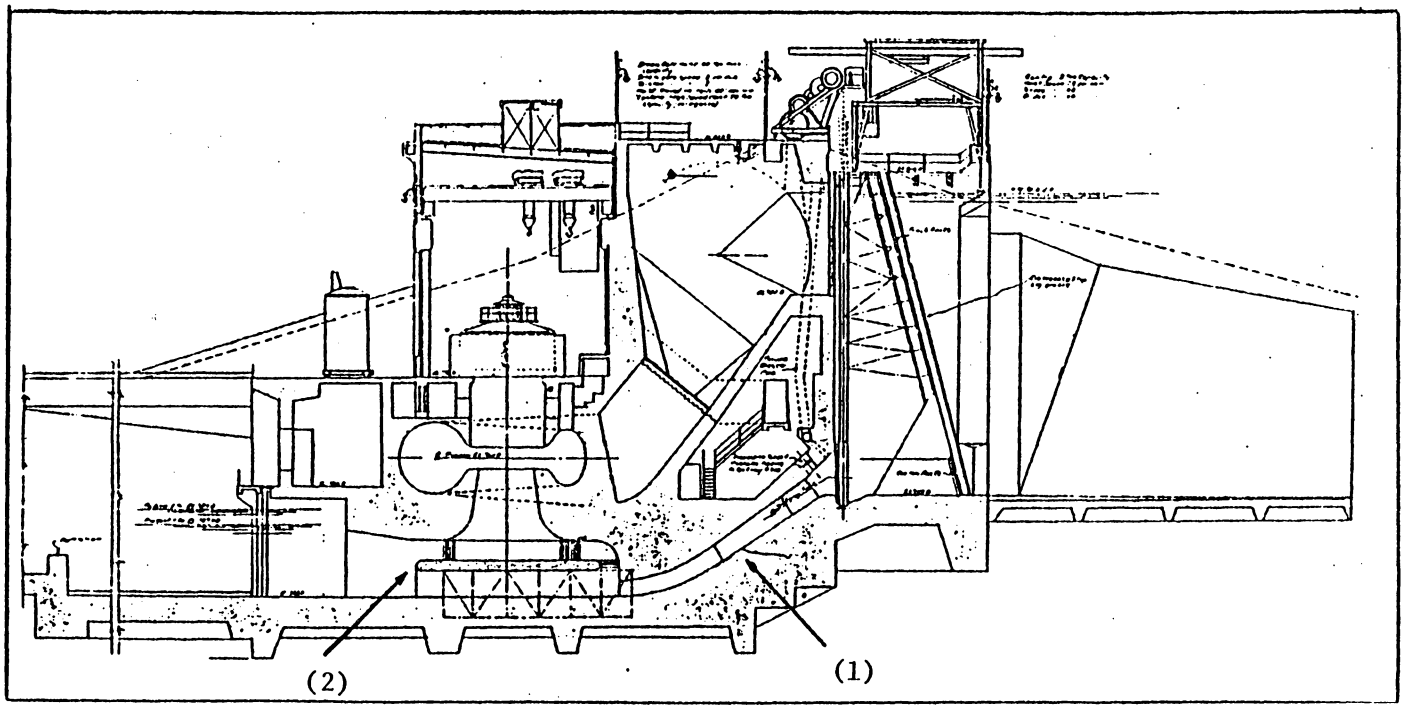

Figure 5. Hodenpyl Plant with Tefft Tube (1) and White Hydraucone Regainer (2), [15]

a lower pressure at the turbine exit, resulting in full power output capability under gross heads which have been reduced by as much as 20 per cent. An experimental turbine designed by Henry Ford and Thomas Edison on the Henry Ford farms was capable of developing its rated power at one-half the normal head [17]. The concept here was a discharge accelerator built into the tailrace which utilized excess flow.

Several of these systems are similar in principle to the current design being evaluated at VPI&SU. However, these devices were designed for intermittent use during high water periods rather than for continuous service with a reduced turbine size.

The use of annular injection slots to increase both effective head and mass flow in freestream machines has been demonstrated in the Run of River Ducted Turbine [18] and the Grumman Diffuser Augmented Wind Turbine [19]. The developers of the Run of River Ducted Turbine claim power production capabilities at gross heads below 0.2m.

2.2 Diffusers

While the amount of material being published on the subject of hydraulic draft tube design seems to have declined substantially over the past several decades, there has been considerable interest in the basic fluid mechanics of diffuser flow during the same period. The majority of the work has been experimental although there have been several recent papers presenting computational approaches for rectangular [20] and conical [21] diffusers. Performance, design, and optimum geometries have been the subject of experimental studies by

Kline, Abbott and Fox [22], Reneau, Johnston, and Kline [23], Ward-Smith [24] and Carlson, Johnston, and Sagi [25], all dealing with rectangular geometries. Sovran and Klomp [26] deal with rectangular, conical and annular geometries in a comprehensive work.

Conical diffusers, probably the most common diffuser type, have received considerable attention. Early work was summarized in 1938 by Patterson [27] in what has long been considered the standard work. Literally all the research of the next twenty-five years was summarized in 1964 by McDonald and Fox [28] who found the available data completely inadequate and impossible to correlate. It became apparent to them that the important parameters in diffuser flow were not controlled or even understood in the early experiments. They found that diffuser performance tends to vary with flow regime and other factors as yet unknown. Their research considered the effects of Reynolds number and geometry on diffuser performance. They found that for flows having an inlet Reynolds number above 75,000 there was no appreciable Reynolds number effect on pressure recovery.

Other researchers have investigated other parameters. Cockrell and Markland [29] studied the effect of inlet momentum thickness and in the Creare Diffuser Data Book [30], Runstadler et al. claim that diffuser performance can be correlated quite well in terms of a blockage factor which is related to the displacement thickness. Explicit correlations for this data have been developed by Thompson [31].

It should be pointed out that although studies such as that of McDonald and Fox fall short of a complete understanding of diffuser

flow, they do provide performance maps, lines of first appreciable stall and lines of optimum performance which are adequate for most engineering applications.

Undoubtedly the main reason that diffuser flow is so difficult to predict analytically is the presence of stall. Stalling flow is very common in diffusers. In fact several of the studies mentioned above [26,28] report that optimum performance often occurs under conditions of partial or transitory stall. Yet full stall and wall separation seriously downgrade a diffuser's performance. Kline [32] has stated that boundary layer theory alone cannot predict the onset or behavior of stall. Moses and Chappell [33] and Woolley and Kline [34] discuss computation approaches to stalled flow in diffusers. Experimental studies such as that of Smith and Kline [35] and Ashjaee, Johnston, and Kline [36] continue to lay the groundwork for the further understanding of this phenomenon.

In some diffuser applications, such as the one presently under investigation, the effect of non-uniform inlet profiles can be very important. There have been several experimental studies in this area [37,38,39] with some rather interesting results. All of these studies found that there were some cases where diffuser performance was improved by inlet non-uniformities. There were also cases of stalled core flow where deep inlet wakes were present.

One of the most important types of diffuser inlet condition which is found to occur frequently in turbomachinery is swirling flow. Traditionally, swirling flow in the turbine discharge has been

considered a consequence of off-design operation which is to be avoided if possible since the kinetic energy carried by the whirl component is almost entirely lost in the diffuser. Wirasinghe [40], however, found that in some cases, mild swirl (less than a 15 degree swirl angle) would tend to flatten diffuser velocity profiles, decreasing centerline velocities and increasing the velocity of the fluid over the wall. This resulted in a delay of wall separation. His data showed continued improvement throughout the mild swirl range except in very wide-angled diffusers where the core flow began to stall at the higher swirl angles. Markowski and Lohmann [41] reported premature separation at the inner walls of annular diffusers with swirl addition.

As the understanding of diffusers continues to grow new concepts for improving them continue to appear in the literature. The improvements are generally directed toward either increasing the efficiency or reducing the overall length. A diffuser can be shortened without any loss in area ratio if a larger divergence angle can be tolerated. However, this is where wall separation quickly becomes a problem. One approach to this problem, which has been used by several researchers [42,43,44], is a vane system which effectively turns a very wide angled diffuser into several diffusers with more moderate flow angles. Senoo and Nishi [45] have successfully tested the use of fixed vortex generators mounted in the diffuser walls to energize the boundary layer with a resulting improvement in performance. Moon [46] used distributed suction to remove the low velocity fluid near the wall, preventing separation and improving pressure recovery as well.

The final method of diffuser performance enhancement to be discussed here is the use of annular injection at the inlet which is the concept being applied in the VPI&SU Draft Tube Project. The concept was previously tested by Ramaprian [47] and Nicoll and Ramaprian [48] in 1970. This research involved three diffuser angles with fixed injection area ratios. When fluid was injected along the wall, each diffuser showed a net improvement in pressure recovery. Most dramatic was the improvement in the widest angled diffuser (30°) which was stalling severely without injection. An analytical model similar to the one used in the current project was also developed.

Fieldner and Gessner [49] applied the concept of tangential injection to rectangular diffusers where the injection slot size and divergence angle could be varied more easily. Their results confirmed Ramaprian's conclusion that injection is effective in improving overall performance. They also showed that the slot width is a significant parameter.

Duggins [50] investigated conical diffusers with tailpipes. He studied the effect of injection flow direction and found axial injection to be superior to meridional since less injection flow was required in this mode.

Frankfort [51] varied the location of the jets and found that the best performance occured with the jets in the diffuser inlet plane.

These studies have demonstrated the effectiveness of annular injection in improving diffuser performance and have refined the technique to some degree. However, none of these studies were concerned with

hydraulic draft tubes where the injected fluid would not come from an external source. This application is the basis of the present study.

The use of peripheral jets for pumping applications is discussed by Mussalli et al. [52]. Exley and Brighton [53] reported cases of stalling secondary flow in jet pumping arrangements with high velocity ratios.

It is clear that a number of researchers have responded to the problem of diffuser wall separation by recognizing the possibility of improving diffuser performance through some means of momentum exchange between the inviscid core flow and the rapidly decelerating flow near the wall. The concept has been shown to be effective in some cases. The limiting factor seems to be the onset of core stall when too much momentum is transferred from this region into the outer flow.

3. DRAFT TUBE PROJECT DEVELOPMENT

The following section briefly outlines the methods and results of the first two phases of the current draft tube project. This will help to provide a sense of continuity for the final phase which is the primary subject of this thesis. A complete description of each of these phases is provided in Ref. (54) and (55).

3.1 One-Dimensional Analysis

The investigation began with a simplified one-dimensional analysis which was developed to estimate the pressure recovery and system performance for varying injection rates as determined by the bypass area ratio and the velocity ratio. The analysis makes use of the following simplifying assumptions:

1) Steady, one-dimensional flow throughout
2) Uniform velocity profiles at each section
3) No wall friction in the mixing tube
4) All pressure rise from mixing occurs in the mixing tube
5) All pressure rise from deceleration occur in the diffuser
6) Constant turbine efficiency
7) Constant diffuser pressure recovery coefficient

The model for this analysis is presented in Fig. 6.

The results of this analysis showed that the full output power of a conventional turbine could be realized with a smaller turbine using bypass flow at a slightly reduced efficiency, see Fig. 7. It should be

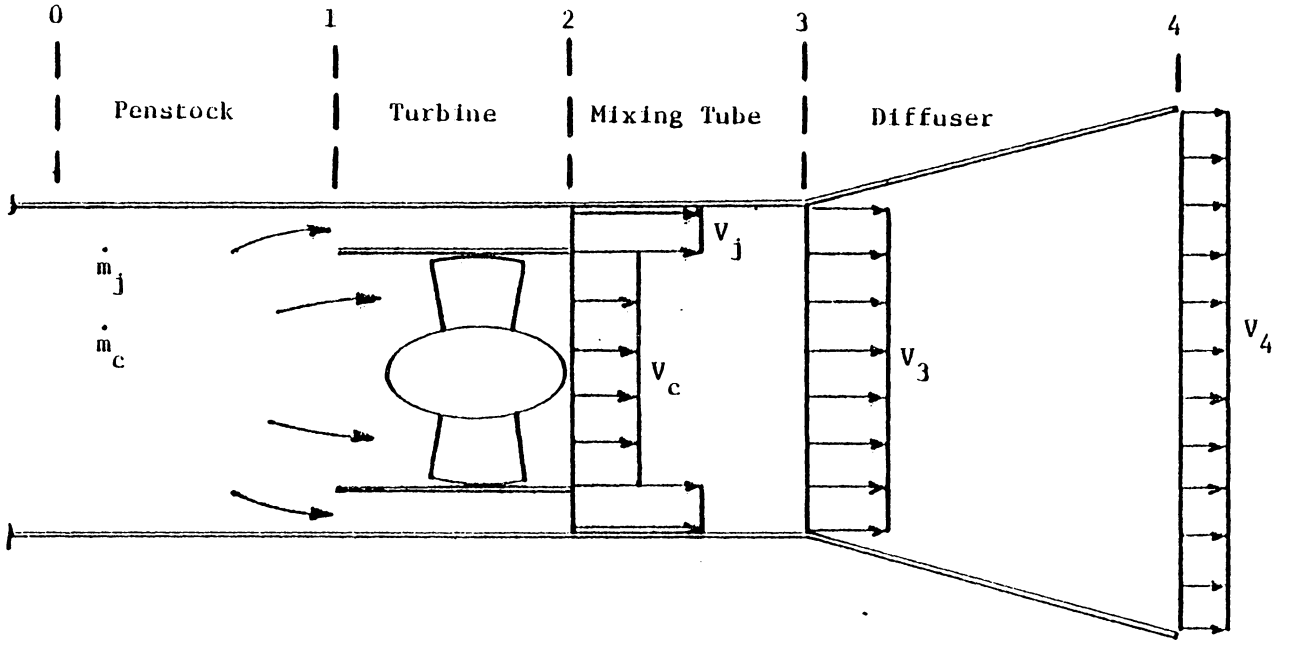

Figure 6. Model for One-Dimensional Analysis [54]

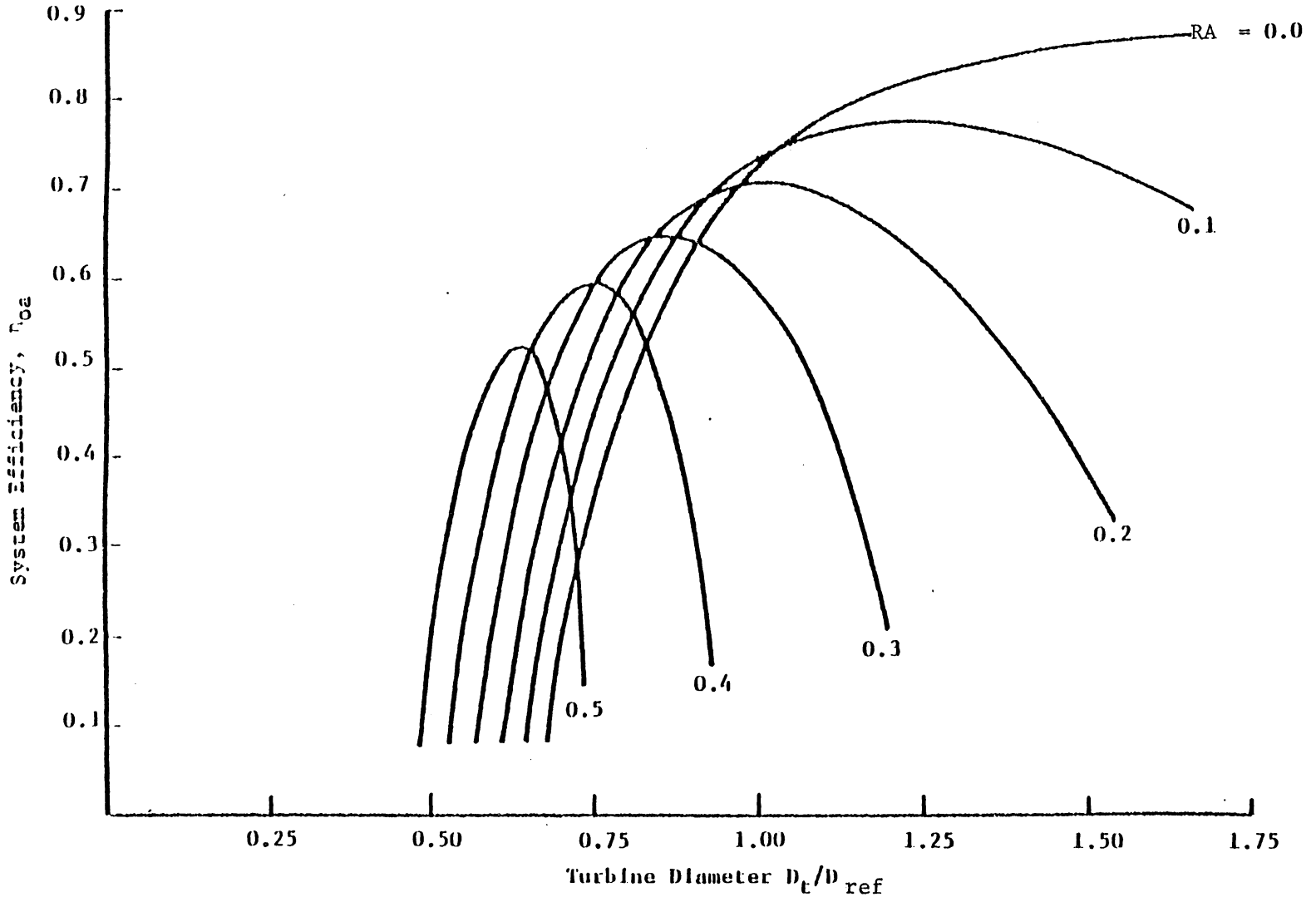

Figure 7. Results of One-Dimensional Analysis [54]

pointed out that the efficiency referred to here is that based on the entire available flow and not just the flow through the turbine. These results indicate that a substantial net benefit might be realized from this system due to the decreased capital expenditure made possible by turbine size reduction.

3.2 Two-Dimensional Diffuser Model

The next step was to develop a more sophisticated analysis which would include viscous effects and cross-stream variations in the flow field. A finite-difference approach was selected, based on the implicit method of Patankar and Spalding [56], a two-dimensional marching technique which has been used successfully in previous investigations [47] of diffusers with wall jets. The solution technique, which solves the Navier-Stokes equations in streamline coordinates takes advantage of the parabolic nature of diffuser flow in which the influence of downstream conditions is negligible in comparison with upstream effects.

The pressure at each downstream location is guessed and iterated upon until continuity is satisfied by the wall streamline location. The turbulent viscosity is calculated with the Prandtl mixing length model, using the Van Driest correction near the wall. With each guess of the downstream pressure, the complete velocity distribution at that location is determined by a tridiagonal matrix algorithm and when the correct pressure is found, the program marches to the next downstream location. It should be pointed out that this program is based on the assumption of no pressure gradient in the cross-stream direction, and

that there is no swirl in the flow. The required inputs are the bypass, diffuser, and mixing tube geometry and the inlet velocity distribution and pressure. The program provides a complete description of the diffuser flow field and values of the pressure recovery coefficient, which is defined as

$$C_p = \frac{P_4 - P_2}{\frac{1}{2}\rho V_c^2} \quad , \tag{3.1}$$

are given as a function of axial position (see Fig. 6). Figure 8 is a flow chart of the numerical analysis and Fig. 9 is an example of the program output in graphical form. Note that the horizontal lines are streamlines while the vertical lines represent the velocity profiles.

The accuracy of the program was confirmed using the experimental apparatus shown in Fig 10. The laboratory model test used air flow with the pressure drop due to the turbine being simulated with wire mesh screen blockage. A comparison of the numerical analysis with the experimental test results is shown in Fig. 11. As the figure indicates, the agreement was generally very good.

The results of both the computer model and the laboratory model tests indicate that significant improvements in pressure recovery can be realized with this system. Further study follows in Phase Two of the project.

3.3 Phase Two - Performance Maps

In the second phase of the project, extensive use was made of the

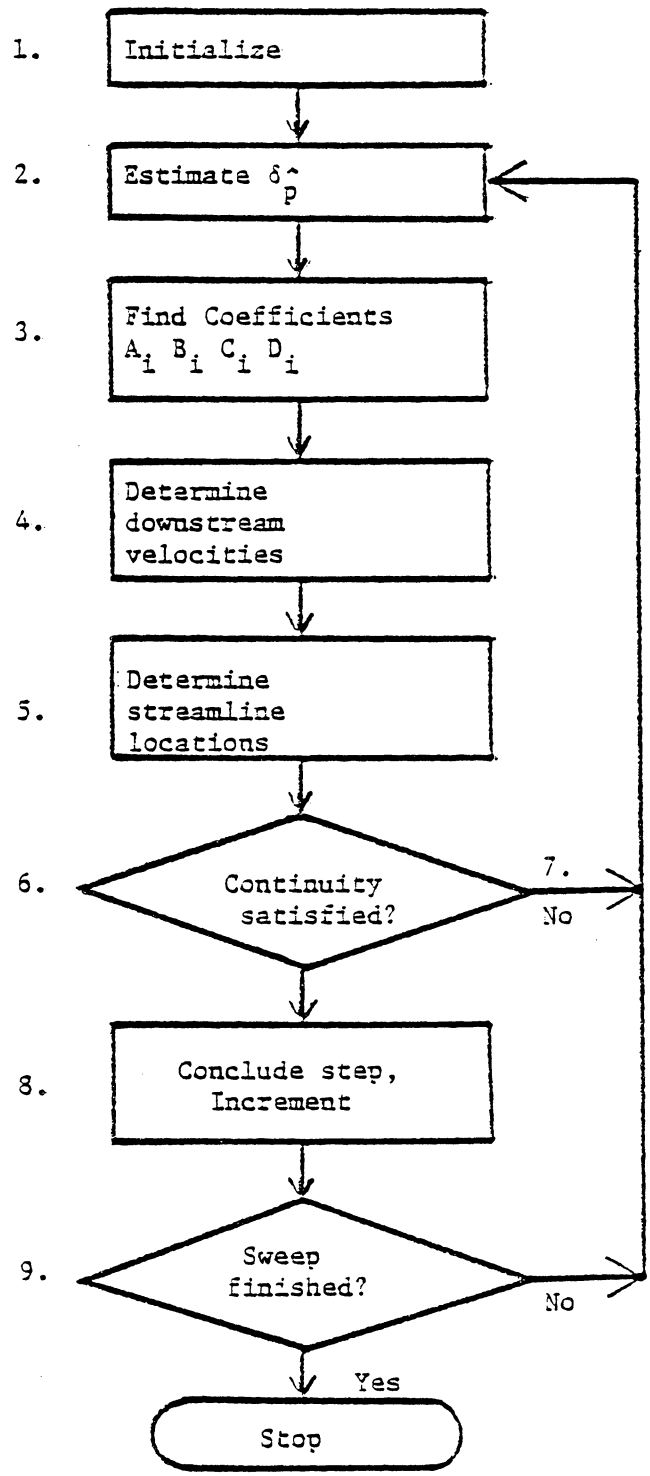

Figure 8. Flow Chart of the Numerical Analysis [54]

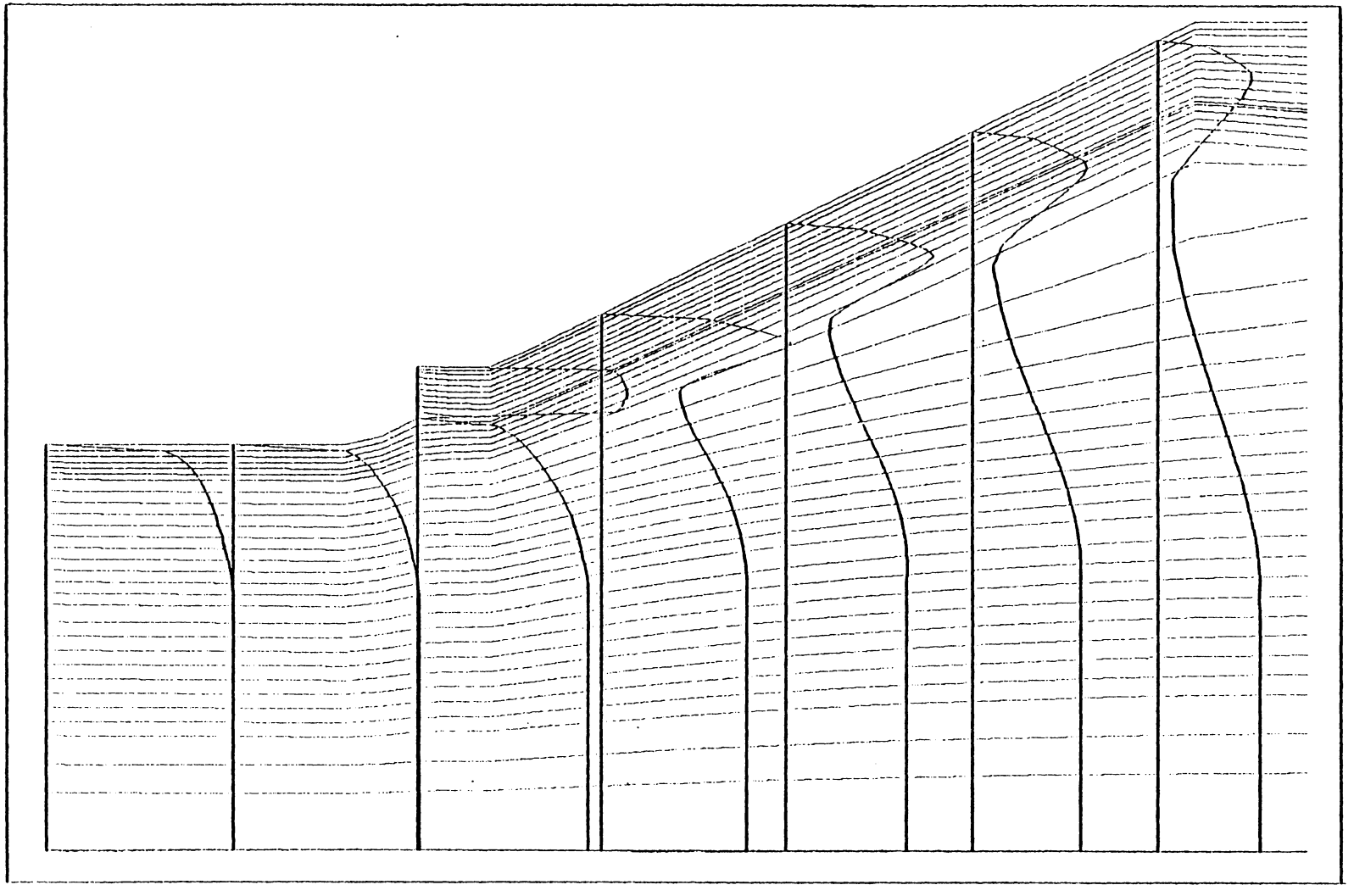

Figure 9: Results of the Numerical Analysis [54]

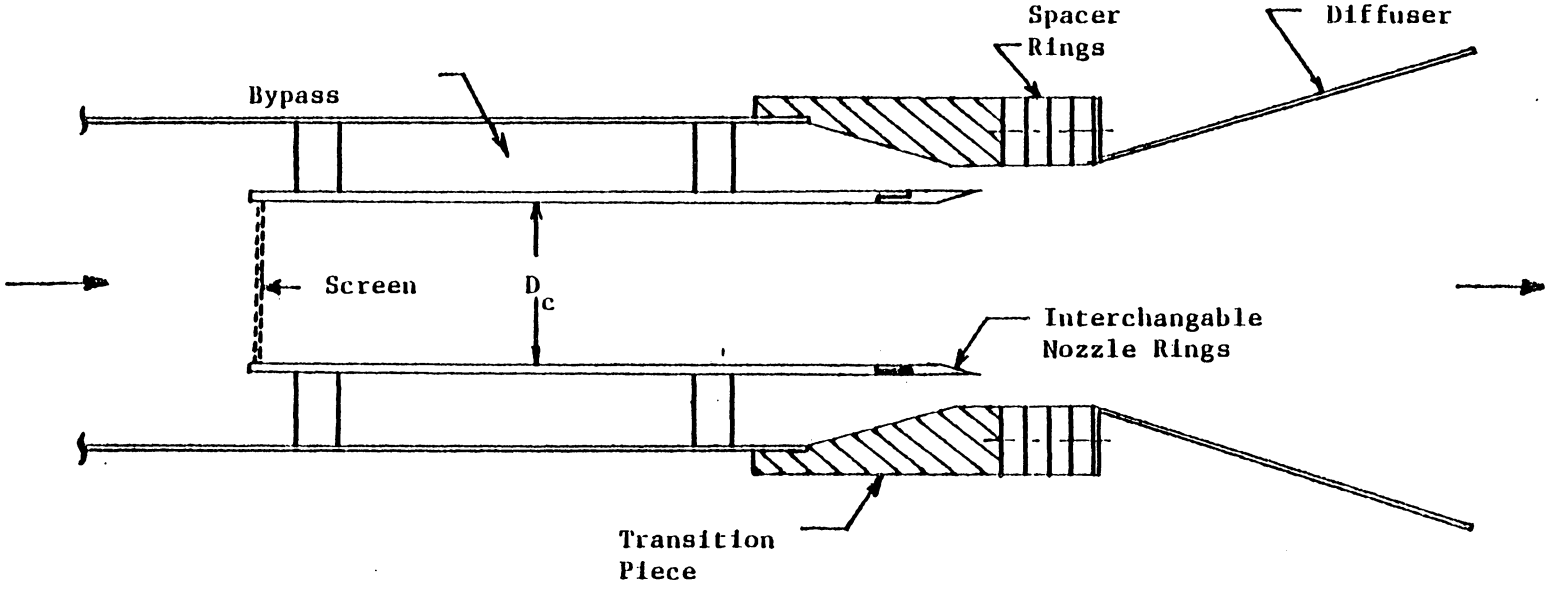

Figure 10. Schematic Diagram of the Experimental Apparatus [54]

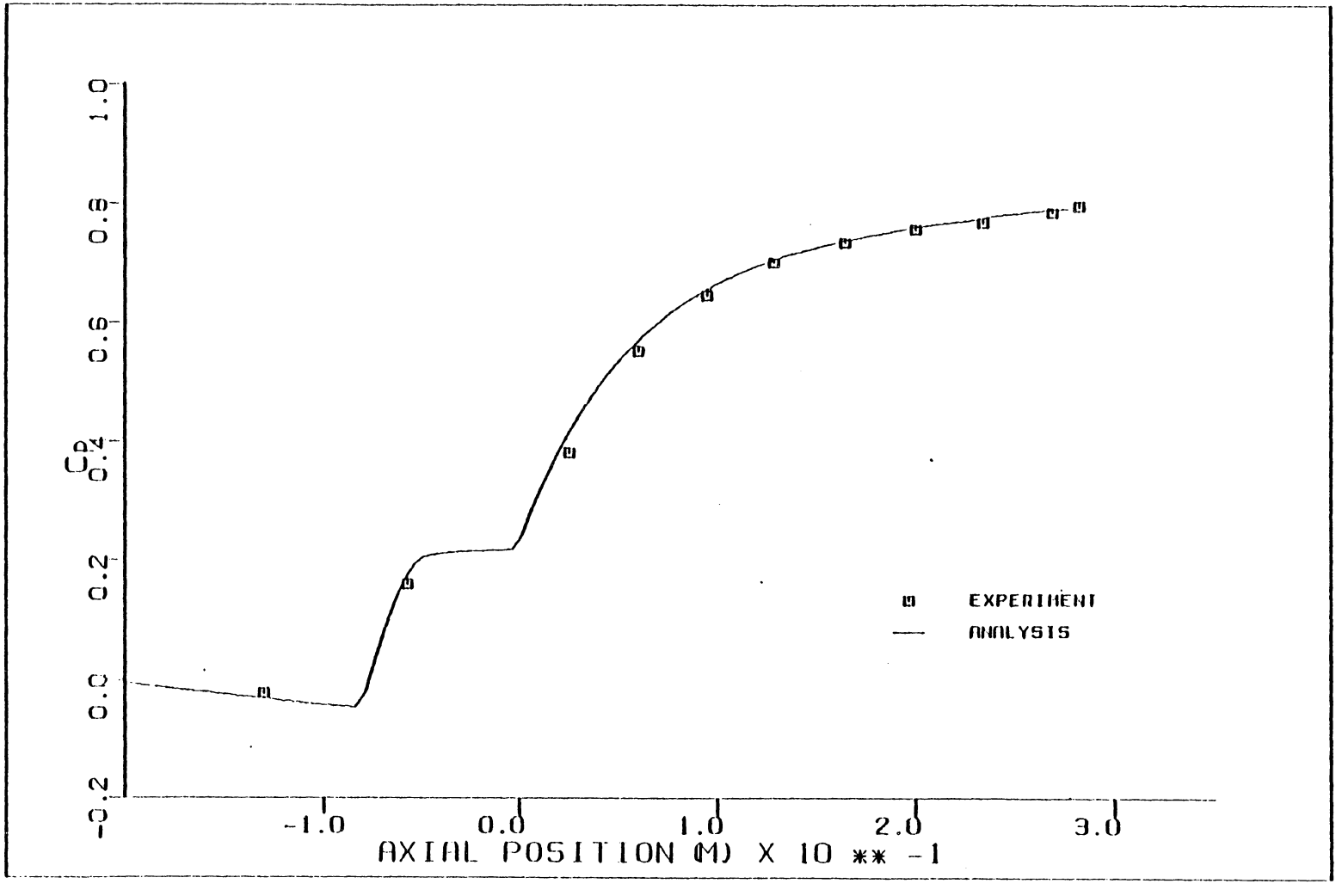

Figure 11. Comparison of Prediction with Experiment: Pressure Recovery, Phase One [54]

diffuser program to predict the operating characteristics of the diffuser-bypass system under typical low-head hydro-power conditions. The program was executed for a large variety of geometries and flow conditions in order to determine those situations where the diffuser-bypass concept would be beneficial.

In this investigation, the bypass area ratio which is defined as

$$RA = A_j/(A_j + A_c) \tag{3.2}$$

is allowed to range from 0 to 0.5, while the diffuser cone half-angle ranges from 0 to 40 degrees. The bypass area ratio and the velocity ratio which is defined as:

$$RV = V_{j\ max}/V_{c\ max} \tag{3.3}$$

completely specify the amount of injection for a given set of inlet conditions. The assumed inlet velocity profiles are given by

$$\frac{U}{U_{max}} = \left(\frac{y}{\delta}\right)^{1/7} \tag{3.4}$$

in the core and by

$$\frac{U}{U_{max}} = \left[\frac{y}{\delta}\right]^{1/25} \tag{3.5}$$

in the wall jet. These profiles are shown in Fig. 12.

The results of this parametric study show beneficial effects of fluid injection under two distinct sets of operating conditions. Under the first condition a small amount of injection is combined with a wide

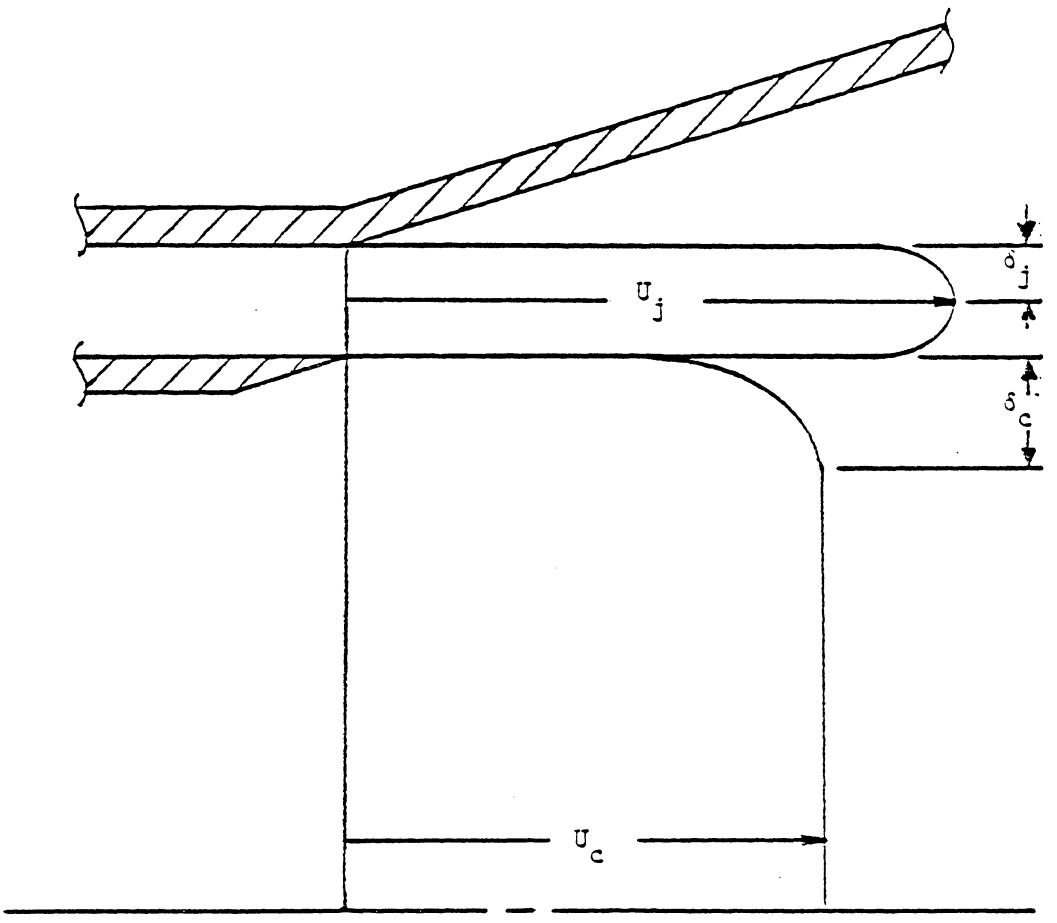

Figure 12. Idealized Inlet Velocity Profile [54]

diffuser angle to yield a very short and effective flow diffusing system. The fluid in the jet acts to energize the wall boundary layer preventing separation and allowing very effective pressure recovery with cone half-angles of 20 degrees and greater. Figure 13 is a performance map of the boundary layer control (BLC) system for bypass area ratios of 0.05 and 0.10. It was found that values of RA below 0.05 did not affect pressure recovery while values above 0.10 were not efficient since too much bypass was required for the improvement shown.

The second set of conditions which was found to be beneficial consisted of a relatively large injection rate with a small diffuser angle. The considerable amount of momentum present in the jet provided a jet-pumping effect which produced a substantial pressure rise across the diffuser. A performance map of the jet-pumping or ejector-diffuser system is shown in Fig. 14. The pressure rise due to this jet-pumping effect begins in the mixing tube which lies between the turbine exit and the diffuser inlet. This mixing tube also serves to moderate the effect of the gross non-uniformity in the turbine exit plane profile which would be likely to stall in the adverse pressure gradient of the diffuser. The computer model predicts the occurence of centerline stall in mixing tubes less than four diameters long for all of the area ratios considered. The occurence of core stall also limits the size of the cone half-angle which can be used with this system.

Several conclusions can be drawn about the merits of these two mechanisms. The BLC system provides an effective method of reducing diffuser length without any corresponding loss in performance. The

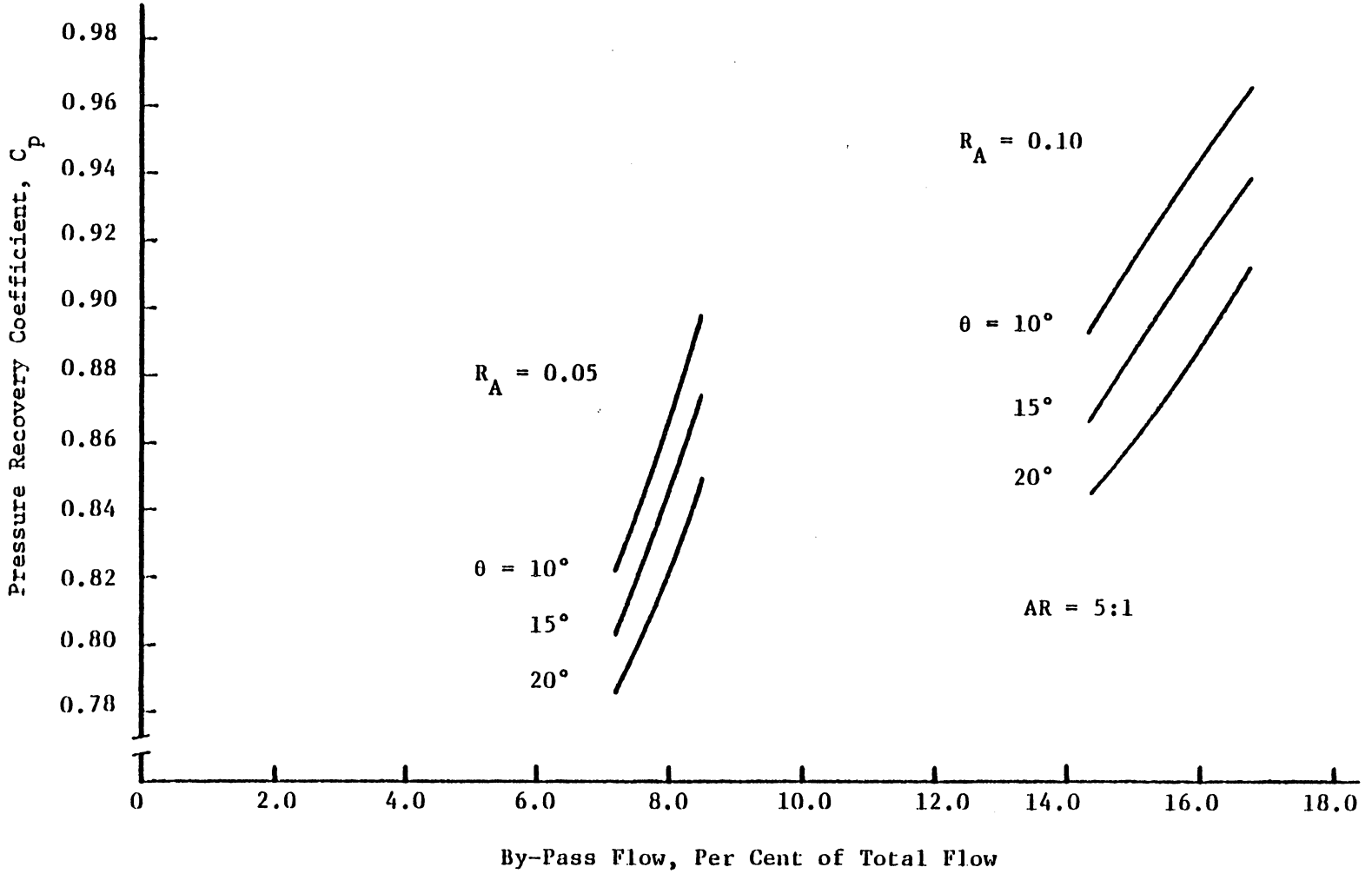

Figure 13. Diffuser Performance with BLC [55]

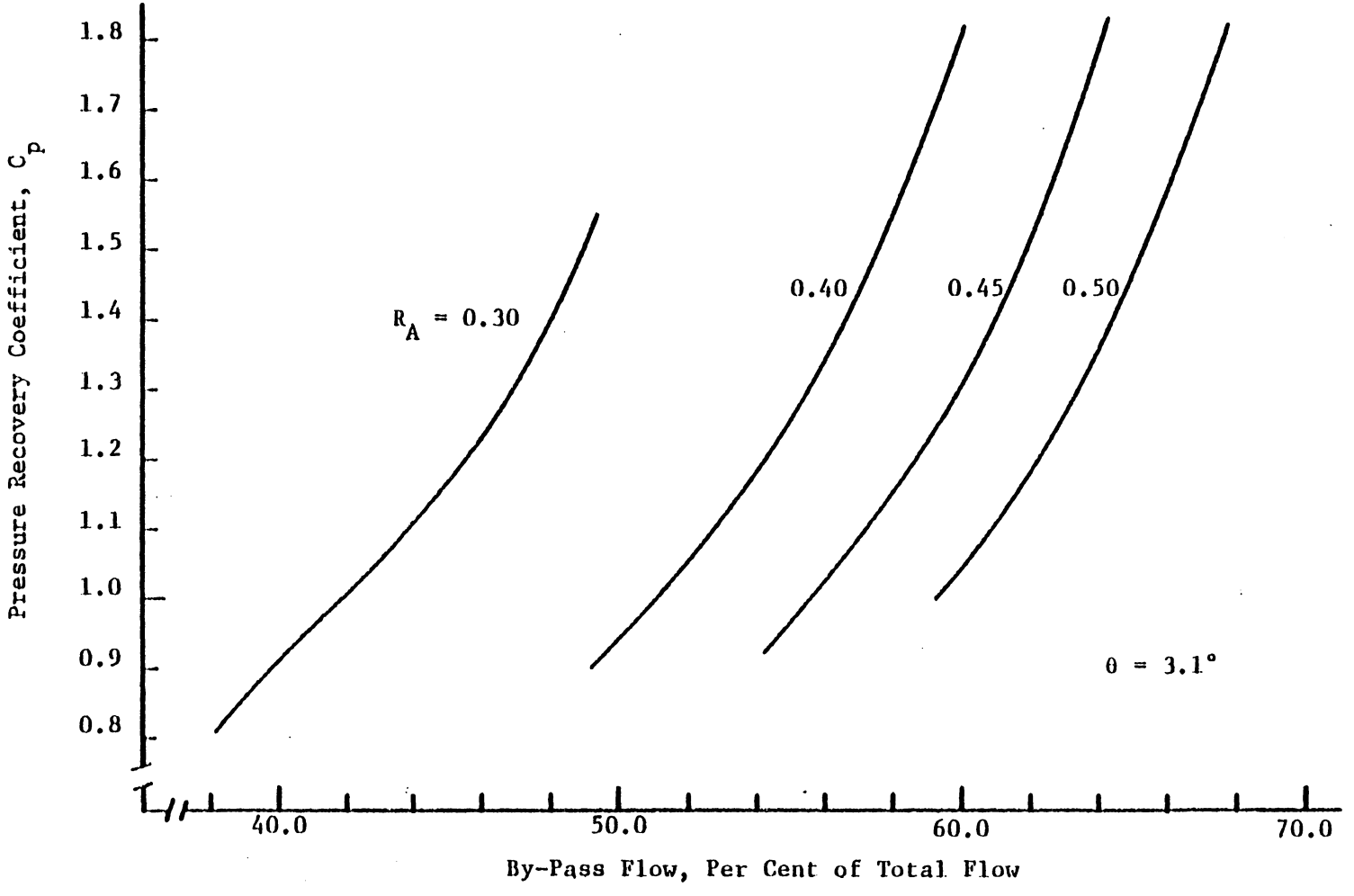

Figure 14. Ejector-Diffuser Performance [55]

pressure recovery coefficients shown compare quite favorably with those of conventional diffusers. The importance of a short draft tube is felt particularly in vertical installations where excavation costs as well as cavitation considerations weigh heavily in the overall design process.

The impressive pressure recovery characteristics of the jet-pumping system make it the prime candidate for a turbine size reduction program. The high rate of kinetic energy conversion in the flow stream which passes through the turbine helps to offset the loss of available energy in the bypass flow.

3.4 Revised System Model

With the operating characteristics of the various diffuser-bypass combinations specified by the performance maps, the system performance estimates of Phase One can be brought one step closer to reality. The system modelling program presented in Phase One was revised to include the results of the numerical diffuser analysis in the form of polynomial curve fits of C_p as a function of the amount of flow bypassed.

The results of this analysis for the BLC system are presented in Table 1. The data clearly shows that boundary layer control can be used to appreciably reduce the length requirement for a draft tube with only a slight sacrifice in overall efficiency. It is clear that the area ratio of 0.05 produces the same length reduction at less expense and is therefore the preferred choice.

TABLE 1

BLC System Performance [55]

THETA, degrees	R_A	$\eta_{o/a}$,%	ℓ/D_2	
4.0	0.0	80.0	8.84	(Baseline)
7.0	0.0	75.0	4.00	(Typical)
10.0	0.05	76.2	3.51	
10.0	0.10	72.2	3.51	
15.0	0.05	75.4	2.31	
15.0	0.10	71.2	2.31	
20.0	0.05	74.5	1.70	
20.0	0.10	70.2	1.70	

η_t = 90%

TVR = 0.742

Figure 15 shows the results for the jet-pumping system in graphical form. The performance of a conventional system is also presented for comparison purposes. These results indicate that a 10-20 per cent reduction in turbine diameter can be achieved with no loss in the system efficiency. On the other hand, for a given turbine as much as 10 points in overall efficiency can be gained with the jet pumping system. Of course either of these improvements would require a substantial amount of additional flow which may or may not be available. Economic optimization which will be discussed later will determine under what circumstances this system will be practical. Clearly the relationship between the turbine size and the overall system cost will play a major role in this decision.

The expression TVR which is used in the above figures refers to the turbine velocity ratio which is defined as

$$TVR = V_c/\sqrt{2\ g\ H_{eff}}\ . \qquad (3.6)$$

This is a turbine design parameter which is related to the work extracted by the turbine. The values of 0.75 which is given is a typical value for ultra low-head turbines. The dots on the system performance curves represent design points based on this value of TVR.

3.5 Experimental Model Design

On the basis of these optimization studies, it was decided that a model of the ejector diffuser system would be constructed and tested in

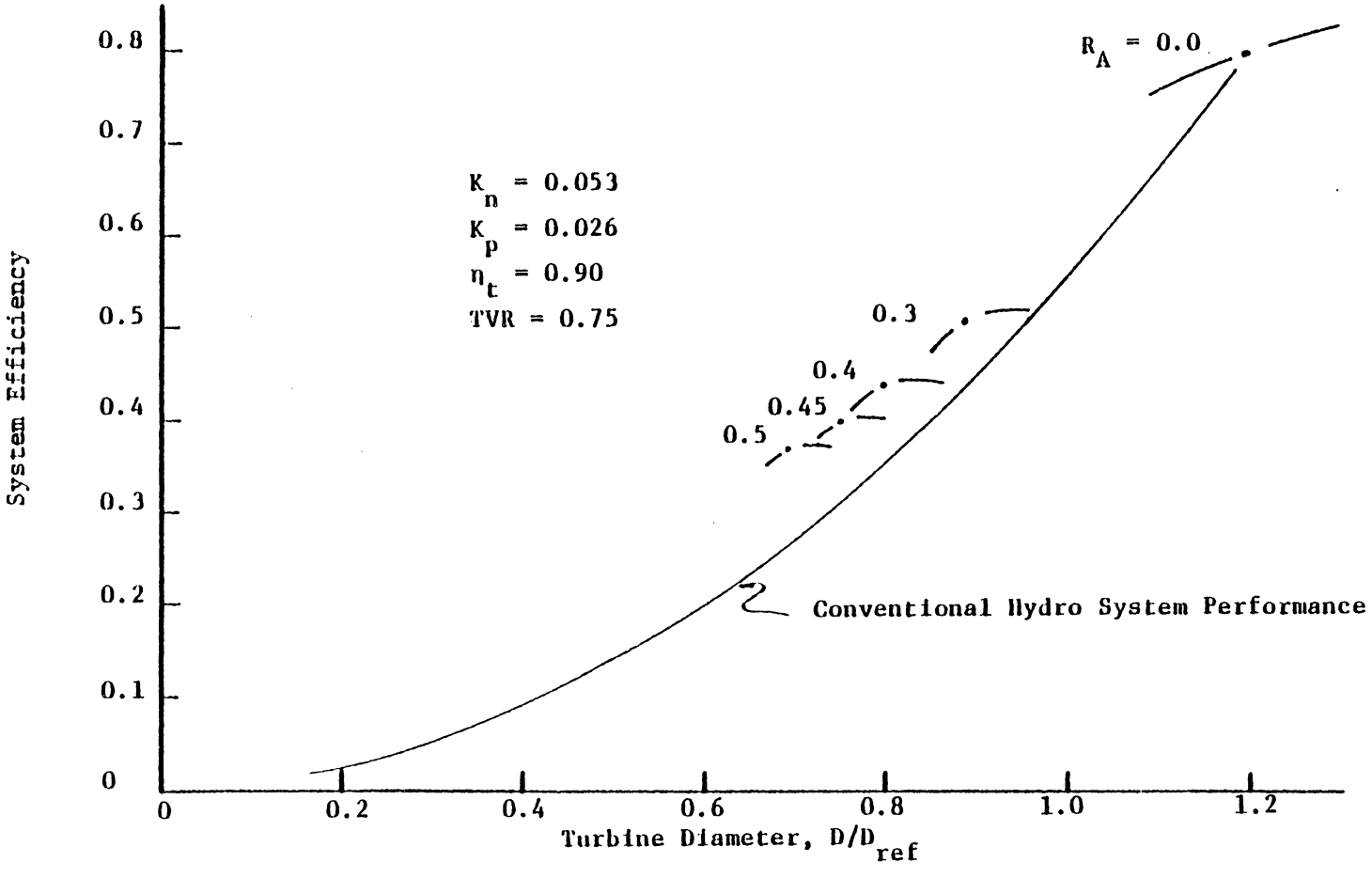

Figure 15. Ejector-Diffuser System Performance [55]

the laboratory to demonstrate the principles involved. The final stage of phase two in the project was the specification of the system components.

The system was chosen to have a bypass area ratio of 0.45 with a mixing tube length of 5 diameters. The diffuser cone angle was chosen to be 4.5 degrees. The design head is 3 meters and the design flow through the turbine is 0.44 m^3/sec. The fixed inlet guide vanes were designed to produce a free vortex flow which is swirl free under design conditions. The turbine runner is a 1940 Rodney Hunt model number 4. It is a fixed blade propeller-type runner with four blades and an outside diameter of 9.68cm. Figure 16 is a photograph of the runner.

The design performance specifications of the model system are given in Table 2. The individual components are discussed in more detail in the following section.

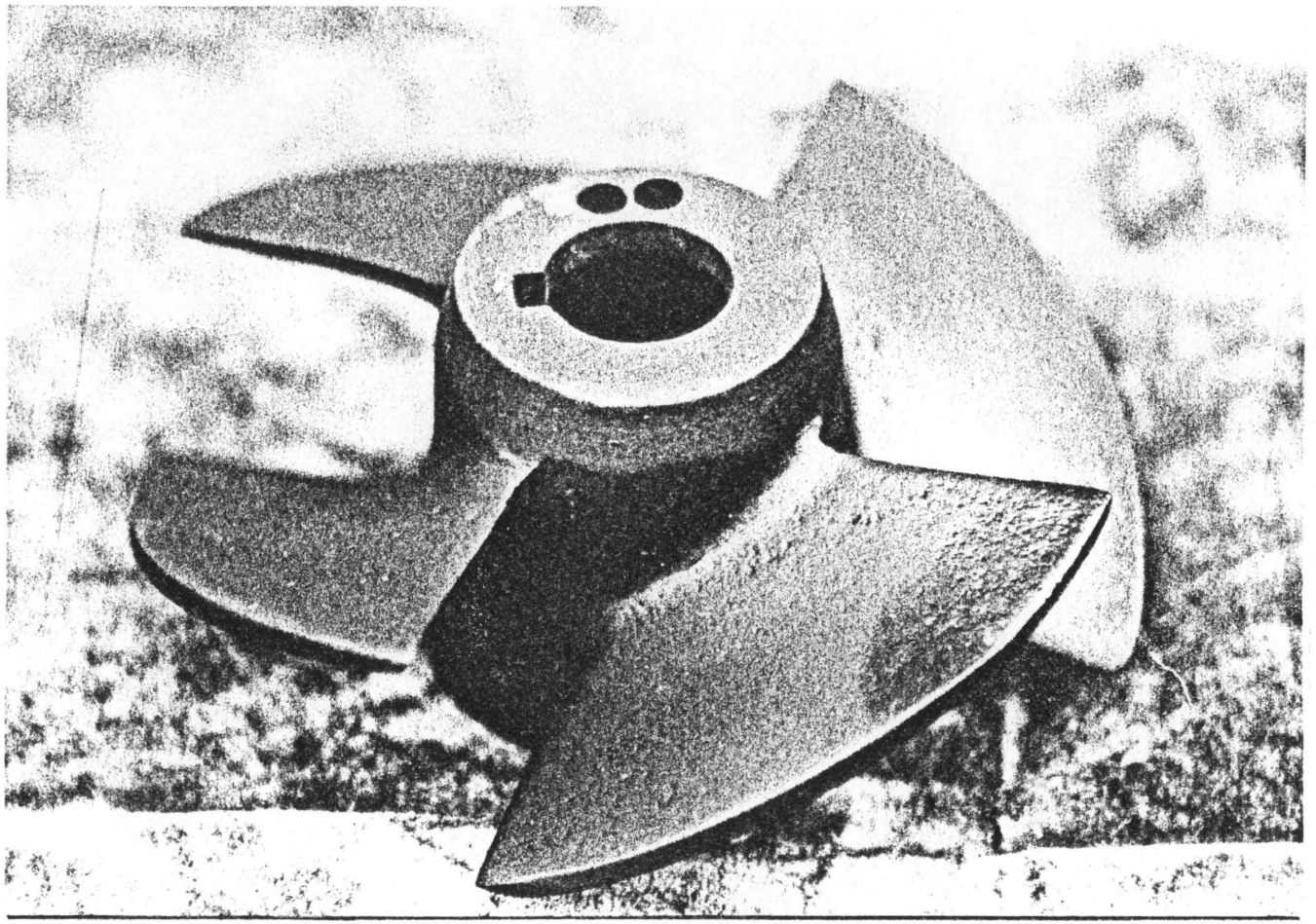

Figure 16. Photograph of Model Turbine Runner

TABLE 2

EXPERIMENT DESIGN PERFORMANCE SPECIFICATIONS

Design Head	3.0 m
Design Core Flow Rate	0.044 m^3/s
Specific Speed	980 (metric hp)
Velocity Ratio, RV	1.66
Turbine Velocity Ratio, TVR	0.731
Bypass Area Ratio	0.45
Diffuser Area Ratio	4:1
Diffuser Cone Half-Angle	4.5°
Mixing Tube Length	5D
Jet Nozzle Area Ratio	1.83:1
Power Output	1.2 kW
Turbine Efficiency	0.90

4. EXPERIMENTAL STUDY

The following section contains a detailed description of the experimental study which was conducted at VPI&SU in order to confirm the principles discussed above in an actual hydropower system and to validate the computer model. The construction of the experimental apparatus is discussed, along with the experimental layout, instrumentation, procedure, and experimental uncertainty.

4.1 Construction of Apparatus

The experimental model was designed to meet the performance specifications outlined in Table 2. The actual scale of the model was determined by the runner used, the available flow in the laboratory facility, and the cost. In order to produce an effective model at a reasonable cost, off-the-shelf hardware was used whenever possible. In addition, the use of standard pipe sizes in the turbine bypass housing, the turbine nacelle, and the mixing tube sections helped to reduce costs. With the exception of the turbine runner, shaft, bearings and seals, all of the components of the system were fabricated by the shop personnel. A summary of the system dimensions is presented in Table 3.

4.1.1 Draft Tube

The draft tube was constructed from 20 gage galvanized sheet metal. The conical shape was obtained by rolling the metal on a 1.22 m (48 in.) rolling mill. The edges were joined using a standard lap joint.

TABLE 3

EXPERIMENTAL MODEL SPECIFICATIONS

Turbine Runner

Diameter	$d_o = 9.68 \pm 0.01$ cm	$d_i = 3.80 \pm 0.01$ cm	$d_m = 7.35 \pm 0.02$ cm
	$\alpha_{o1} = 23 \pm 1°$	$\alpha_{i1} = 45 \pm 1°$	$\alpha_{m1} = 29 \pm 1°$
	$\beta_{o1} = 76 \pm 1°$	$\beta_{i1} = 61 \pm 1°$	$\beta_{m1} = 70.2 \pm 1°$
	$\beta_{o2} = 77 \pm 1°$	$\beta_{i2} = 61 \pm 1°$	$\beta_{m2} = 73.3 \pm 1°$

Diffuser

Overall Length	86.92 ± 0.10 cm
Inlet Diameter	12.82 ± 0.10 cm
Outlet Diameter	25.64 ± 0.20 cm
L/D_1	6.78

Turbine/Bypass Assembly

Inlet Diameter	15.57 ± 0.01 cm
Outlet Diameter	13.29 ± 0.01 cm
Overall Length	17.78 ± 0.02 cm

Turbine Nacelle

Inside Diameter	9.86 ± 0.01 cm
Outside Diameter	10.16 ± 0.02 cm

Mixing Tube

Inlet Diameter	13.29 ± 0.01 cm
Outlet Diameter	12.82 ± 0.01 cm
Overall Length	39.89 ± 0.02 cm

A 0.9525 cm (3/8 in.) thick flange with a 22.86 cm (9 in.) OD was brazed to the throat to permit a bolted connection to the mixing tube outlet. Two steel rings with a 0.76 cm x 0.76 cm cross section were brazed to the cone to provide additional hoop strength and rigidity. The inlet diameter was 12.82 $\pm$ .10 cm and the outlet diameter was 26.58 $\pm$ .20 cm, providing an area ratio of 4.00 $\pm$ 0.12. The overall diffuser length was 86.92 $\pm$ 0.2 cm giving an included half angle of 4.526 degrees $\pm$ 0.11 degrees. Pressure taps were installed as described in section 4.3. The draft tube is shown in Fig. 17.

4.1.2 Turbine/Bypass Assembly

The turbine/bypass assembly is a dual-purpose subsystem which is the heart of the diffuser-ejector concept. The assembly provides both a housing for the turbine and inlet guide vanes as well as the annular bypass channel for the accelerating jet. Figure 18 shows a cross-sectional view of this assembly. The outer housing consists of a 17.78 cm (7 in.) long section of schedule 40 15.24 cm (6 in.) steel pipe which has been machined to an inside diameter of 15.57 $\pm$ 0.01 cm. The nacelle, which houses the turbine and guide vanes, is made of 9.83 cm ID thin wall cold drawn steel tubing with a wall thickness of 1.52 mm. The nacelle is supported by four faired struts which are welded to a support ring which slides over the nacelle and fastens with set screws. The tapered nozzle ring was machined of stainless steel and pressed into place. After the inlet guide vanes were installed and the stator mounted in place with machine screws, the entire nacelle with support rings

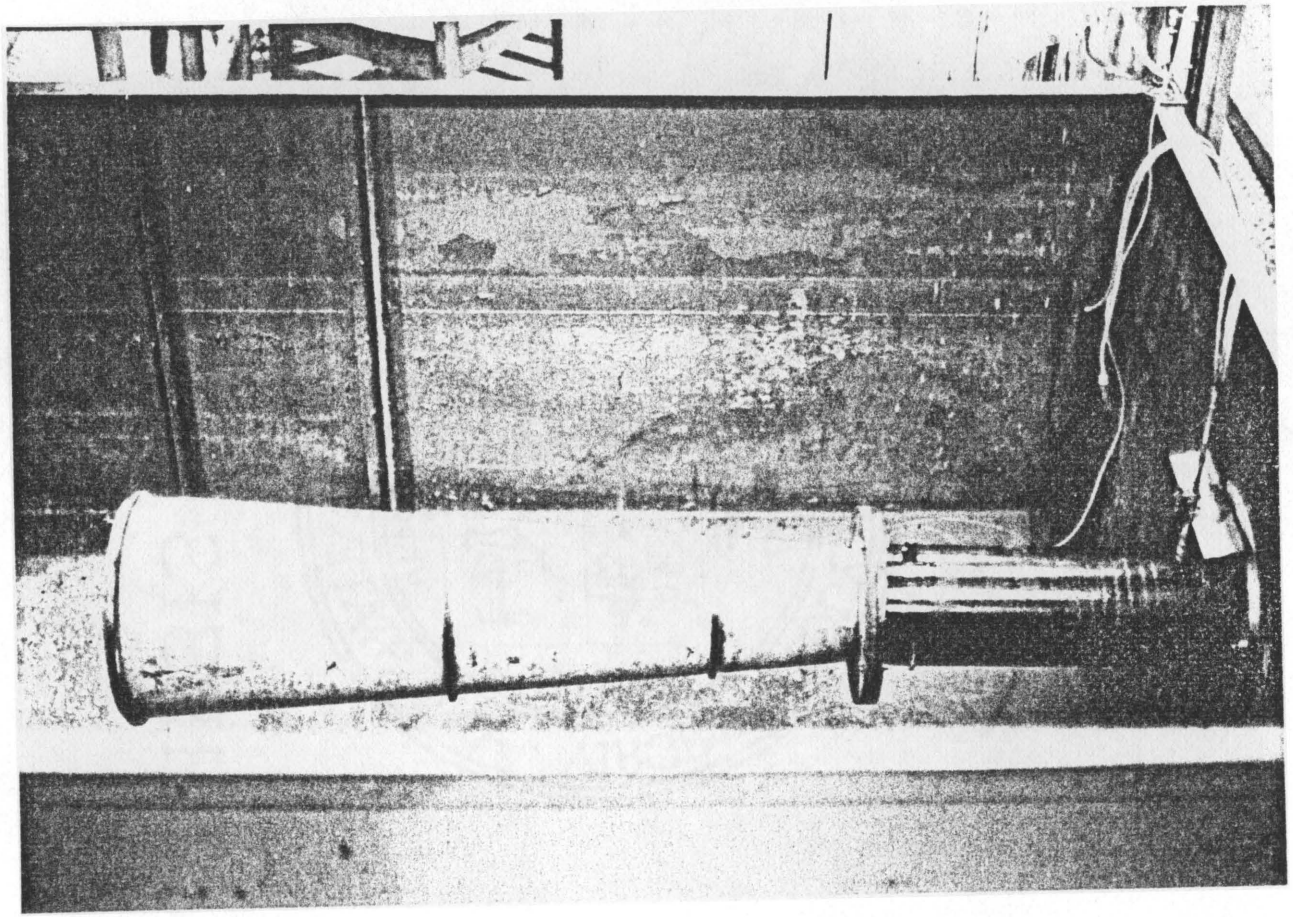

Figure 17. Photograph of Experimental Draft Tube

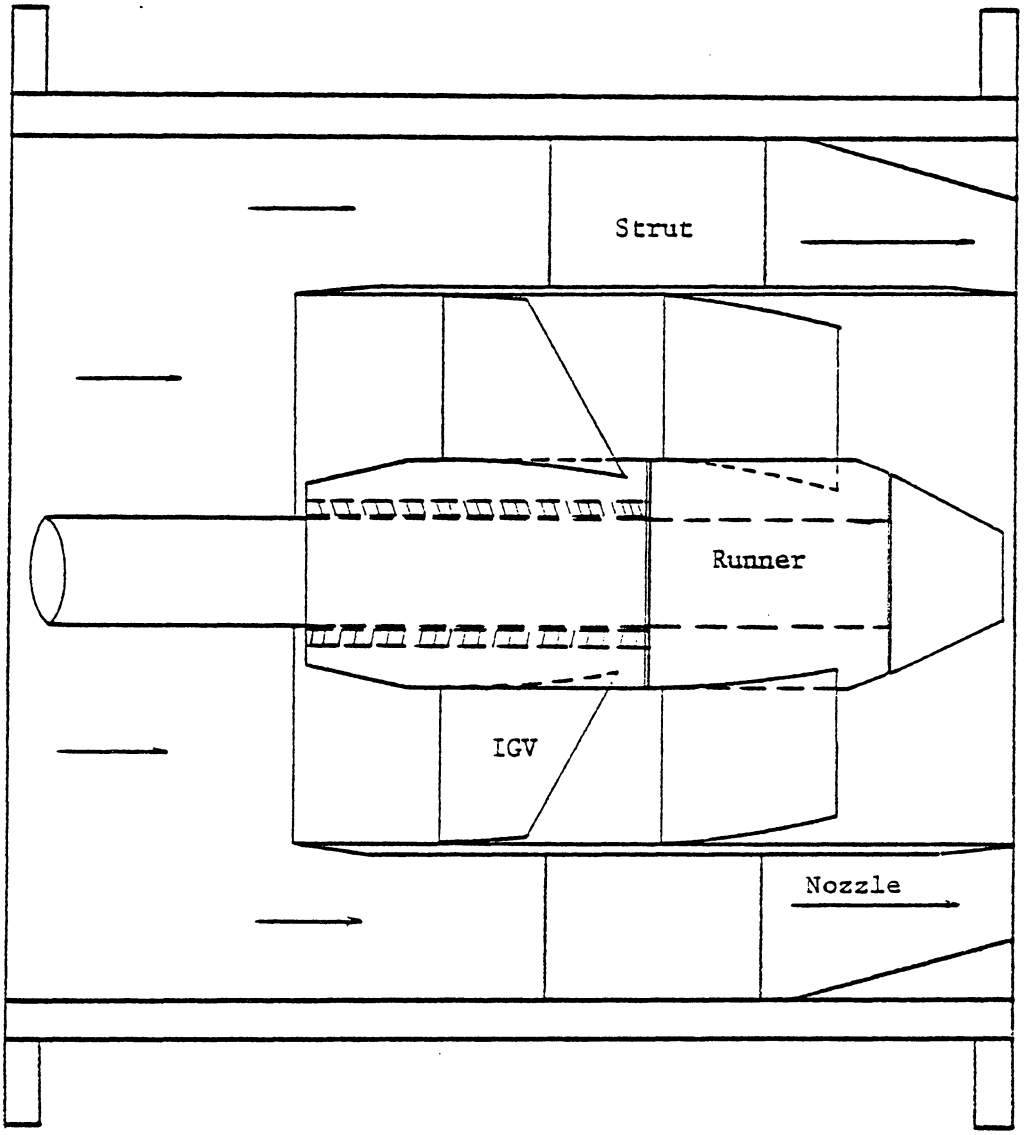

Figure 18. Turbine/By-Pass Assembly [55]

and struts was turned on the lathe to the inner housing diameter to ensure that the shaft would be centered. Figure 19 shows the turbine bypass assembly.

Inlet Guide Vanes (Stator)

The stator subassembly serves two functions in supporting the shaft with a sleeve bearing as well as turning the inlet flow by means of fixed guide vanes. The hub was machined from bar stock to a 3.8 $\pm$ 0.002 cm outside diameter with an overall length of 5.62 $\pm$ 0.01 cm. The front 1.54 cm tapers down to 3.09 $\pm$ 0.002 cm to provide for a more aerodynamic profile. The hub is then bored to accommodate the "oilite" sleeve bearing with a 1.905 cm ID. The guide vanes themselves are fashioned from pieces cut from a standard 10.2 cm (4 in.) steel pipe in an ingenious method described by Myatt in reference [60].

Figure 20 shows the required cuts. The blades are then machined to a 0.476 cm thickness, the leading edge ground to a rounded point while the trailing edge is cut, surfaced and finished by hand. The finished blades are then welded to the hub, held in place by means of a temporary holding jig. The stator is shown in Figures 21 and 22.

4.1.3 Mixing Tube Construction

Table 2 shows that a mixing tube length of 5 diameters is specified. This amounts to a total length of 66.45 cm. The tubes were constructed from standard 12.7 cm (5 in.) schedule 40 pipe. Rather than

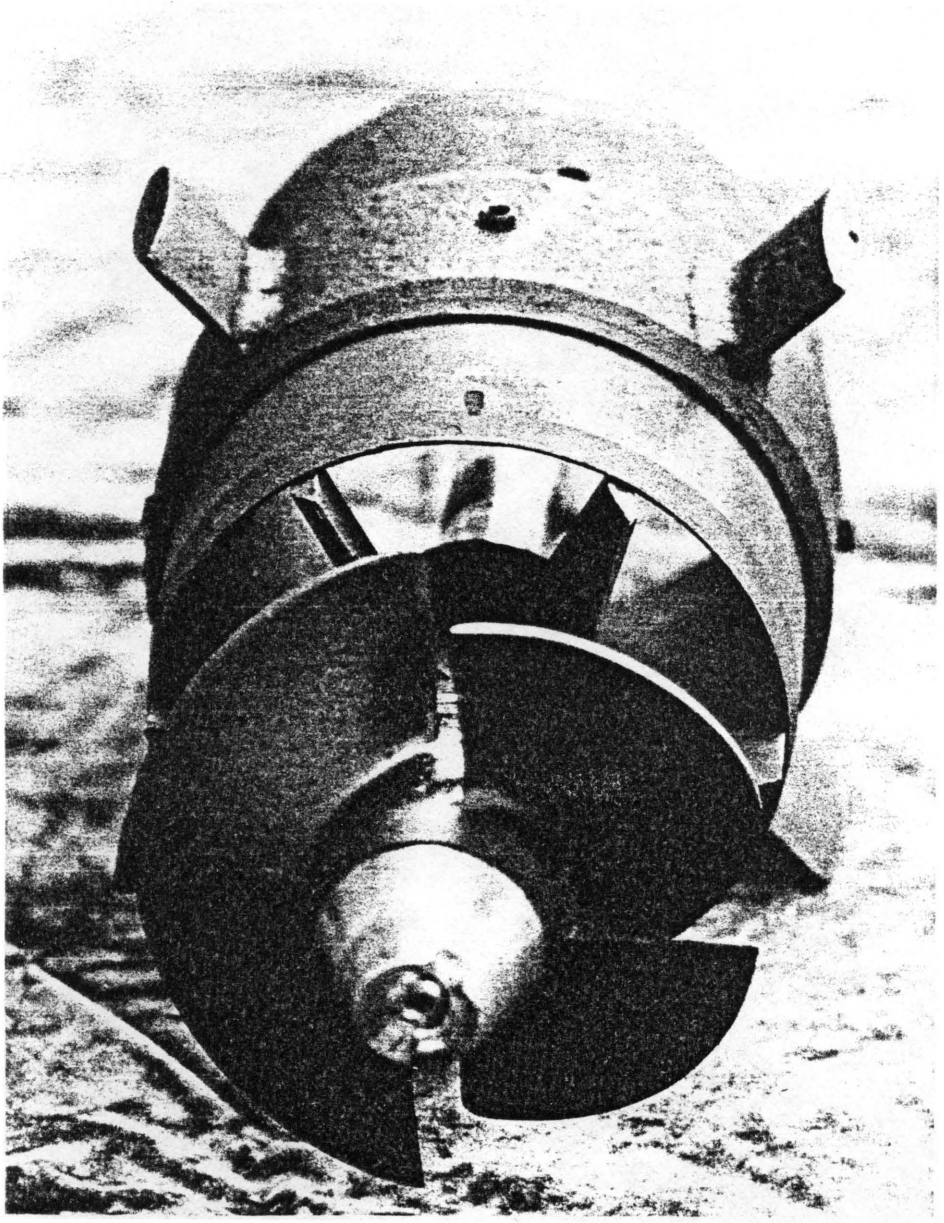

Figure 19. Exploded View of Turbine/Bypass Assembly

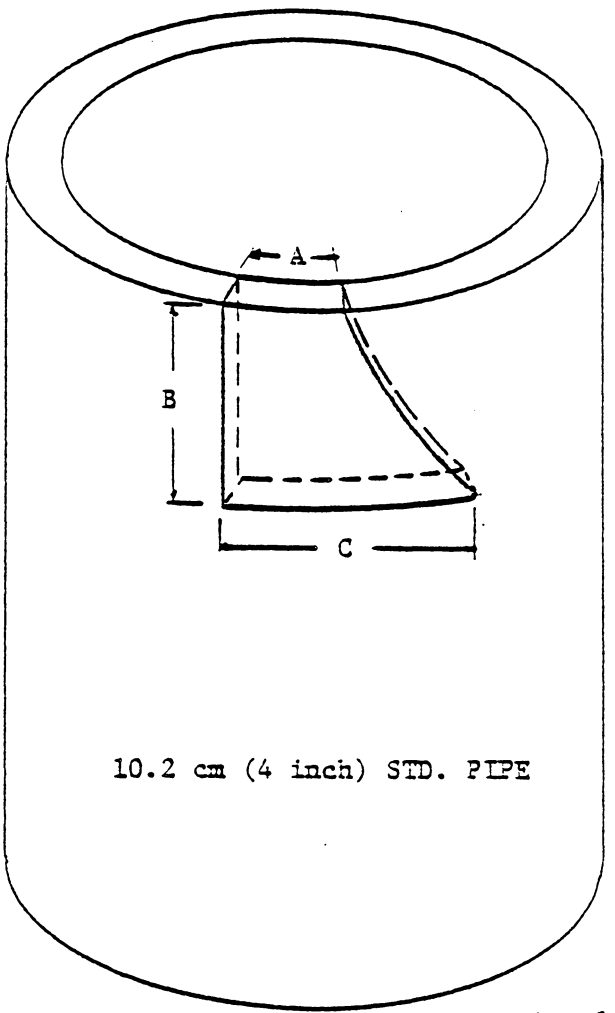

Figure 20. IGV Construction [55]

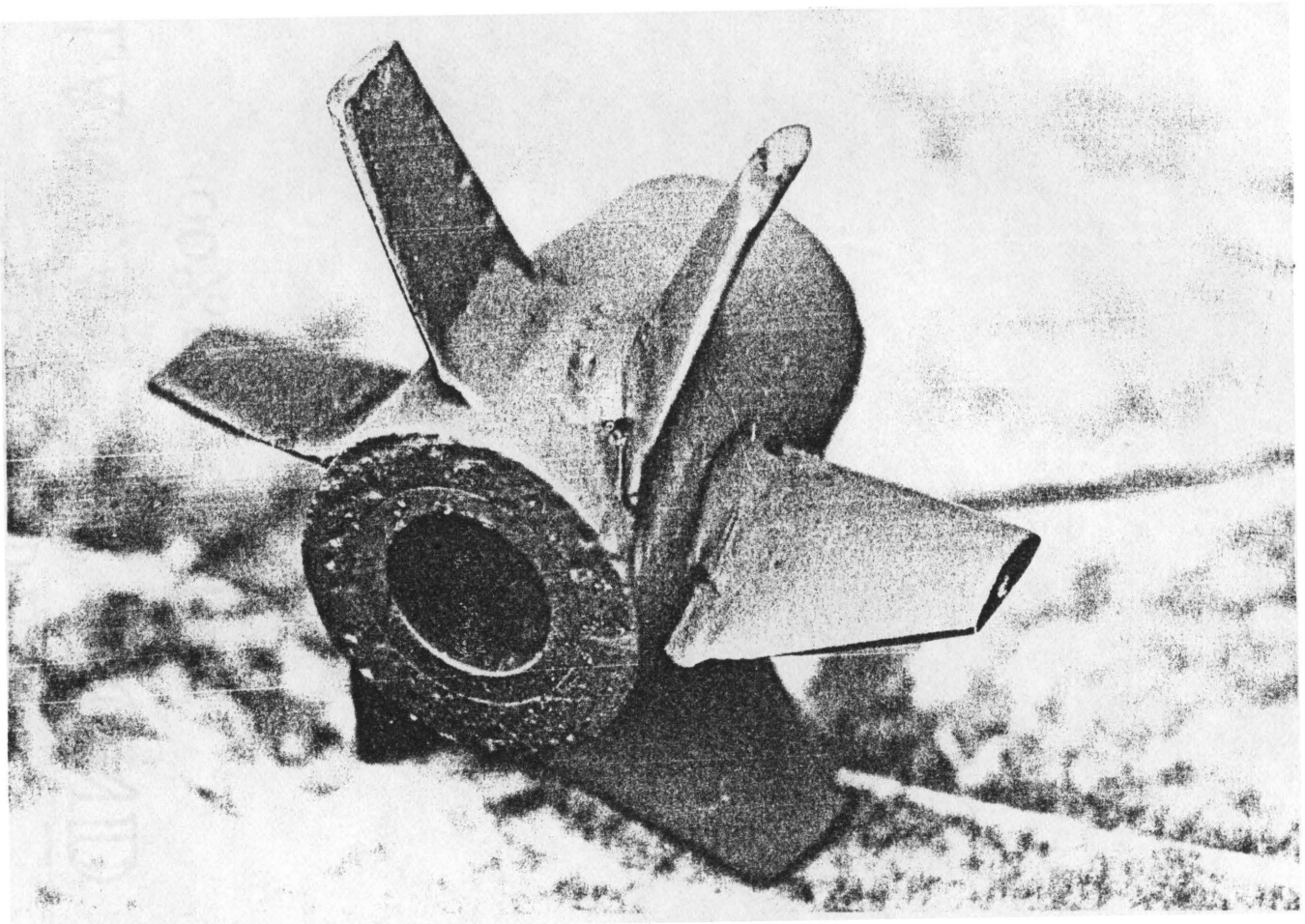

Figure 21. Photograph of Stator Assembly

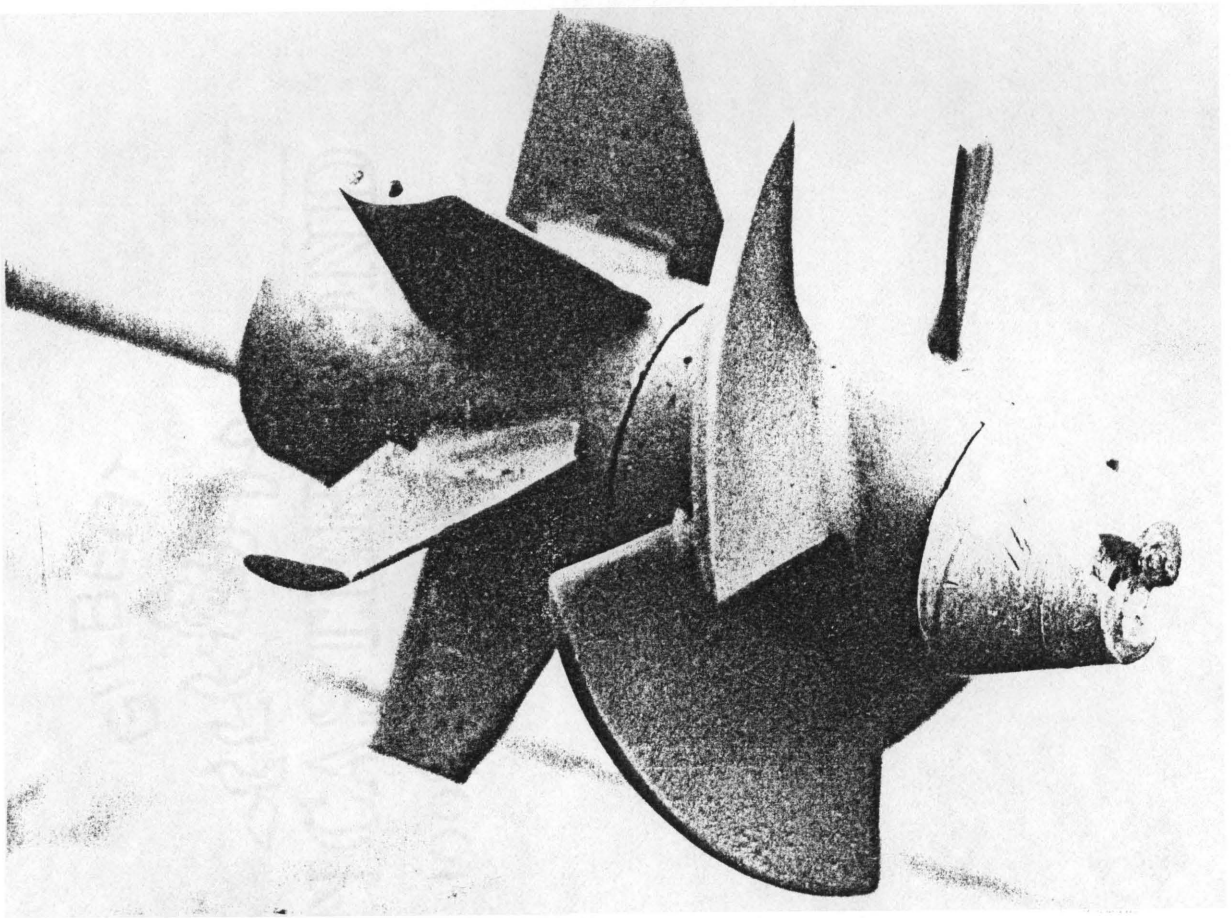

Figure 22. Photograph of Rotor and Stator

machine the entire length to the required 13.28 cm (5.23 in.) dimension, it was decided to use this dimension at the mixing tube entrance, tapering down to the standard pipe ID 12.82 (5.047 in.) over the length of approximately one diameter. Furthermore, it was decided to produce the mixing tube in two sections, one being two diameters long and the other being three diameters long. This gave increased flexibility in the experiment configuration as well as simplified construction and handling. The mixing tube flanges were matched identically to those of the diffuser and the turbine/bypass assembly and were welded to the pipe.

4.1.4 Shaft, Bearing and Seals

The turbine shaft, which had been used previously with the Rodney Hunt turbine is a 1.905 cm (3/4 in.) stainless steel shaft. The shaft is accessible to the load by means of a hole in the inlet elbow. A welded boss at the point of penetration contains the bearing and the required seals. A Fafnir 7204 angular contact bearing is used to support the thrust load. A schematic of this arrangement is given in Fig. 23. It was necessary to turn, then step up the shaft in order to obtain the proper fit in the bearing.

4.2 Test Facility and Layout

The experimental model was tested in the Department of Mechanical Engineering Hydraulics Laboratory. This location was chosen for the

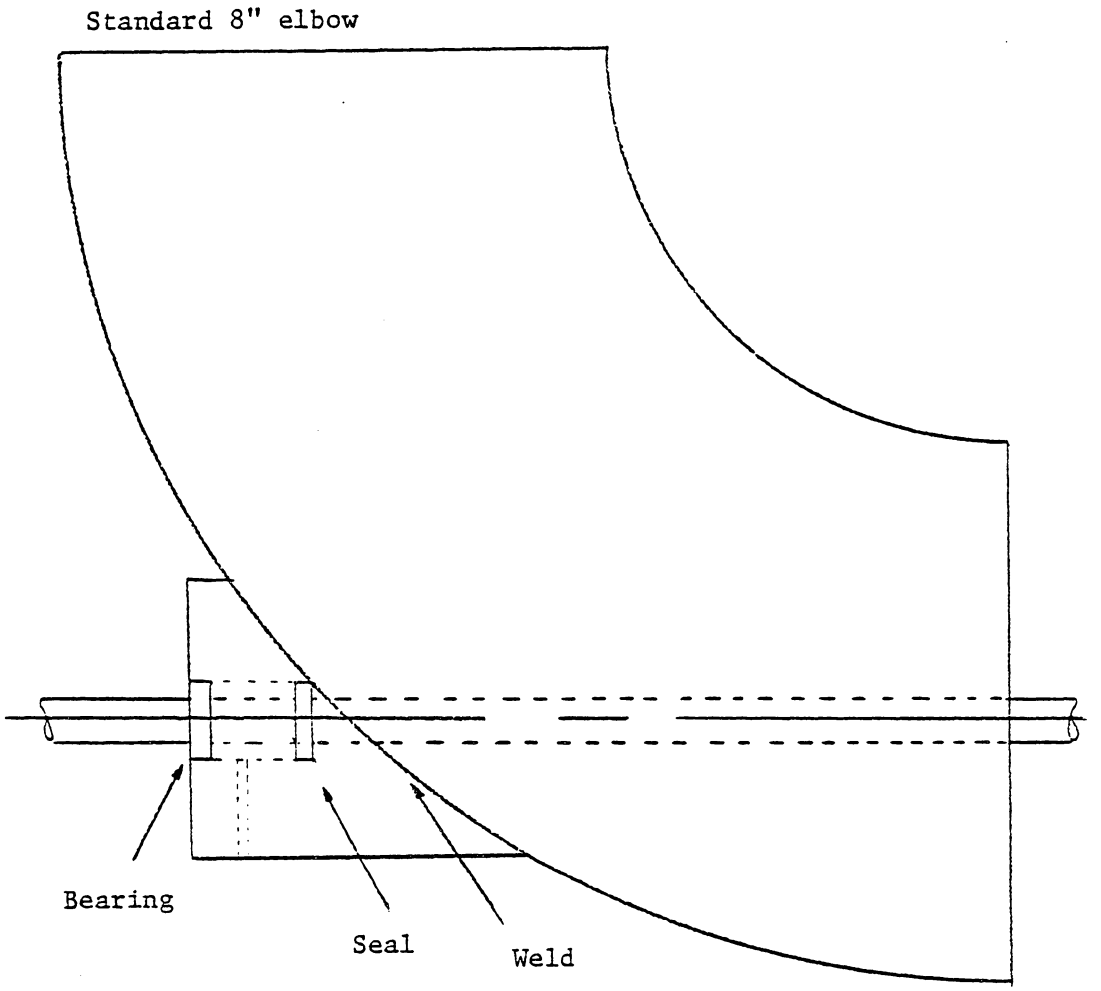

Figure 23. Schematic of Shaft Support Assembly

availability of a high volume centrifugal supply pump, a large discharge tank and a 20.32 cm (8 in.) venturi flowmeter.

The supply pump used was manufactured by the Newport News Shipbuilding Company. It has a maximum rated discharge of 0.1896 m^3/sec (3000 gpm) at a head of 37 m (120 ft). The pump discharge reaches the turbine by means of a 20.32 cm diameter pipeline. A bypass leg allows a portion of the pump discharge to be diverted so that conditions at the turbine can be controlled by a set of valves.

The discharge tank is an open rectangular basin with a capacity of 4 m^3. The tank was equipped with a weir plate and a level gauge to measure discharge but for this test, the venturi flowmeter was moved onto the supply line to provide considerably better accuracy. The tank was found to be capable of handling up to approximatley 0.1 m^3/sec before the overflow limit was reached. A scale drawing of the supply line and venturi meter is presented in Fig. 24. An inlet length in excess of the required six diameters is provided for the venturi, as shown.

4.3 Instrumentation

The venturi flow meter mentioned in the previous section was manufactured by the Builder's Iron Foundary of Providence RI. The meter was designed to measure flows in the range for 0.04 to 0.25 m^3/sec. The throat diameter is 10.16 cm (4 in.) which means the inlet/throat area ratio is 4.0. The standard ASME discharge coefficient for a venturi meter of this type is 0.983 [58]. The pressure across the

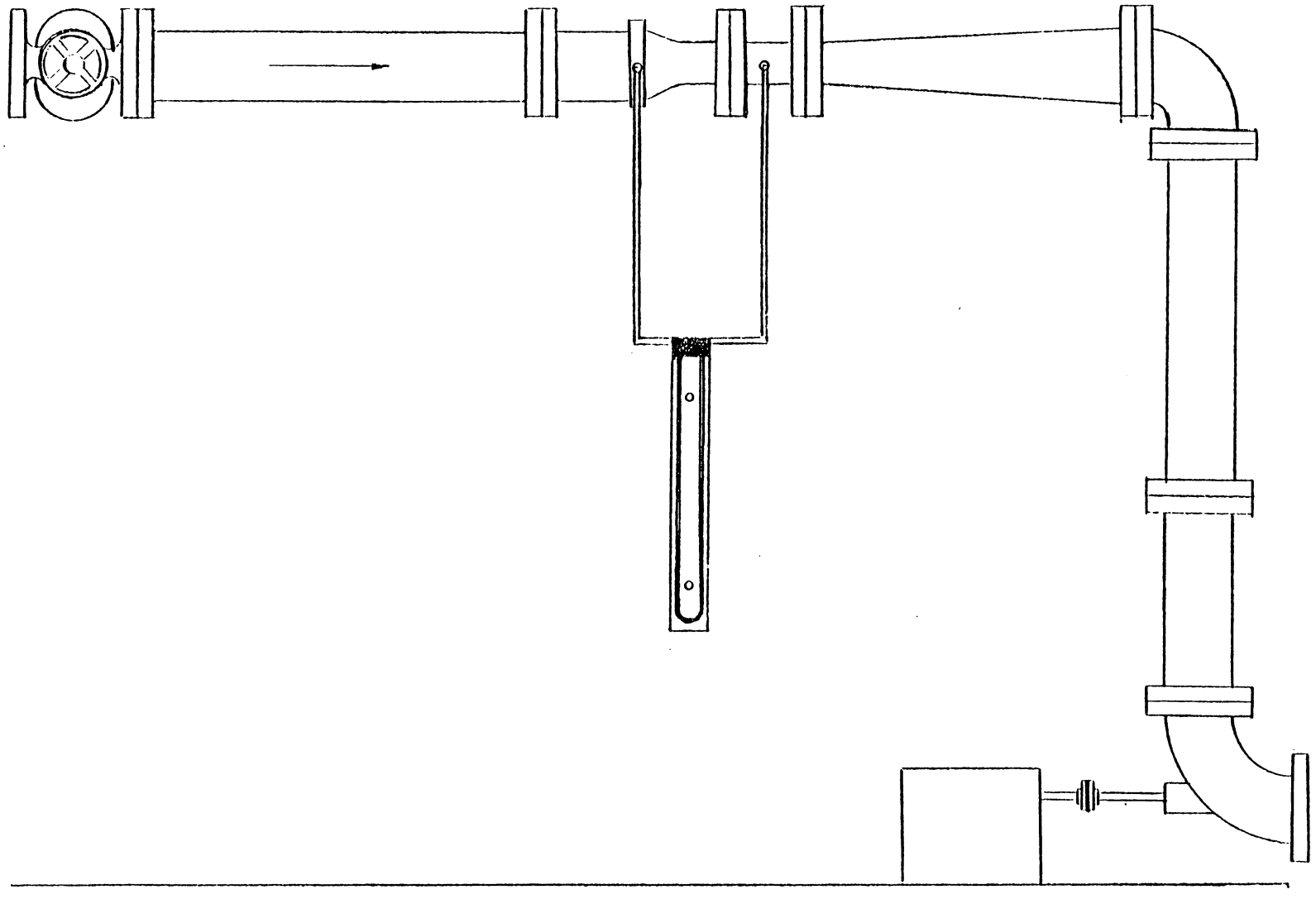

Figure 24. Water Supply Line With Venturi Flowmeter

venturi is measured by means of a 91.44 cm (36 in.) U-tube manometer manufactured by Meriam Instruments. The manometer is graduated in inches and tenths and the operating fluid is mercury. The resulting equation for conversion is given by

$$Q(m^3/sec) = 0.0214 \sqrt{\Delta p(inHg)} \quad . \tag{4.1}$$

Considering the unsteadiness of the flow, the precision of the manometer and the estimate of the discharge coefficient, it is estimated that the uncertainty of the flow measurement is $\pm$ 0.05 in Hg or $\pm$ 0.00012 m^3/s which represents less than 1 per cent of the flow rate which was used in the test.

The rotational speed of the turbine shaft was measured using a General Radio model 1531 strobotac which was calibrated at 3600 rpm to be within $\pm$ 10 rpm.

The turbine was loaded by means of a torque converter which was adapted from a Go-Power model DY-7D water brake. The brake was supplied with a regulated water supply to ensure constant loading.

The torque output was determined by measuring the tangential force applied by the water brake through a stranded steel wire to an aluminum cantilever beam arrangement which was equipped with two strain gages. The strain gages were connected to a Vishay/Ellis-11 bridge amplifier equipped with a model 11-AG bridge completion module. The torque measuring system was calibrated on-location with standard weights and is estimated to be within $\pm$ 0.5 per cent. The cantilever beam arrangement is shown in Fig. 25.

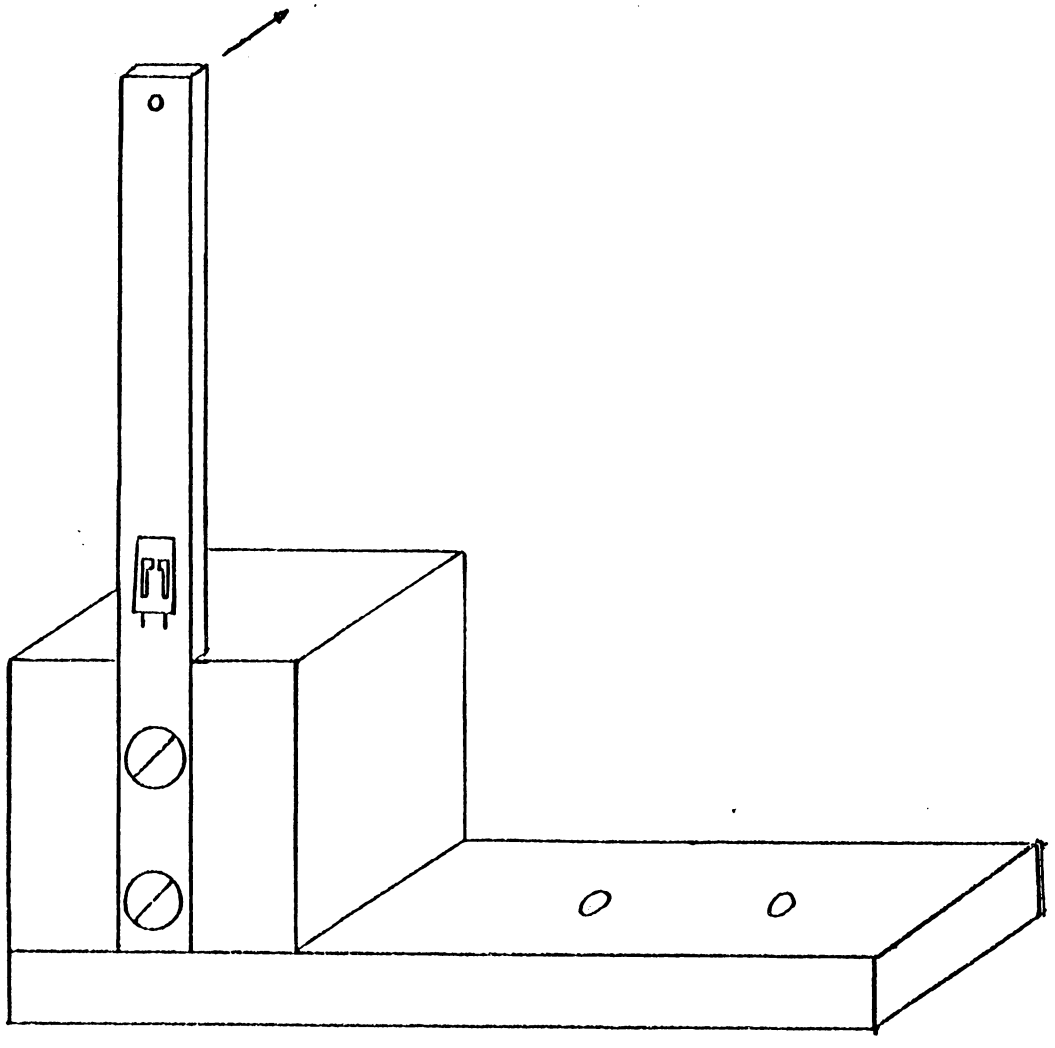

Figure 25. Cantilever Beam Arrangement Used for Torque Measurement

The measurement of static and total pressures was performed using standard cleanout manometers filled with mercury. The pressures which were consistently below atmospheric were referenced to the atmosphere, while the positive gage pressures were referenced to the tailwater by means of a submerged line. This reading was related to the gage pressure by the expression

$$p = \rho g \, [z_s - z_p + (SG - 1)h] \tag{4.2}$$

The manometer readings can generally be considered accurate to within 1.3 mm (0.05 in.) unless otherwise noted. The total pressure at the turbine inlet was measured by a simple impact probe located approximately halfway between the wall and the turbine shaft.

The total pressure at the turbine exit was measured by means of the yaw probe which is illustrated in Fig. 26. The probe was constructed of 0.8 mm (1/32 in.) stainless steel tubing mounted in a 6.4 mm (1/4 in.) diameter stainless steel shell. The pressure signals from the two 45 degree balance ports were connected across a Statham model 8737 pressure transducer which was connected to a Tektronix Oscilloscope equipped with a 3666 carrier amplifier. The alignment of the probe in the flow direction was then indicated by a zero line on the oscilloscope screen. The swirl angle could then be read from the direction of the pointer on the protractor scale. Considering unsteadiness in the flow and parallax in the scope and protractor readings the swirl angle precision is estimated to be $\pm$ 3 degrees. The total pressure is then measured from the center hole which is connected to a manometer. The radial location

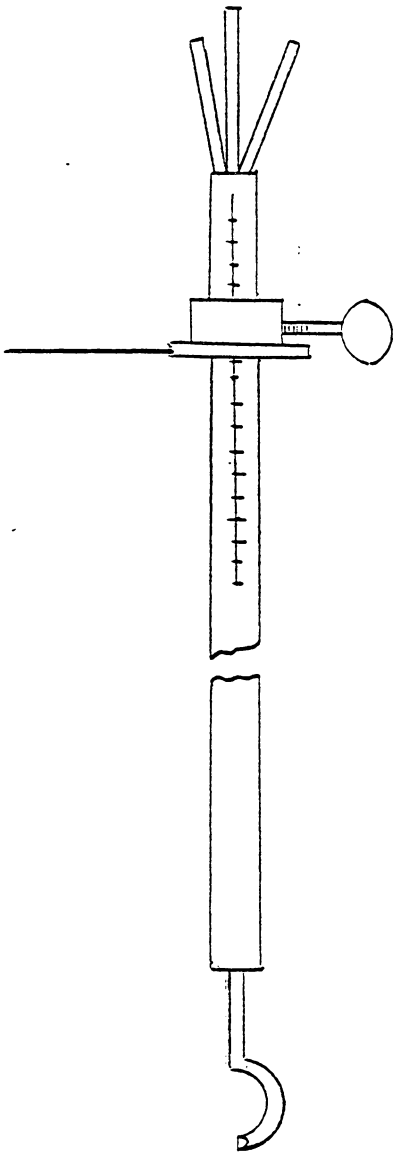

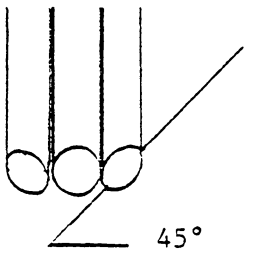

Detail of Probe Tip

Figure 26. Yaw Probe

of the yaw probe is the mean radius of the rotor which is defined by:

$$r_m = \left[\frac{r_h^2 + r_t^2}{2} \right]^{\frac{1}{2}} \tag{4.3}$$

The location of all the pressure taps is given in Fig. 27.

4.4 Experimental Procedure

Due to the highly turbulent and unsteady nature of the flow in the turbine discharge, it was desired to repeat the various flow field measurements a number of times. In order to keep the experimental work load manageable it was decided to use a single set of inlet conditions (flow and gross head) for the study. These inlet conditions can be generalized under similar operation by use of the non-dimensional parameters Q/ND^3 and H/N^2D^2. The capacity of the discharge tank was a constraint in the amount of flow which could be used in the testing. A flow rate of 0.0957 m^3/sec was achieved without difficulty. This flow rate would allow the turbine the design flow rate of 0.044 m^3/sec if 54 per cent of the flow, or less, were bypassed.

With the gross head and flow rate fixed, the study is reduced to a single indepent parameter, the rotational speed, which is controlled by the turbine loading.

In the present study, the rotational speed was varied from 2200 to 3600 rpm. This range was defined by the capabilities of the water brake and was judged to be adequate for the purposes of this project. Figure 28 shows this apparatus.

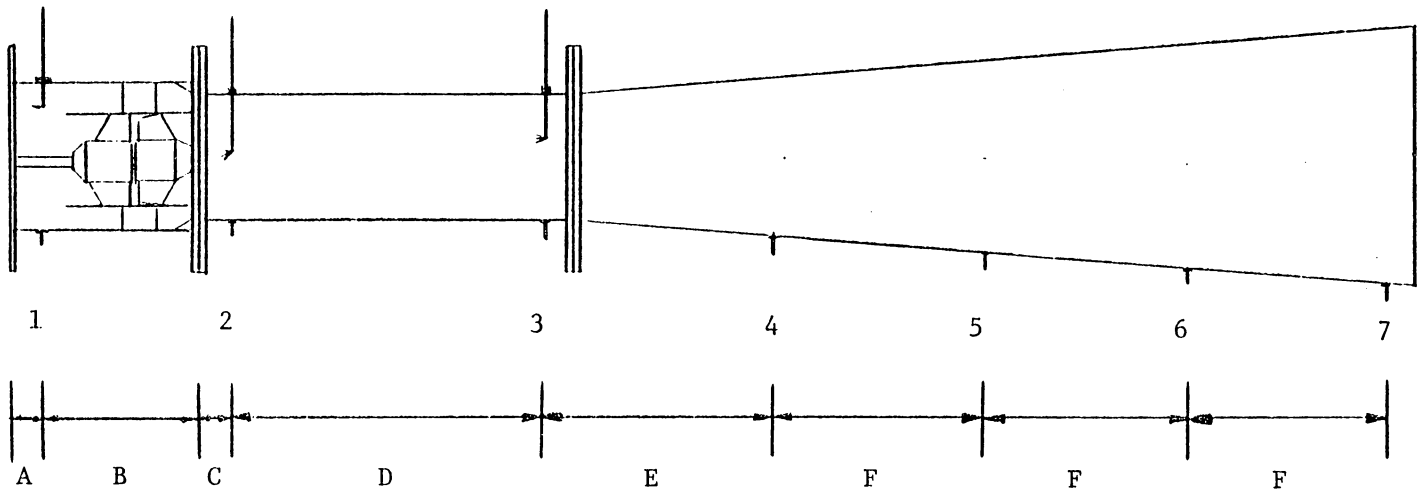

A = 2.78 cm
B = 15.00 cm
C = 5.58 cm
D = 31.82 cm
E = 24.6 cm
F = 20.03 cm

Figure 27. Location of Pressure Taps

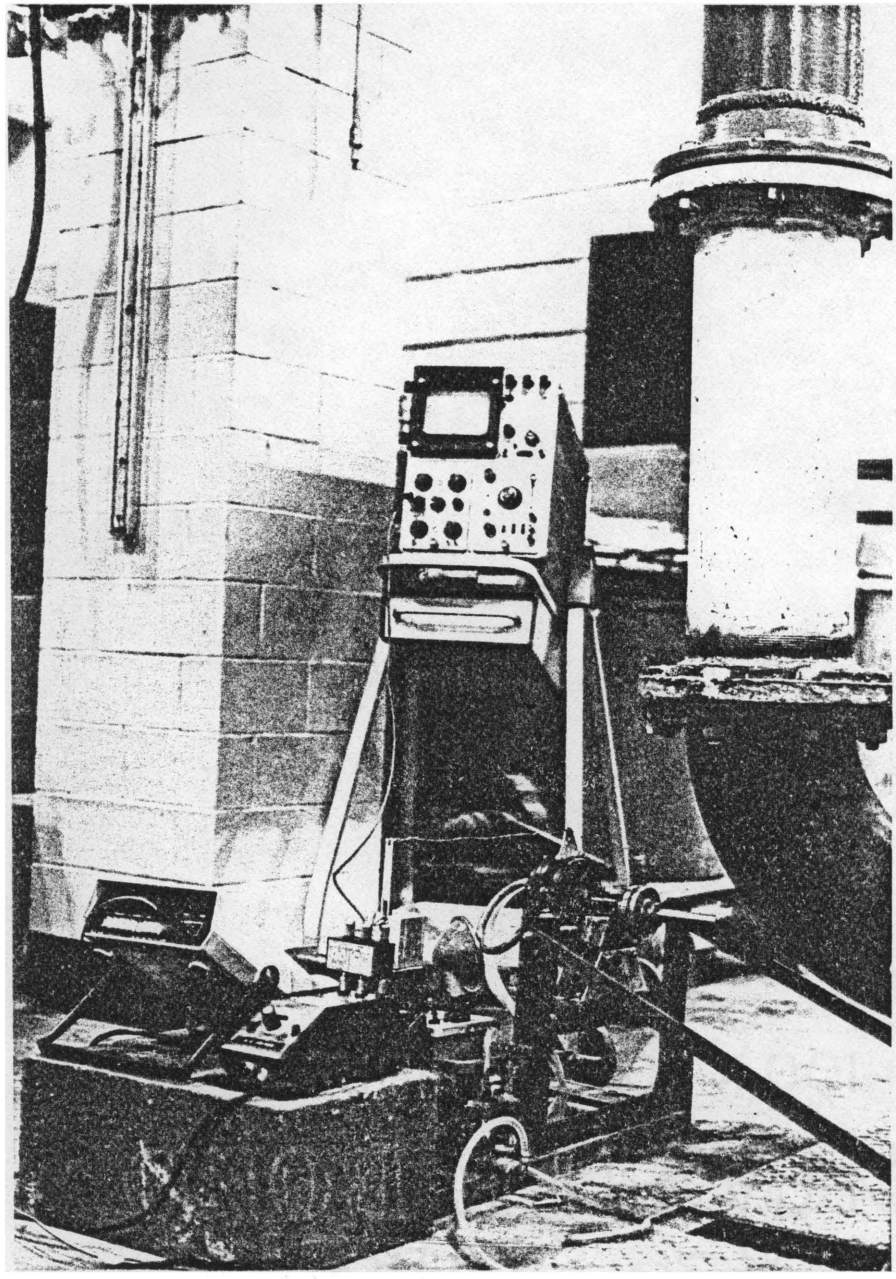

Figure 28. Experimental Apparatus

With the turbine loaded and operating at a given speed, the torque and static pressures could be read directly. The total pressure at the inlet was also read directly after the incoming flow angle was confirmed to be constant with N and fixed. The total pressure at the turbine exit could be measured after the swirl angle, α_2 was determined. To find the swirl angle, the yaw probe was pivoted at the mean radius until the pressures at either balance port were equal. At this point the swirl angle and the total pressure could be read and recorded.

This procedure was repeated at intervals of 100 RPM until the entire range of speeds was covered.

4.5 Uncertainty Analysis

The experimental uncertainty of the results which are presented in Chapter 5 was determined by the method of Kline and McClintock as presented in Ref. [59]. These uncertainties have been calculated based on nominal values of the measured variables which represent the maximum uncertainty within the range of this experiment. The results of this analysis are presented in Table 4.

TABLE 4

EXPERIMENTAL UNCERTAINTIES

	Measured Variables		
P	Pressures	±	0.169 kPa
N	Rotational Speed	±	10 rpm
F_D	Force (Dynamometer)	±	0.032 N
D_{tot}	Diameter (discharge)	±	0.006 cm
D_{core}	Diameter (core)	±	0.012 cm
r	Radius (Torque Converter)	±	0.051 cm
	Calculated Variables		
Q	Total Flow Rate	±	0.00012 m^3/sec
Q_{core}	Core Flow Rate	±	0.0016 m^3/sec
V_J	Jet Velocity	±	0.25 m/s
V_C	Core Velocity	±	0.21 m/s
P_c	Corrected Pressure	±	0.235 kPa
A_{core}	Core Area	±	0.00002 m^2
T	Torque	±	0.01593 N-m
P_{out}	Power Output	±	0.0625 kW
P_{in}	Power Supplied	±	0.0167 kW
η	Efficiency of Rotor	±	0.0269
C_p	Pressure Recovery Coefficient	±	0.084

5. EXPERIMENTAL RESULTS

This chapter presents the results of the experimental study. The data are compiled to reflect the performance of the system in terms of pressure recovery and turbine efficiency. In all cases, average values of the data are used which are subject to the experimental uncertainty calculations of section 4.6.

5.1 Pressure Recovery

The average values of the wall static pressures and the total pressures at the turbine inlet and exit are presented in Table 5 as a function of the turbine rotational speed. The pressure recovery coefficient C_p is plotted in Fig. 29 as a function of the non-dimensional flow rate. This allows generalization of the results to other similar machines, or other flow rates. Figure 30 gives the results in terms of head augmentation.

It should be pointed out that these results are based on the wall static pressures which will tend to increase with swirl in the flow, particularly at the turbine exit. This is a two-dimensional effect which is not considered in the definition of the pressure recovery coefficient, see Eq. 3.1.

For a flow with a small radial velocity component, the radial momentum equation can be written

$$\frac{\partial p}{\partial r} = \frac{\rho c_\theta^2}{r} > 0 \qquad (5.1)$$

TABLE 5

EXPERIMENTAL RESULTS: PRESSURE

N (RPM)	P1 (PA)	P2 (PA)	P3 (PA)	P4 (PA)	P5 (PA)	P6 (PA)	P7 (PA)
2200.00	15375.88	-24307.20	-25320.00	-6920.80	-2700.80	0.0	506.40
2300.00	15219.50	-24644.80	-25826.40	-7089.60	-2532.00	-168.80	675.20
2400.00	14906.73	-23969.60	-25320.00	-7427.20	-2700.80	-506.40	506.40
2500.00	14593.96	-23294.40	-24982.40	-7427.20	-2869.60	-168.80	168.80
2600.00	14437.58	-22956.80	-24982.40	-7427.20	-3038.40	-168.80	675.20
2700.00	14124.81	-22619.20	-24982.40	-7427.20	-2869.60	-168.80	675.20
2800.00	13812.04	-22450.40	-24644.80	-7427.20	-2869.60	-168.80	675.20
2900.00	13499.27	-22281.60	-24307.20	-7427.20	-3038.40	-168.80	675.20
3000.00	13186.51	-21944.00	-23969.60	-7258.40	-3207.20	-168.80	675.20
3100.00	13030.12	-21944.00	-24138.40	-7258.40	-3207.20	-168.80	675.20
3200.00	12717.36	-21775.20	-23969.60	-7089.60	-3376.00	-168.80	675.20
3300.00	12248.20	-21606.40	-23969.60	-7089.60	-3376.00	-168.80	675.20
3400.00	11935.44	-21606.40	-23969.60	-6752.00	-3376.00	-168.80	675.20
3500.00	11622.67	-21606.40	-23800.80	-6752.00	-3544.80	-168.80	675.20

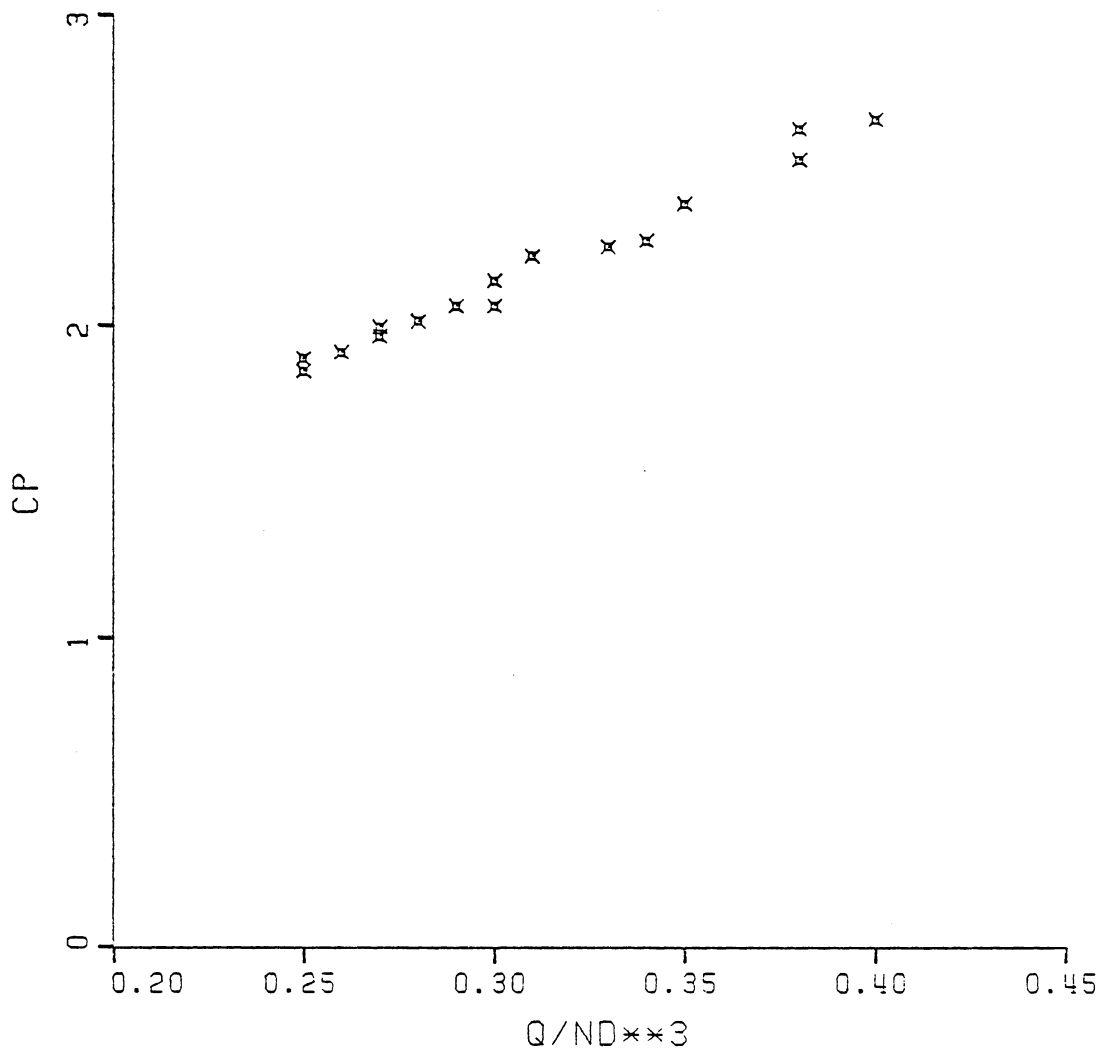

Figure 29. Experimental Results: Pressure Recovery

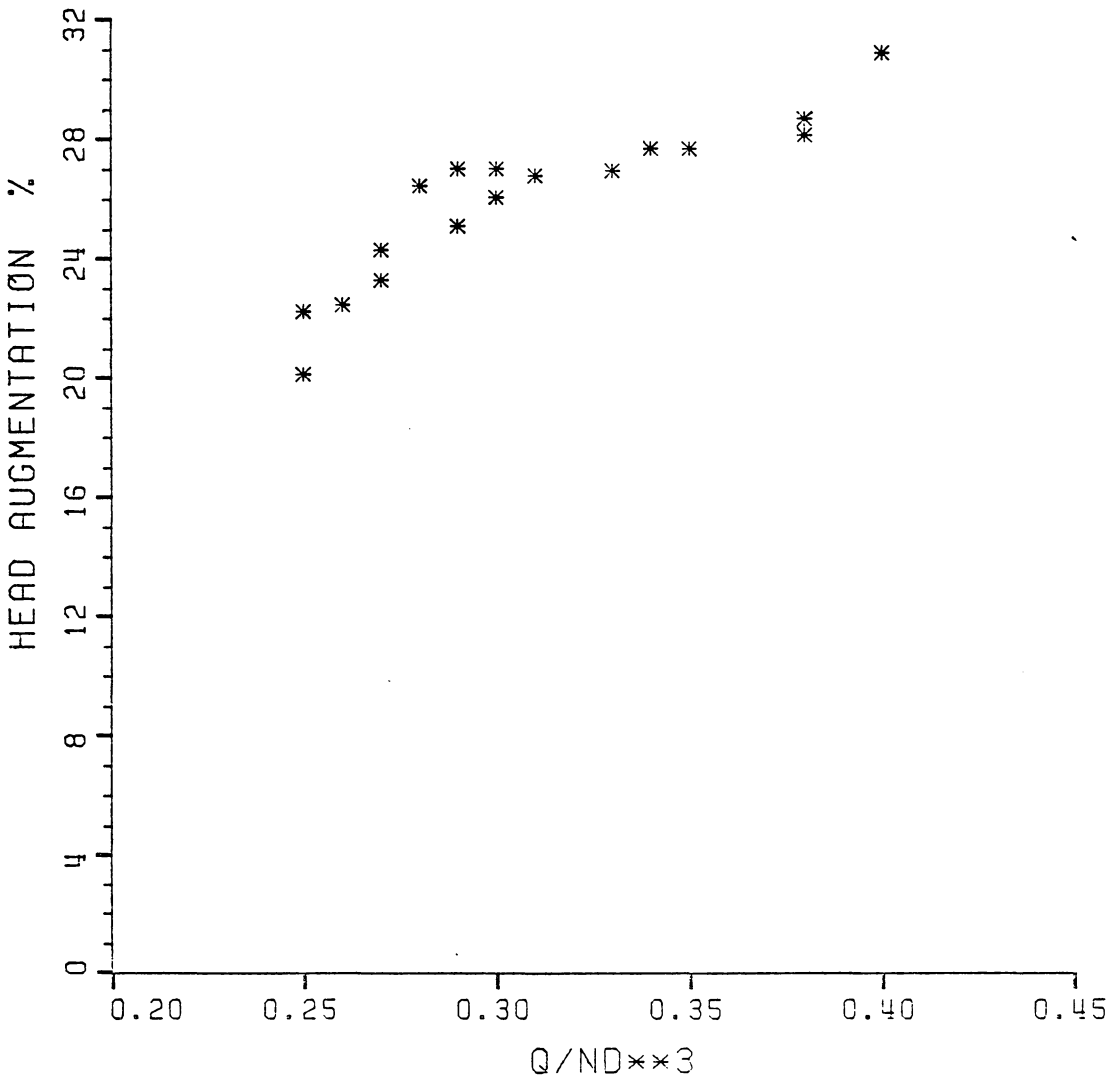

Figure 30. Experimental Results: Head Augmentation

This is sometimes called the radial equilibrium condition. There is not enough information available here to integrate Eq. 5.1, but it should be clear by examination that the net result of a swirl component is to increase the static pressure at the wall. This means that the values of C_p which are presented in Fig. 29 will be conserative since the difference term, $p_7 - p_2$ will be reduced. Figure 31 shows the exit swirl angle as a function of the rotational speed. Values of C_p as a function of X are plotted in Fig. 32 for several values of α_2.

It is clear from these data that a significant increase in the effective head across the turbine has been achieved as a result of the injection of fluid through the bypass. Furthermore the head augmentation increases with increased injection as illustrated by Fig. 33.

5.2 Turbine Performance

The characteristic curve for the experimental turbine is presented in Fig. 34. This simply shows the chracteristic performance in terms of the total system without regard for the flow being bypassed around the turbine. It has already been shown in section 5.1 that the result of fluid injection has been to increase the effective head across the turbine. Since this was accomplished at the expense of a portion of the total flow, it is desirable to know the net result upon the total system performance.

Figure 35 shows the measured power output as a function of the non-dimensional flow rate. The relationship between this parameter and the bypass is illustrated in Fig. 36. It should be recalled that since the

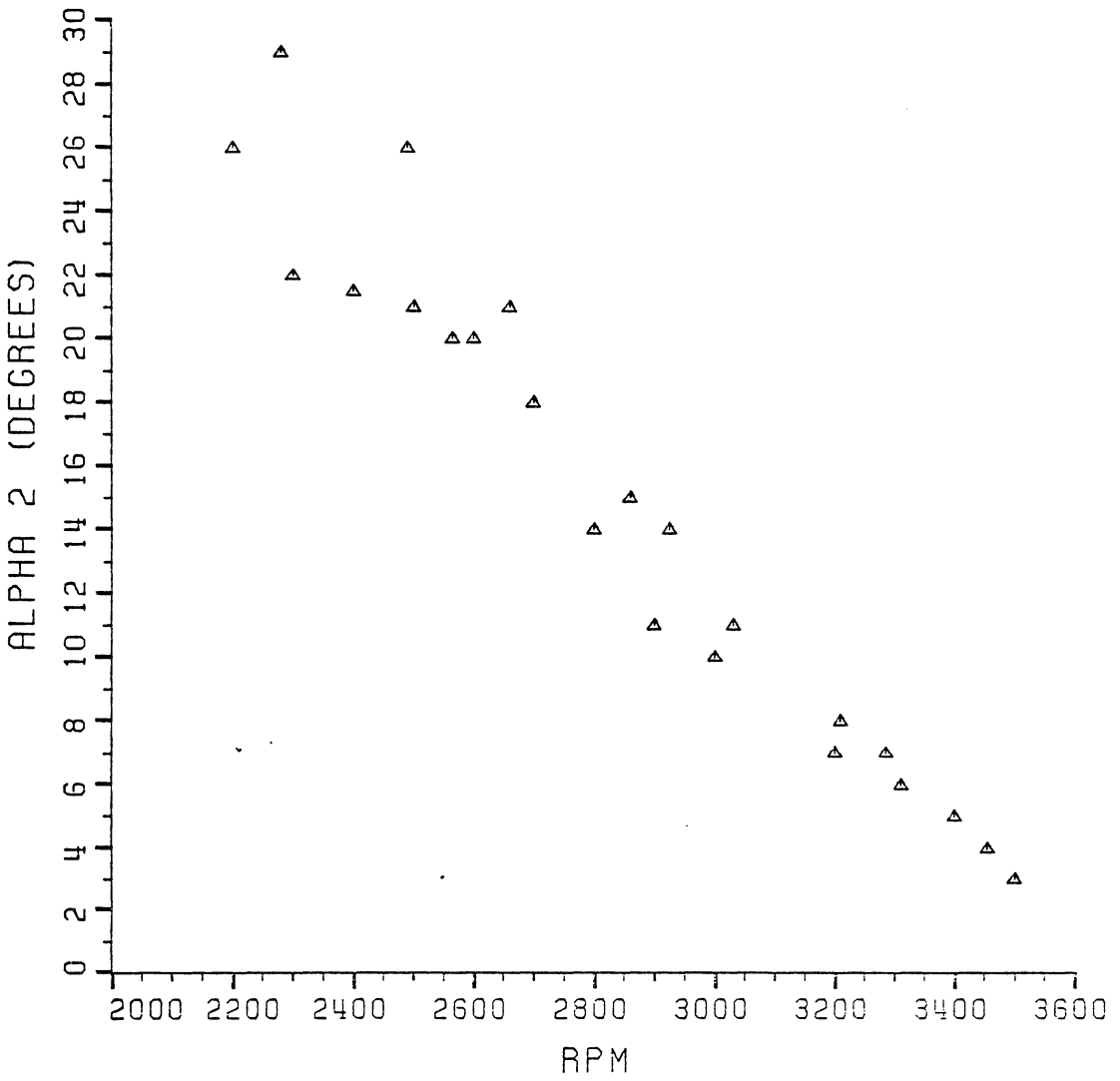

Figure 31. Experimental Results: Exit Swirl Angle

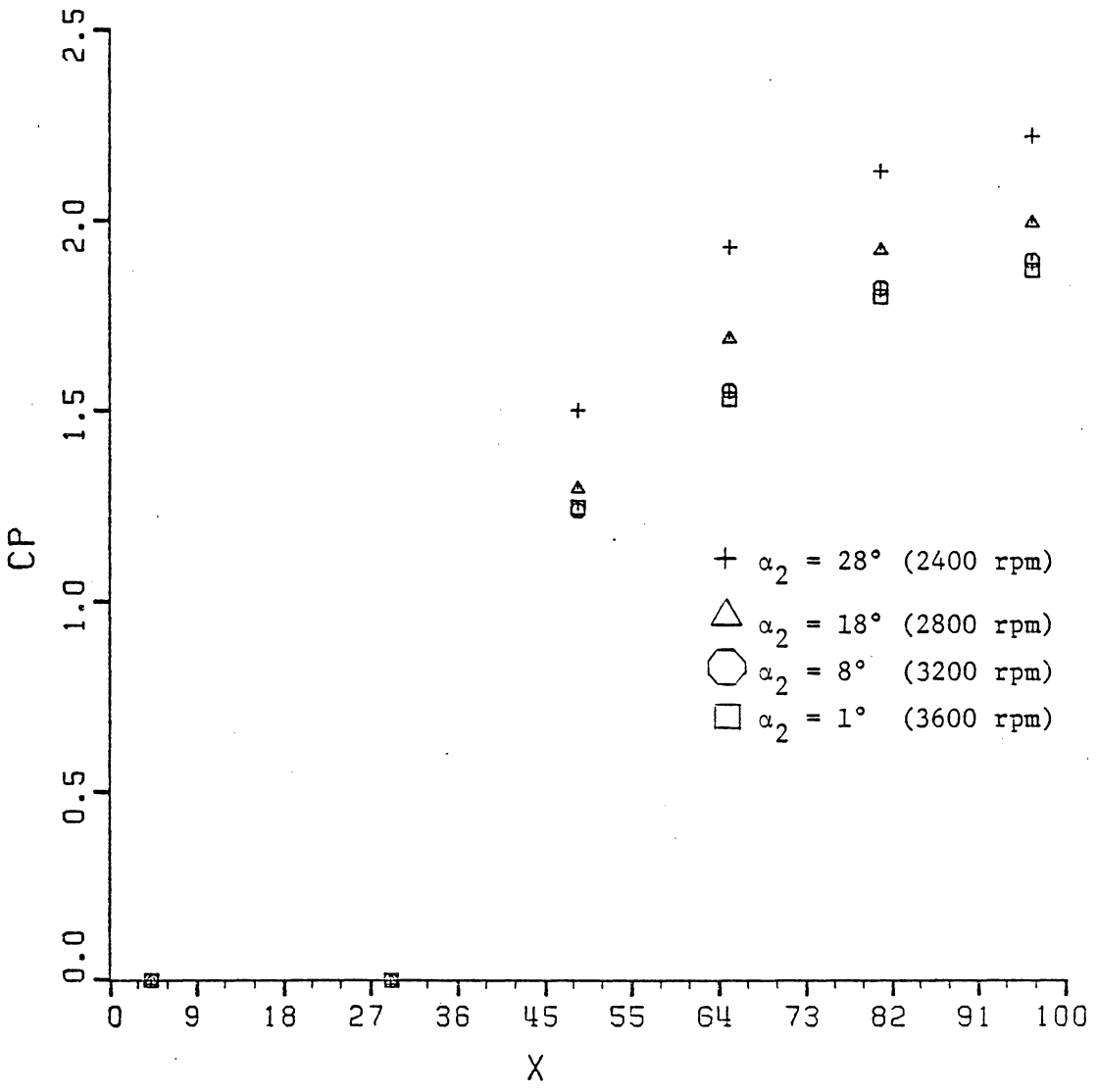

Figure 32. Experimental Results: C_p for Various Swirl Angles

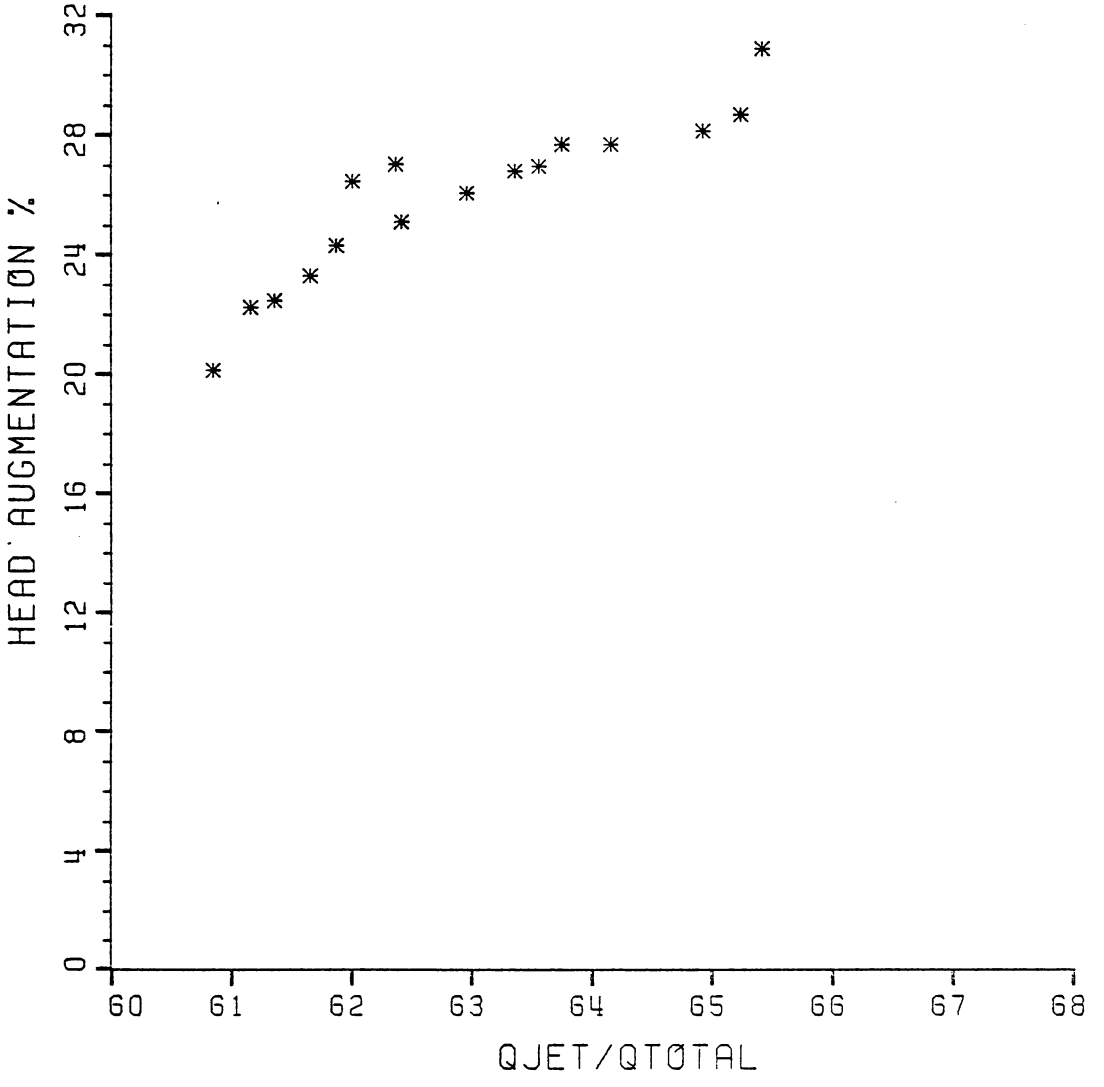

Figure 33. Experimental Results: Effect of Bypass

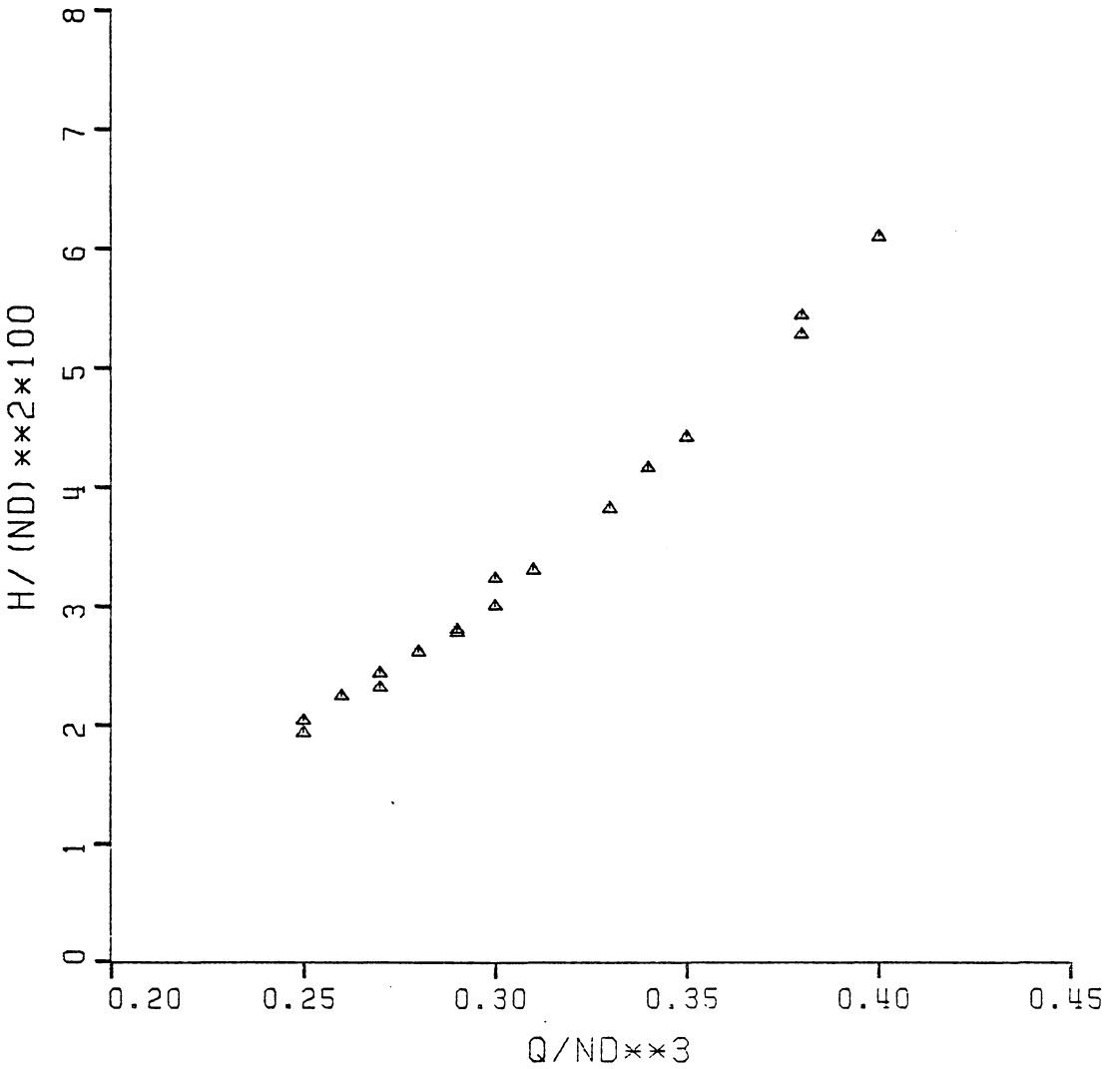

Figure 34. Experimental Results: System Characteristic

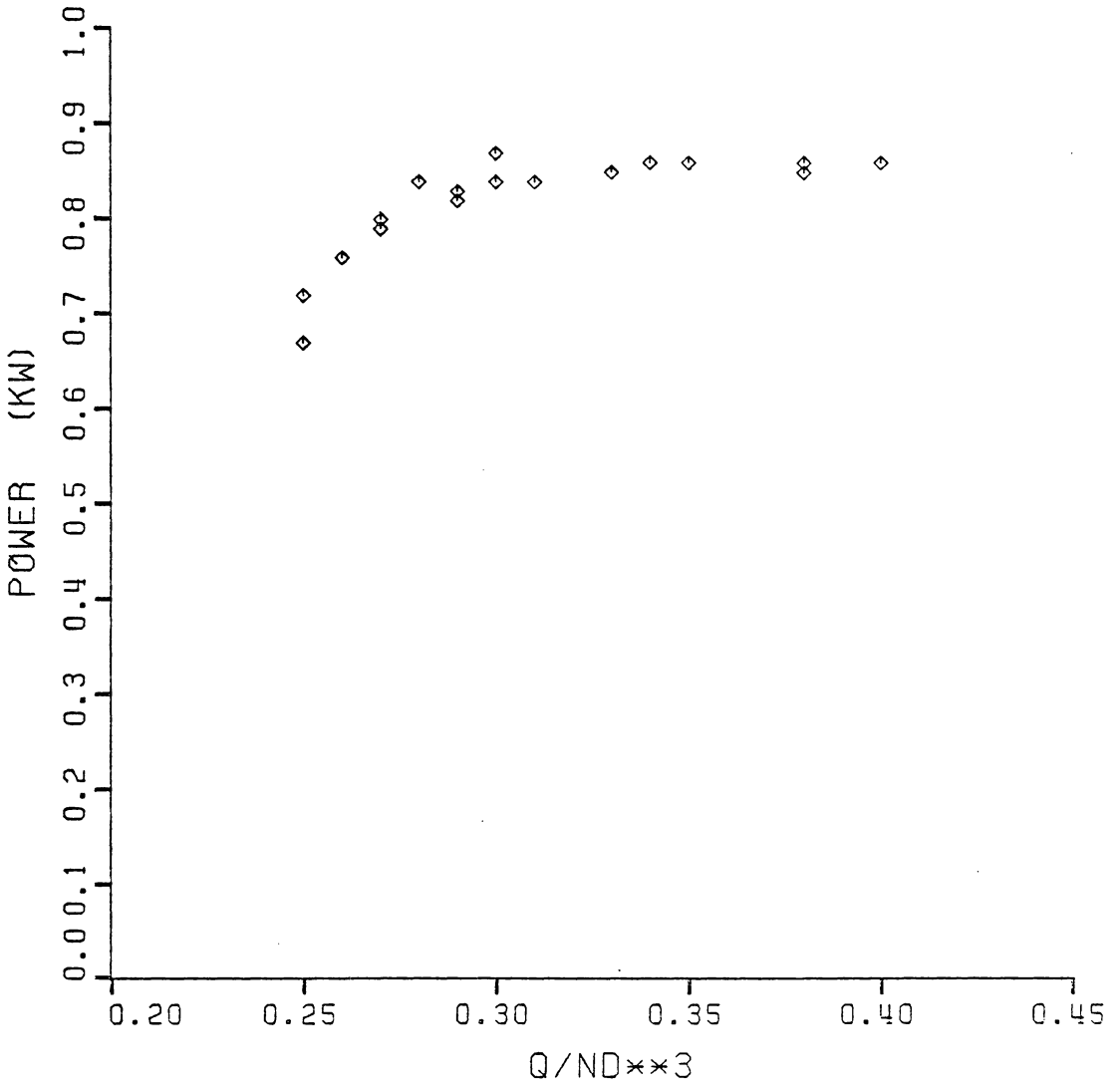

Figure 35. Experimental Results: Power Output

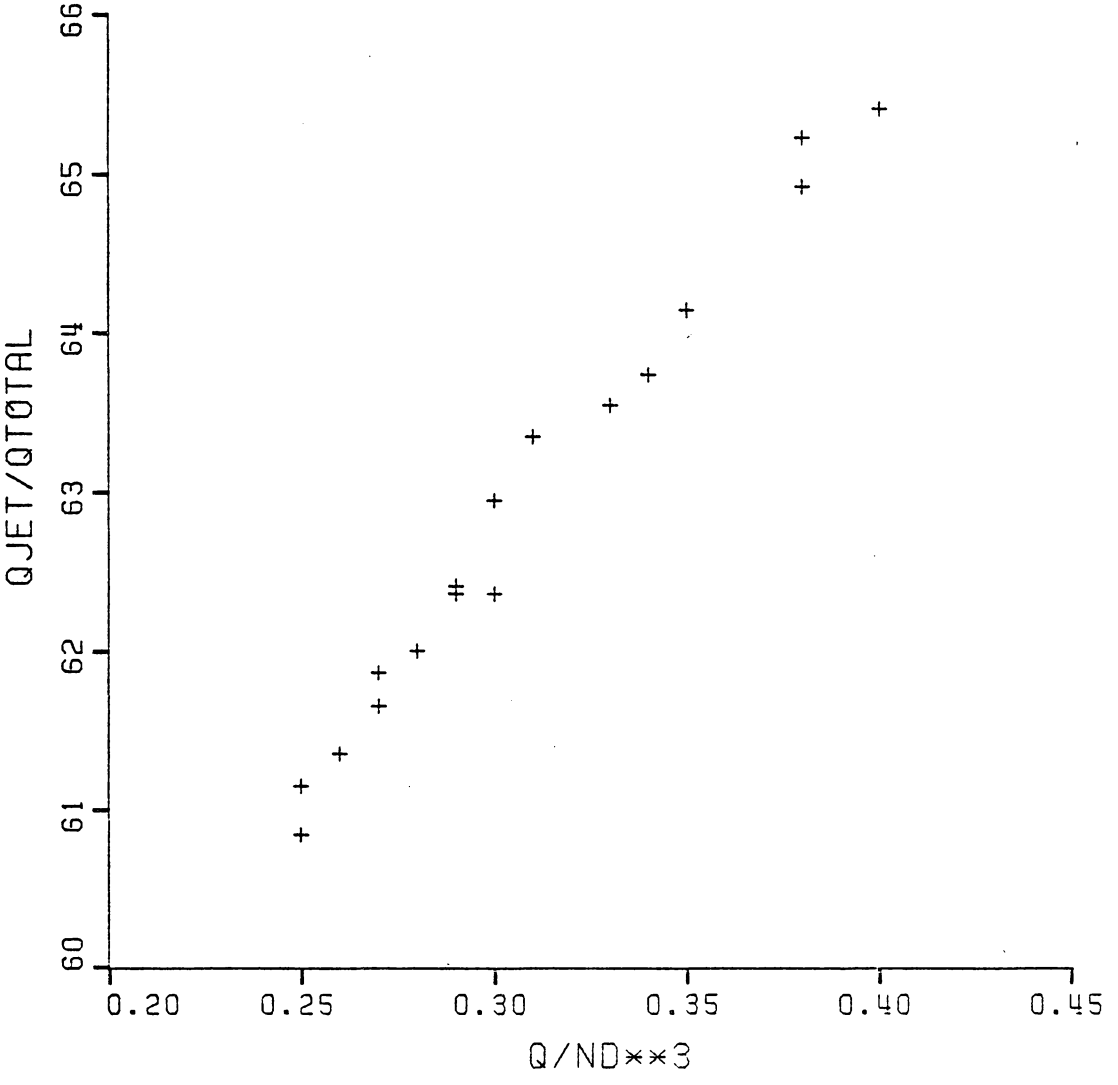

Figure 36. Experimental Results: Variation of Bypass

data which are presented here were obtained for a single flow rate, the parameter Q/ND^3 is simply proportional to N^{-1}. The turbine efficiency was computed by the equation

$$\eta_t = \frac{T\omega}{\rho g H_{eff} Q_{core}} \tag{5.2}$$

This efficiency was then corrected for size by the Moody formula [7] which gives

$$\eta_{tc} = 1 - (1 - \eta_m) \left[\frac{N_m D_m^2}{N_{ref} D_{ref}^2} \right]^{1/5} \tag{5.3}$$

where the subscript m denotes the model. This is a standard scaling procedure which compensates for Reynolds number effects. The reference rotational speed is determined by similar operation so that

$$N_{ref} = \left[\frac{H_{ref} N_m^2 D_m^2}{H_m D_{ref}^2} \right]^{1/2} \tag{5.4}$$

The reference values were taken from a typical 1 MW tubular turbine [60]. The resulting turbine efficiencies, shown in Fig. 37 represent very reasonable values for a low head propeller turbine. This helps to confirm the validity of the experimental model.

The corrected values of the turbine efficiency were used to determine the overall system efficiency given by

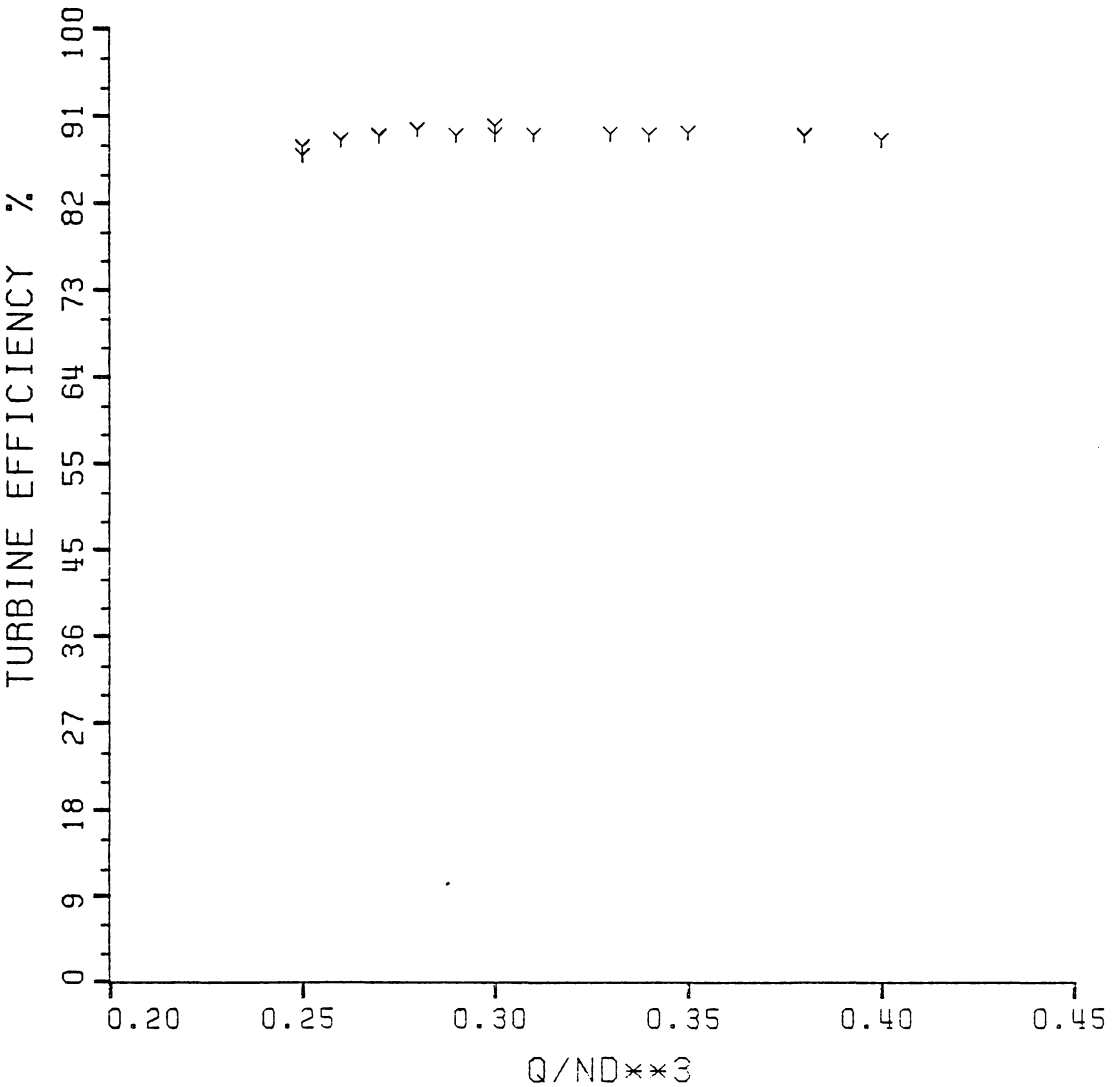

Figure 37. Experimental Results: Turbine Efficiency

$$\eta_{OA} = \eta_{tc} \frac{H_{eff}}{H} \frac{Q_{core}}{Q_{total}} \tag{5.5}$$

The overall efficiency remains fairly constant over the range of rotational speeds investigated. There is an influence of the turbine bypass flow rate upon the efficiency, but this effect cannot be insolated in the present experiment.

Having demonstrated the principle of head augmentation in an actual laboratory model, the experimental results can now be used to test and improve the computer model so that extrapolations can be made to full scale systems.

6. ANALYSIS

In this section, the performance of the experimental model is compared with the numerical analysis. Several discrepanices are found and possible explanations are considered. A revised model is presented and the predictions of the modified computer model are compared with the experiment. The revised model is then used to generate new performance maps for full scale systems. These maps are then used as a basis for economic evaluation. The section closes with a discussion of the problem of cavitation.

6.1 Comparison of Experimental Results with Numerical Model

Early testing of the laboratory model showed that a mixing tube length of three diameters could be tolerated without stall, contrary to the predictions of the computer model. This indicated that some modification of the computer program would be necessary in order to achieve a realistic representation of the performance of an actual hydropower system. Figure 38 shows the flow field predicted by the original model. Centerline stall is seen to occur quite early with a considerable loss in the pressure recovery. The program, which matched the experimental results discussed in section 3.1 quite well (see Fig. 11), would not predict the results presented in Chapter 5 when simply modified to fit the geometry and physical properties of that experiment.

It is helpful to consider the differences that exist between the two experiments. In the first test, air was used as the working fluid

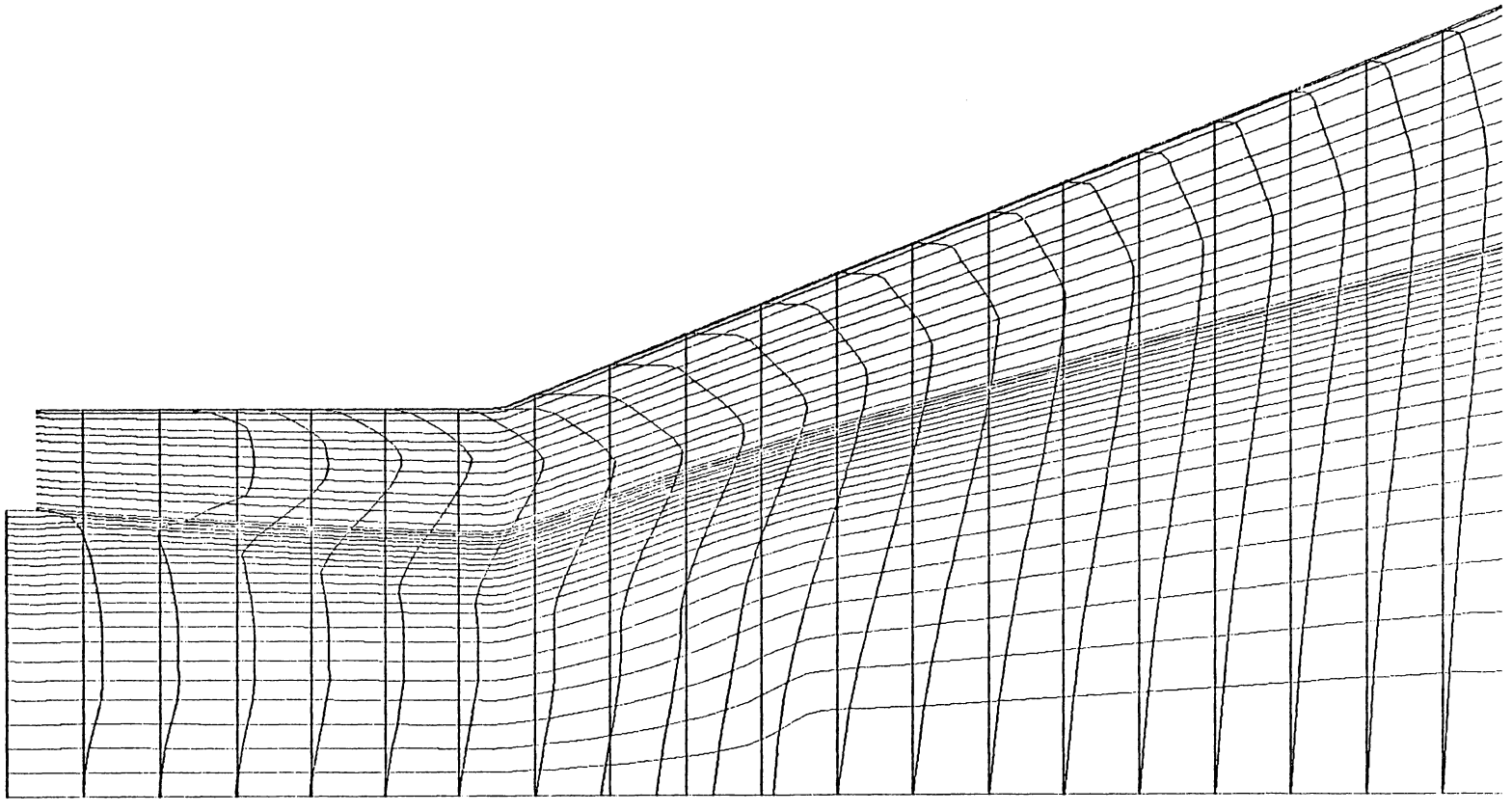

Figure 38. Velocity Profiles Showing Core Stall

and the pressure drop of the turbine was simulated by a wire screen. In the second experiment, water was used with an actual turbine that was loaded and operated under a variety of conditions. Among the factors which might be changed in going from the first to the second experiment are:

1) physical properties,
2) mixing tube inlet velocity profile,
3) freestream turbulence,
4) kinematic properties, and
5) presence of swirl in the flow.

The physical properties are easily handled by the program as a part of the input data. The presence of swirl in the flow violates the assumption of no cross-stream pressure gradient and cannot be incorporated into the program without major revision. However, the laboratory model can be operated at a nearly swirl-free condition, which the program should be able to simulate, after the remaining three factors have been incorporated into it.

The mixing tube inlet velocity profile will reflect the presence of the turbine upstream in a non-uniform profile which might be represented by a hub wake as a possible inprovement over the velocity profiles described earlier in section 3.1. A simplified hub wake model was applied to the inlet core flow where

$$\frac{u}{u_{max}} = 1 - WKD\ [\cos\ (\frac{y}{y_w}\frac{\pi}{2})] \qquad y \leq y_w \qquad (6.1)$$

where WKD represents the wake depth, and y_w indicates the width of the wake. The addition of the wake to the inlet velocity profile resulted in a slight improvement in the pressure recovery, although the increased non-uniformity of the flow seemed to expedite the core stall phenomenon. Figure 39 shows the modified velocity profile.

The premature prediction of centerline stall is a consequence of an inadequate mixing model which is a function of the remaining two factors, the freestream turbulence and the kinematic properties, notably the turbulent viscosity.

The turbulent viscosity model which was used in the program was based on Pradtl's mixing length hypothesis which states

$$\mu_t = \rho \ell^2 \left| \frac{\partial u}{\partial r} \right| \qquad (6.2)$$

where ℓ is the mixing length. The calculation is carried out using the Escudier model [54] which divides the flow into two distinct layers, an inner layer and an outer layer. In the outer layer the mixing length is taken to be a linear function of the distance from the wall except for very close to the wall where the Van Driest correction is applied. In the inner layer the mixing length is equal to a constant value which is proportional to a characteristic length δ.

In the original model the characteristic length is taken to be the thickness of the shear layer, which has been shown to be a reasonable

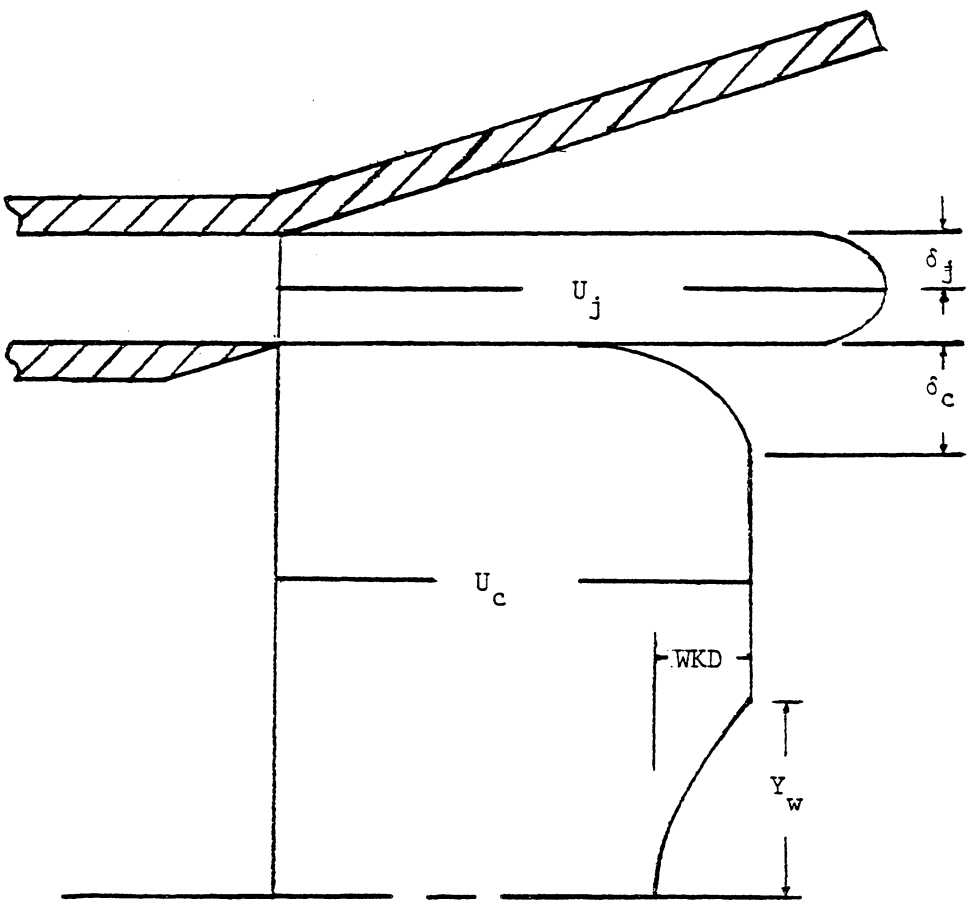

Figure 39. Revised Model Inlet Velocity Profile

assumption for turbulent free jets [61] but does not necessarily represent the highly turbulent mixing found in the discharge of a turbine. Moore and Moore [62] have been successful using a characteristic length equal to the radius of the diffuser for highly turbulent diffuser flows. For the case of a diffuser with a sudden expansion immediately upstream, their calculations based on this value of δ compared very well with experimental data.

When this value of δ was submitted to the computer model, the results were encouraging. The model no longer predicted centerline stall for the laboratory model conditions and the values of C_p at the diffuser exit were only slightly below the measured values. Figure 40 is a schematic of the revised viscosity model compared with the original model. The inlet velocity profiles are included to illustrate the location of the transitional points. Note that the mixing length is determined by

$$\ell = \kappa y \left[1 - \exp\left(\frac{y}{26\mu} \sqrt{\rho\mu \, \partial u/\partial r} \right)\right] \tag{6.3}$$

or

$$\ell = \lambda\delta \tag{6.4}$$

whichever is the smaller value. In the original model, δ is equal to the thickness of the local shear layer. The constants κ and λ were taken as 041 and 0.09 respectively [54]. In the revised model, δ takes on the value of the diffuser radius and does not change with radial position.

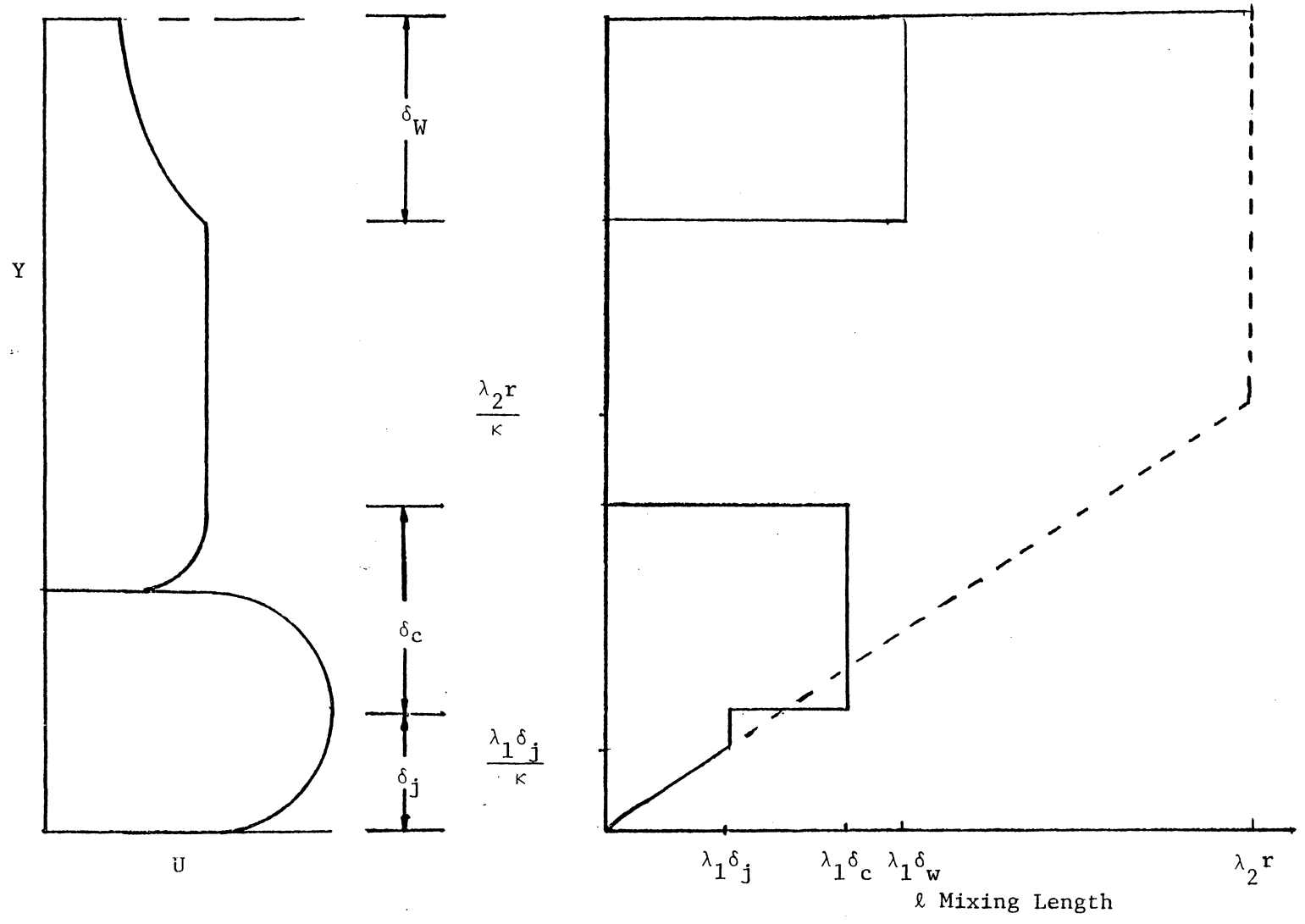

Figure 40. Schematic of Revised Mixing Length Model

With the revised viscosity model, it became possible to vary the inlet velocity profile without creating centerline stall. A parametric study of the various hub wake profiles showed very good agreement when a wake width equal to 35 per cent of the core diameter with a 20 per cent velocity deficit at the centerline was used. The actual hub diameter was equal to 30 per cent of the core.

The final modification which was made to the program to essentially "fine-tune" the match with the data, was to increase the value of λ from 0.090 to 0.095. This was a strictly empirical step which provided a slightly better match with the experimental points.

Figure 41 shows the comparison of the model with the experimental data for C_p as a function of axial position at 3600 rpm. Note that the model follows the shape of the experimental points, and matches the value of the exit C_p to within 2 per cent. The flat region on the curve at low X values represents the mixing tube. Note that while the program calls for the pressure to rise and then fall, the experimental data show no pressure variation at all.

One possible explanation for this discrepancy, could be the presence of swirl at the turbine exit. Although the measured flow was found to be nearly swirl free at the mean radius location, it is possible that there could be some swirl in the flow near the wall. This would tend to cause an artifically high wall static pressure at this location (see Eq. 5.1). The result is a slightly reduced value of C_p throughout the mixing tube and diffuser. Any swirl in the discharge would tend to mix out by the second station giving a more realistic,

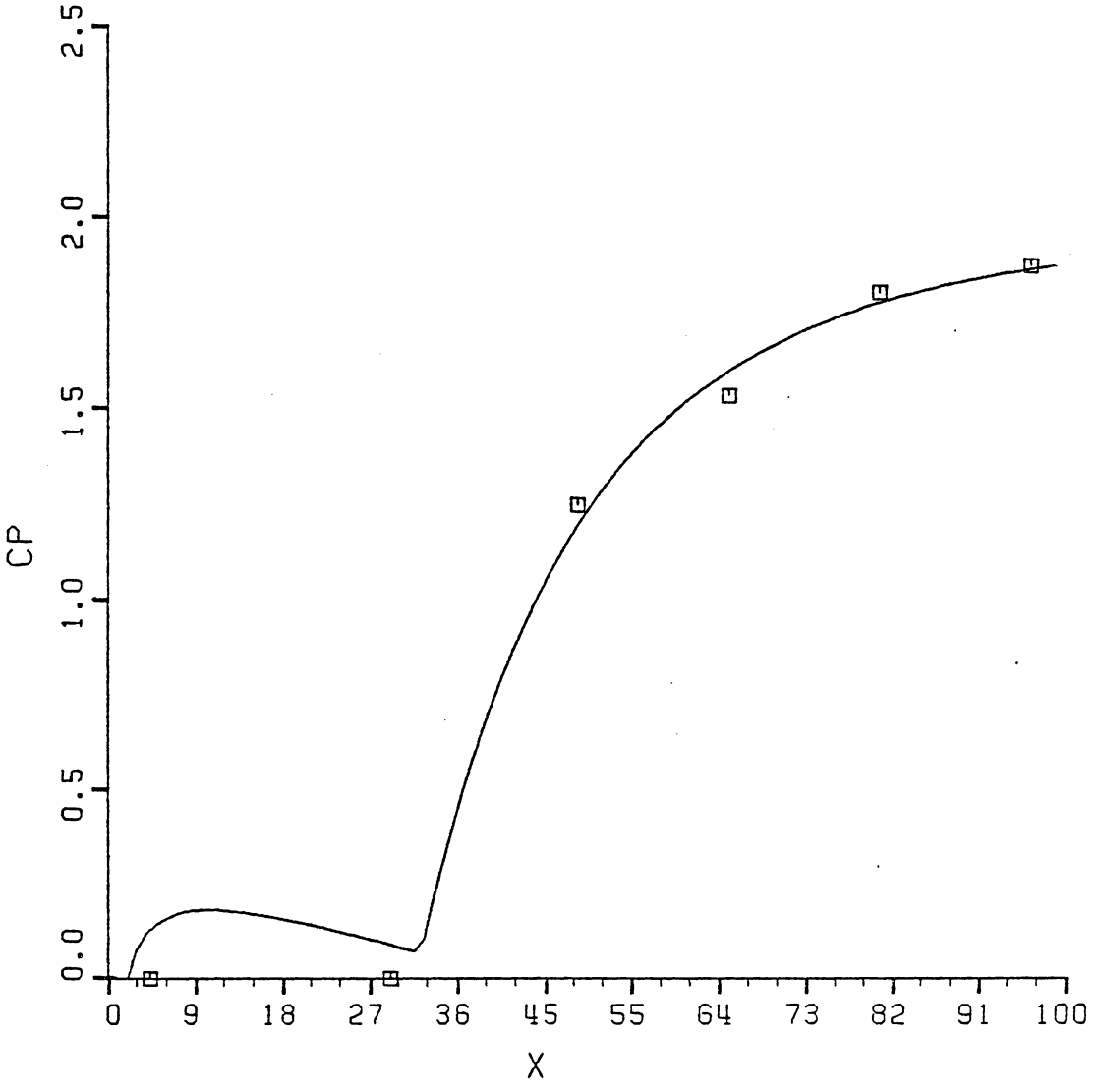

Figure 41. Comparison of Experiment With Model

lower static pressure there. If the actual pressure recovery were approximately equal to increase in wall static pressure due to swirl at the first station, the result would be no apparent change in the value of C_p along the mixing tube.

Any attempt to optimize mixing tube geometry for pressure recovery would require the resolution of this point. More static pressure data, and a more detailed knowledge of the flow field in the mixing tube would be helpful. However, the primary objective of this computer model was to be able to predict the overall pressure recovery for the system and this has been accomplished with reasonable accuracy.

6.2 Revised Performance Maps

Before proceeding to the overall system analysis with the new diffuser flow model, it was necessary to develop new performance maps. The procedure used here was essentially the same as that used by Myatt [55]. The bypass area ratio and the velocity ratio for each flow considered were combined into a new independent variable corresponding to the fraction of the total flow which was bypassed. For a given value of RA, each value of RV produces a unique bypass fraction. The performance maps give C_p as a function of the bypass fraction with RA as a parameter.

In order to give a realistic representation of a full size hydropower system, it was necessary to scale the diffuser performance by the Reynolds number based on the turbine diameter given by

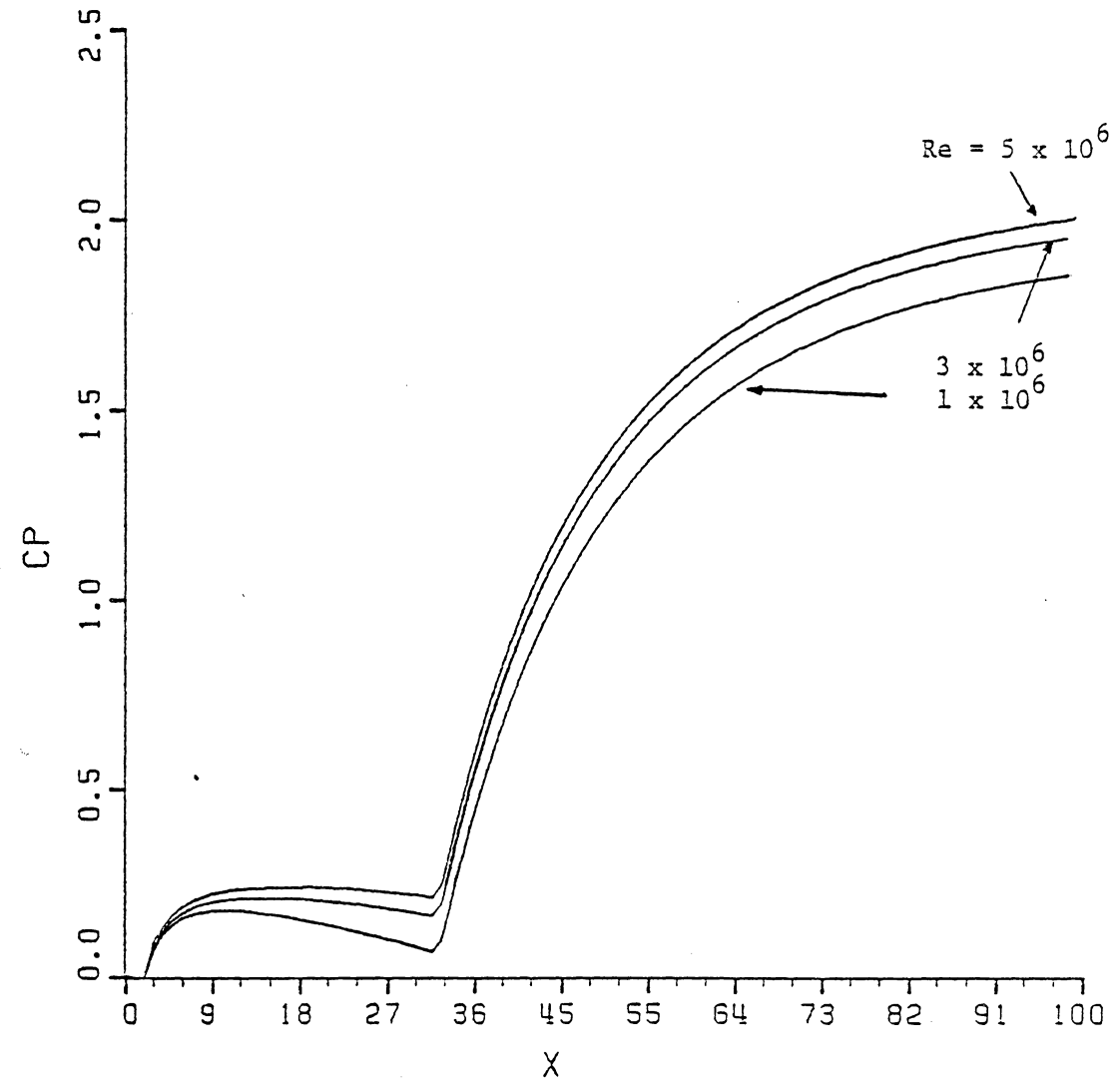

Figure 42. Effect of Reynolds Number on Pressure Recovery

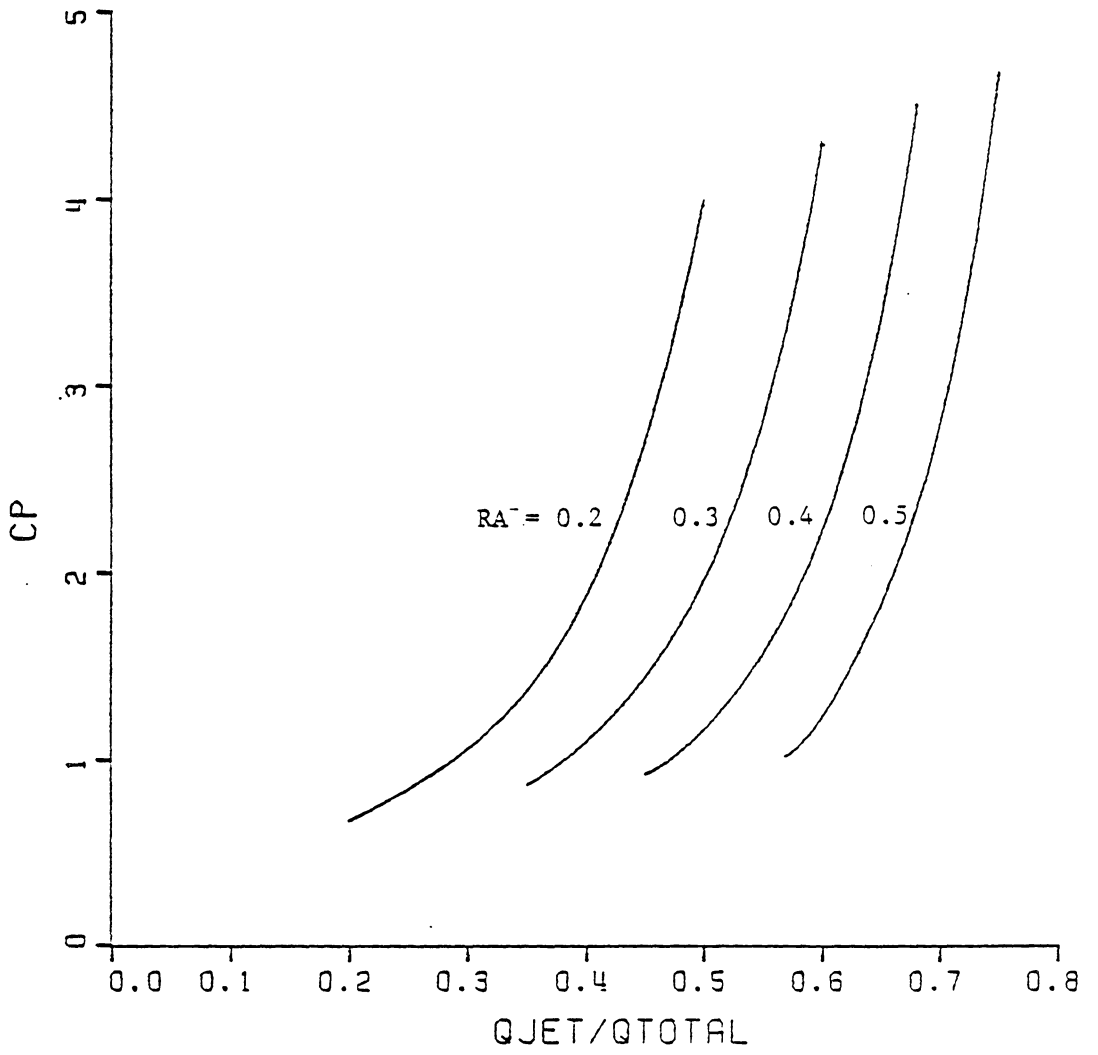

Figure 43. Revised Performance Maps

$$Re = \frac{\rho V D}{\mu} \qquad (6.5)$$

Typical small low-head turbines have Reynolds numbers in the range from 4 to 8 x 10^6. The experimental model had a Reynolds number of 920,000. The value of 5 x 10^6 was chosen as a typical value for a small, ultra-low-head turbine. Figure 42 shows the effect of Reynolds number on the pressure recovery coefficient calculated by the program. It should be pointed out that a Reynolds number of 5 x 10^6 is relatively small for a tubular low-head turbine, which means that the pressure recovery predictions given by the system model will be somewhat conservative.

Figure 43 shows the performance maps which were used in the final system program. The curves which are shown were obtained directly from a curve-fit of the diffuser program output. The curve fits were developed for each area ratio and are presented in the Appendix with the system program listing. Intermediate values of area ratio used in the program were obtained by interpolation.

6.3 Full Scale System Performance

With the diffuser program improved and the new performance maps in hand, it is now possible to return to the original system model for a reasonable approximation of how the overall hydropower system will perform with the ejector-diffuser pressure recovery system in the place of a conventional draft tube. To best represent the system performance in terms which can be evaluated economically as well as technically, several modifications were made to the original system model. The new

system model is in dimensional form covering the range of head and capacity which is of interest in this report. A turbine cost correlation, which is primarily a function of the effective head is then applied to determine when in fact the system is cost-effective.

The input matrix to the system model can be represented by a three-dimensional array which is defined by the generator output capacity, ranging from 200 to 500 kW, the net head, ranging from 2 to 5 meters, and the bypass area ratio ranging from 0 to 0.5. The first step was to establish a realistic model of a conventional low-head system. This was accomplished by correlating the data presented on a set of performance curves for Allis Chalmers 4-bladed tubular turbines [63]. The curve fit equations, which are included in the program listing, give the turbine diameter as a function of net head, with power as a parameter. An overall efficiency based on the net head is then defined as

$$\eta_{OA} = \frac{\eta_T \, \eta_G \, H_{eff}}{H} \tag{6.6}$$

where the value of the effective head is determined by the diffuser performance. It is important to make this distinction since turbine efficiencies are generally presented with reference to the actual head across the turbine rather than the net head, which can be thought of as the total pressure at the turbine inlet relative to the tailwater. A turbine efficiency, η_t, of 0.90 was used and η_{gen} was taken as 0.95. For the conventional draft tube performance, a C_p of 0.8 was chosen as a typical value for a good diffuser. With the power, net head, turbine

diameter and C_p specified, the overall efficiency was fixed implicitly. This value was found to be 76.7% and was taken as a constant for all cases although it is a very weak function of V_c. The variation was found to be less than 1.5% between the rated power and the computed power in all cases. With this information, Q is obtained directly as well as the flow area for the conventional system and the effective head. The turbine cost is then calculated as a function of effective head using the data given in reference [64]. The costs are updated using the W.P.R.S. Hydro Cost Index, which according to Sheldon [65], has followed the inflation rate very accurately.

At this point the program is incremented to the first bypass area ratio. The performance of this system is based on the same net head, total flow rate, and total flow area as the conventional system. In other words, it is as if the conventional turbine and housing were disconnected from the penstock and the modified system installed in its place. The difference being that in this system the turbine only fills a portion of the pipe, creating an annular space through which flow is bypassed. In order to compute the power output of this sytem it is necessary to find the amount of flow through the turbine and the effective head across it. Since the geometry and the inlet pressure are known, this amounts to finding V_c, V_J and p_2. The equations which must be solved are the conservation of mass, which can be written as:

$$V_3 = V_c \ (RVRA + 1 - RA), \tag{6.7}$$

and the momentum equation through the jet which is given by

$$\frac{\hat{p}_2}{\gamma} = \frac{\hat{p}_o}{\gamma} + \frac{V_o^2}{2g} - \frac{V_J^2}{2g}(1 + K_n). \tag{6.8}$$

Additional equations are provided by the diffuser performance maps which give C_p as a function of the bypass flow rate, the definitions of RV and C_p, and the net head. This results in a set of six unknowns and six equations which is most easily solved by an iterative method where RV is the free unknown. A value of RV is guessed and continuity is applied to determine V_c and V_J. At this point the bypass fraction can be calculated and a value of C_p obtained from the performance map curve fits. The momentum equation is then used to determine whether these values are correct. When the iteration process is completed the effective head is found from equation (1.4) and power can be computed by

$$P = \eta_t \eta_g Q_{core} H_{eff} \tag{6.9}$$

where Q is smaller and H_{eff} is generally larger than the conventional system. The cost per kilowatt can then be calcuated as a basis for comparison. The performance data for the 2-500 kW systems are presented in Tables 6-9.

6.4 Economic Analysis

Figure 44 shows the ratio of the cost per kilowatt of a low-head

TABLE 6

PERFORMANCE DATA: 200 KW SYSTEM

PGEN (KW)	HEAD (M)	RA	RV	QCORE (CU.M/S)	POWER (KW)	COST ($1000)	HEFF (M)	CP	BYP	DIAM (M)	RATIO
200.0	2.00	0.00	0.00	13.32	200.	931.	1.79	0.80	0.000	2.00	1.00
200.0	2.00	0.20	2.08	8.76	160.	747.	2.18	1.32	0.342	1.79	1.00
200.0	2.00	0.25	2.37	7.45	154.	678.	2.47	1.95	0.441	1.73	0.94
200.0	2.00	0.30	2.63	6.27	135.	627.	2.57	2.41	0.530	1.68	0.99
200.0	2.00	0.35	3.56	4.56	119.	525.	3.13	5.49	0.657	1.61	0.94
200.0	2.00	0.40	4.83	3.16	88.	472.	3.35	10.49	0.763	1.55	1.14
200.0	2.50	0.00	0.00	10.65	199.	808.	2.24	0.80	0.000	1.68	1.00
200.0	2.50	0.20	2.05	7.04	160.	647.	2.72	1.30	0.339	1.51	0.99
200.0	2.50	0.25	2.33	6.00	154.	588.	3.07	1.90	0.437	1.46	0.94
200.0	2.50	0.30	2.57	5.07	135.	543.	3.20	2.32	0.524	1.41	0.98
200.0	2.50	0.35	3.45	3.73	121.	457.	3.88	5.11	0.650	1.36	0.93
200.0	2.50	0.40	4.65	2.60	91.	406.	4.18	9.77	0.756	1.30	1.09
200.0	3.00	0.00	0.00	8.88	199.	720.	2.68	0.80	0.000	1.46	1.00
200.0	3.00	0.20	2.03	5.89	160.	576.	3.25	1.28	0.337	1.31	0.99
200.0	3.00	0.25	2.30	5.03	154.	524.	3.67	1.85	0.434	1.27	0.93
200.0	3.00	0.30	2.53	4.26	136.	484.	3.82	2.26	0.520	1.22	0.98
200.0	3.00	0.35	3.35	3.17	122.	408.	4.62	4.82	0.644	1.18	0.92
200.0	3.00	0.40	4.51	2.22	93.	358.	5.01	9.20	0.750	1.13	1.06
200.0	3.50	0.00	0.00	7.61	198.	653.	3.12	0.80	0.000	1.30	1.00
200.0	3.50	0.20	2.02	5.06	160.	522.	3.78	1.27	0.335	1.16	0.99
200.0	3.50	0.25	2.27	4.33	155.	475.	4.27	1.82	0.431	1.12	0.93
200.0	3.50	0.30	2.50	3.68	136.	438.	4.44	2.20	0.517	1.09	0.97
200.0	3.50	0.35	3.28	2.75	123.	371.	5.36	4.59	0.638	1.05	0.91
200.0	3.50	0.40	4.39	1.94	95.	323.	5.84	8.73	0.745	1.01	1.03
200.0	4.00	0.00	0.00	6.66	198.	600.	3.56	0.80	0.000	1.17	1.00
200.0	4.00	0.20	2.00	4.44	160.	479.	4.31	1.26	0.333	1.05	0.98
200.0	4.00	0.25	2.25	3.81	155.	436.	4.87	1.79	0.429	1.01	0.93
200.0	4.00	0.30	2.47	3.24	137.	403.	5.06	2.16	0.514	0.98	0.97
200.0	4.00	0.35	3.21	2.44	124.	341.	6.09	4.41	0.634	0.94	0.90
200.0	4.00	0.40	4.28	1.73	96.	295.	6.66	8.33	0.741	0.91	1.01
200.0	4.50	0.00	0.00	5.92	198.	557.	4.00	0.80	0.000	1.07	1.00
200.0	4.50	0.20	1.99	3.95	160.	444.	4.84	1.25	0.332	0.96	0.98
200.0	4.50	0.25	2.23	3.39	155.	405.	5.46	1.77	0.427	0.93	0.92
200.0	4.50	0.30	2.45	2.89	137.	373.	5.68	2.12	0.512	0.89	0.96
200.0	4.50	0.35	3.16	2.19	125.	317.	6.82	4.26	0.630	0.86	0.90
200.0	4.50	0.40	4.19	1.56	97.	273.	7.47	7.98	0.736	0.83	0.99
200.0	5.00	0.00	0.00	5.33	198.	521.	4.44	0.80	0.000	0.99	1.00
200.0	5.00	0.20	1.98	3.57	160.	416.	5.37	1.24	0.331	0.88	0.98
200.0	5.00	0.25	2.22	3.06	155.	379.	6.06	1.75	0.425	0.85	0.92
200.0	5.00	0.30	2.42	2.61	138.	349.	6.30	2.09	0.510	0.82	0.96
200.0	5.00	0.35	3.12	1.99	126.	297.	7.55	4.13	0.627	0.79	0.89
200.0	5.00	0.40	4.11	1.42	99.	254.	8.28	7.67	0.733	0.76	0.97

TABLE 7

PERFORMANCE DATA: 300 KW SYSTEM

PGEN (KW)	HEAD (M)	RA	RV	QCORE (CU.M/S)	POWER (KW)	COST ($1000)	HEFF (M)	CP	BYP	DIAM (M)	RATIO
300.0	2.00	0.00	0.00	19.98	298.	1138.	1.78	0.80	0.000	2.42	1.00
300.0	2.00	0.20	2.02	13.28	240.	901.	2.16	1.27	0.335	2.16	0.98
300.0	2.00	0.25	2.27	11.37	232.	820.	2.44	1.82	0.431	2.10	0.92
300.0	2.00	0.30	2.50	9.65	205.	755.	2.54	2.20	0.517	2.02	0.96
300.0	2.00	0.35	3.28	7.22	185.	639.	3.06	4.60	0.638	1.95	0.90
300.0	2.00	0.40	4.39	5.09	142.	538.	3.34	8.73	0.745	1.87	0.99
300.0	2.50	0.00	0.00	15.98	298.	987.	2.23	0.80	0.000	2.05	1.00
300.0	2.50	0.20	2.02	10.62	240.	781.	2.70	1.27	0.335	1.83	0.98
300.0	2.50	0.25	2.27	9.09	232.	711.	3.05	1.82	0.431	1.77	0.92
300.0	2.50	0.30	2.50	7.72	205.	655.	3.17	2.20	0.517	1.71	0.96
300.0	2.50	0.35	3.28	5.78	185.	554.	3.83	4.61	0.639	1.65	0.90
300.0	2.50	0.40	4.39	4.07	142.	465.	4.17	8.76	0.745	1.59	0.98
300.0	3.00	0.00	0.00	13.32	298.	878.	2.67	0.80	0.000	1.79	1.00
300.0	3.00	0.20	2.02	8.85	240.	696.	3.24	1.27	0.335	1.60	0.98
300.0	3.00	0.25	2.27	7.58	232.	633.	3.66	1.83	0.431	1.55	0.92
300.0	3.00	0.30	2.50	6.43	205.	583.	3.81	2.21	0.517	1.49	0.96
300.0	3.00	0.35	3.29	4.81	185.	493.	4.60	4.62	0.639	1.44	0.90
300.0	3.00	0.40	4.40	3.39	142.	412.	5.01	8.78	0.746	1.38	0.98
300.0	3.50	0.00	0.00	11.42	298.	796.	3.12	0.80	0.000	1.59	1.00
300.0	3.50	0.20	2.02	7.59	240.	631.	3.78	1.27	0.335	1.42	0.98
300.0	3.50	0.25	2.28	6.49	232.	574.	4.27	1.83	0.431	1.38	0.92
300.0	3.50	0.30	2.50	5.51	205.	529.	4.44	2.21	0.518	1.33	0.96
300.0	3.50	0.35	3.29	4.12	185.	446.	5.37	4.63	0.639	1.28	0.90
300.0	3.50	0.40	4.40	2.90	142.	372.	5.84	8.80	0.746	1.23	0.98
300.0	4.00	0.00	0.00	9.99	298.	731.	3.57	0.80	0.000	1.44	1.00
300.0	4.00	0.20	2.02	6.64	240.	579.	4.32	1.27	0.335	1.29	0.98
300.0	4.00	0.25	2.28	5.68	232.	527.	4.88	1.83	0.431	1.25	0.92
300.0	4.00	0.30	2.50	4.82	205.	486.	5.08	2.21	0.518	1.20	0.96
300.0	4.00	0.35	3.29	3.60	185.	409.	6.13	4.64	0.639	1.16	0.90
300.0	4.00	0.40	4.41	2.54	142.	340.	6.68	8.81	0.746	1.12	0.98
300.0	4.50	0.00	0.00	8.88	298.	678.	4.01	0.80	0.000	1.32	1.00
300.0	4.50	0.20	2.02	5.90	240.	537.	4.87	1.27	0.335	1.18	0.98
300.0	4.50	0.25	2.28	5.05	232.	489.	5.49	1.83	0.431	1.14	0.92
300.0	4.50	0.30	2.50	4.28	205.	451.	5.72	2.21	0.518	1.10	0.96
300.0	4.50	0.35	3.29	3.20	185.	380.	6.90	4.64	0.639	1.06	0.90
300.0	4.50	0.40	4.41	2.25	141.	315.	7.51	8.82	0.746	1.02	0.97
300.0	5.00	0.00	0.00	7.99	298.	633.	4.46	0.80	0.000	1.22	1.00
300.0	5.00	0.20	2.02	5.31	240.	502.	5.41	1.27	0.336	1.09	0.98
300.0	5.00	0.25	2.28	4.54	232.	457.	6.11	1.83	0.432	1.06	0.92
300.0	5.00	0.30	2.51	3.85	205.	422.	6.35	2.21	0.518	1.02	0.96
300.0	5.00	0.35	3.29	2.88	185.	355.	7.67	4.65	0.640	0.98	0.90
300.0	5.00	0.40	4.41	2.03	141.	294.	8.35	8.84	0.746	0.94	0.97

TABLE 8

PERFORMANCE DATA: 400 KW SYSTEM

PGEN (KW)	HEAD (M)	RA	RV	QCORE (CU.M/S)	POWER (KW)	COST ($1000)	HEFF (M)	CP	BYP	DIAM (M)	RATIO
400.0	2.00	0.00	0.00	26.64	397.	1305.	1.79	0.80	0.000	2.80	1.00
400.0	2.00	0.20	2.03	17.67	320.	1037.	2.17	1.28	0.337	2.51	0.98
400.0	2.00	0.25	2.29	15.10	309.	945.	2.45	1.85	0.433	2.43	0.93
400.0	2.00	0.30	2.53	12.79	272.	865.	2.55	2.24	0.520	2.34	0.96
400.0	2.00	0.35	3.34	9.52	245.	726.	3.08	4.78	0.643	2.26	0.90
400.0	2.00	0.40	4.48	6.68	187.	607.	3.34	9.11	0.749	2.17	0.99
400.0	2.50	0.00	0.00	21.31	397.	1125.	2.23	0.80	0.000	2.37	1.00
400.0	2.50	0.20	2.03	14.14	320.	898.	2.71	1.28	0.336	2.12	0.99
400.0	2.50	0.25	2.29	12.09	309.	819.	3.06	1.84	0.432	2.05	0.93
400.0	2.50	0.30	2.52	10.25	272.	750.	3.18	2.23	0.519	1.98	0.97
400.0	2.50	0.35	3.32	7.65	246.	631.	3.84	4.72	0.641	1.91	0.90
400.0	2.50	0.40	4.45	5.37	187.	527.	4.18	8.99	0.748	1.83	0.99
400.0	3.00	0.00	0.00	17.76	397.	996.	2.68	0.80	0.000	2.06	1.00
400.0	3.00	0.20	2.02	11.79	320.	799.	3.24	1.27	0.336	1.85	0.99
400.0	3.00	0.25	2.28	10.09	309.	729.	3.66	1.83	0.432	1.79	0.94
400.0	3.00	0.30	2.51	8.56	273.	669.	3.81	2.22	0.518	1.73	0.97
400.0	3.00	0.35	3.30	6.39	246.	563.	4.60	4.67	0.640	1.66	0.91
400.0	3.00	0.40	4.43	4.49	188.	470.	5.01	8.90	0.747	1.60	0.99
400.0	3.50	0.00	0.00	15.22	397.	898.	3.12	0.80	0.000	1.84	1.00
400.0	3.50	0.20	2.02	10.11	320.	723.	3.78	1.27	0.335	1.64	0.99
400.0	3.50	0.25	2.28	8.65	309.	660.	4.27	1.83	0.431	1.59	0.94
400.0	3.50	0.30	2.50	7.34	273.	606.	4.44	2.21	0.518	1.54	0.98
400.0	3.50	0.35	3.29	5.49	246.	511.	5.37	4.64	0.639	1.48	0.91
400.0	3.50	0.40	4.41	3.86	189.	427.	5.84	8.82	0.746	1.42	1.00
400.0	4.00	0.00	0.00	13.32	397.	821.	3.57	0.80	0.000	1.66	1.00
400.0	4.00	0.20	2.02	8.85	320.	664.	4.32	1.27	0.335	1.49	1.00
400.0	4.00	0.25	2.27	7.58	309.	606.	4.88	1.82	0.431	1.44	0.94
400.0	4.00	0.30	2.50	6.43	273.	557.	5.08	2.20	0.517	1.39	0.98
400.0	4.00	0.35	3.28	4.81	247.	470.	6.13	4.60	0.639	1.34	0.92
400.0	4.00	0.40	4.39	3.39	189.	393.	6.67	8.74	0.745	1.29	1.00
400.0	4.50	0.00	0.00	11.84	397.	759.	4.01	0.80	0.000	1.52	1.00
400.0	4.50	0.20	2.01	7.87	320.	615.	4.86	1.27	0.335	1.36	1.00
400.0	4.50	0.25	2.27	6.74	309.	562.	5.49	1.82	0.431	1.32	0.95
400.0	4.50	0.30	2.49	5.72	273.	517.	5.71	2.20	0.517	1.27	0.98
400.0	4.50	0.35	3.27	4.29	247.	436.	6.89	4.57	0.638	1.23	0.92
400.0	4.50	0.40	4.37	3.02	190.	365.	7.51	8.68	0.745	1.18	1.00
400.0	5.00	0.00	0.00	10.65	397.	708.	4.45	0.80	0.000	1.40	1.00
400.0	5.00	0.20	2.01	7.09	320.	575.	5.40	1.27	0.335	1.26	1.00
400.0	5.00	0.25	2.27	6.07	309.	526.	6.10	1.81	0.430	1.22	0.95
400.0	5.00	0.30	2.49	5.15	273.	484.	6.34	2.19	0.516	1.17	0.99
400.0	5.00	0.35	3.26	3.87	247.	408.	7.65	4.55	0.637	1.13	0.92
400.0	5.00	0.40	4.36	2.73	190.	342.	8.34	8.63	0.744	1.09	1.00

TABLE 9

PERFORMANCE DATA: 500 KW SYSTEM

PGEN (KW)	HEAD (M)	RA	RV	QCORE (CU.M/S)	POWER (KW)	COST ($1000)	HEFF (M)	CP	BYP	DIAM (M)	RATIO
500.0	2.00	0.00	0.00	33.30	496.	1421.	1.78	0.80	0.000	3.12	1.00
500.0	2.00	0.20	2.02	22.14	400.	1152.	2.16	1.27	0.335	2.79	1.00
500.0	2.00	0.25	2.27	18.95	387.	1045.	2.44	1.82	0.431	2.71	0.94
500.0	2.00	0.30	2.50	16.08	341.	963.	2.54	2.20	0.517	2.61	0.98
500.0	2.00	0.35	3.28	12.05	308.	817.	3.06	4.59	0.638	2.52	0.92
500.0	2.00	0.40	4.38	8.49	237.	679.	3.34	8.72	0.745	2.42	1.00
500.0	2.50	0.00	0.00	26.64	496.	1222.	2.23	0.80	0.000	2.64	1.00
500.0	2.50	0.20	2.01	17.73	400.	993.	2.70	1.26	0.335	2.36	1.00
500.0	2.50	0.25	2.26	15.18	387.	902.	3.05	1.81	0.430	2.29	0.94
500.0	2.50	0.30	2.49	12.89	342.	833.	3.17	2.19	0.516	2.21	0.98
500.0	2.50	0.35	3.25	9.68	309.	710.	3.82	4.53	0.637	2.13	0.93
500.0	2.50	0.40	4.35	6.83	238.	591.	4.17	8.58	0.743	2.04	1.00
500.0	3.00	0.00	0.00	22.20	496.	1081.	2.67	0.80	0.000	2.30	1.00
500.0	3.00	0.20	2.01	14.78	400.	879.	3.24	1.26	0.334	2.06	1.00
500.0	3.00	0.25	2.26	12.67	387.	799.	3.65	1.80	0.429	1.99	0.94
500.0	3.00	0.30	2.48	10.76	342.	740.	3.80	2.17	0.515	1.92	0.99
500.0	3.00	0.35	3.24	8.09	310.	632.	4.58	4.47	0.635	1.85	0.93
500.0	3.00	0.40	4.32	5.72	239.	527.	5.00	8.47	0.742	1.78	1.01
500.0	3.50	0.00	0.00	19.03	495.	974.	3.12	0.80	0.000	2.05	1.00
500.0	3.50	0.20	2.00	12.68	400.	793.	3.78	1.26	0.334	1.83	1.00
500.0	3.50	0.25	2.25	10.87	387.	722.	4.26	1.80	0.429	1.77	0.94
500.0	3.50	0.30	2.47	9.24	342.	670.	4.43	2.16	0.514	1.71	0.99
500.0	3.50	0.35	3.22	6.96	310.	573.	5.33	4.43	0.634	1.65	0.94
500.0	3.50	0.40	4.29	4.93	240.	479.	5.83	8.37	0.741	1.59	1.01
500.0	4.00	0.00	0.00	16.65	495.	890.	3.56	0.80	0.000	1.85	1.00
500.0	4.00	0.20	2.00	11.10	400.	726.	4.31	1.26	0.333	1.66	1.00
500.0	4.00	0.25	2.25	9.52	387.	661.	4.87	1.79	0.428	1.60	0.94
500.0	4.00	0.30	2.47	8.09	342.	614.	5.06	2.15	0.514	1.55	0.99
500.0	4.00	0.35	3.21	6.10	311.	527.	6.09	4.39	0.633	1.49	0.94
500.0	4.00	0.40	4.27	4.33	241.	441.	6.66	8.29	0.740	1.43	1.01
500.0	4.50	0.00	0.00	14.80	495.	822.	4.00	0.80	0.000	1.69	1.00
500.0	4.50	0.20	2.00	9.87	400.	671.	4.85	1.25	0.333	1.51	1.01
500.0	4.50	0.25	2.24	8.47	387.	611.	5.47	1.79	0.428	1.47	0.95
500.0	4.50	0.30	2.46	7.20	343.	569.	5.69	2.14	0.513	1.42	1.00
500.0	4.50	0.35	3.20	5.44	311.	489.	6.84	4.36	0.633	1.37	0.94
500.0	4.50	0.40	4.25	3.86	241.	409.	7.48	8.21	0.739	1.31	1.02
500.0	5.00	0.00	0.00	13.32	495.	766.	4.45	0.80	0.000	1.56	1.00
500.0	5.00	0.20	1.99	8.89	400.	625.	5.39	1.25	0.333	1.40	1.01
500.0	5.00	0.25	2.24	7.62	387.	570.	6.08	1.78	0.428	1.35	0.95
500.0	5.00	0.30	2.46	6.49	343.	531.	6.32	2.14	0.513	1.31	1.00
500.0	5.00	0.35	3.19	4.90	311.	457.	7.60	4.33	0.632	1.26	0.94
500.0	5.00	0.40	4.24	3.48	242.	383.	8.31	8.15	0.739	1.21	1.02

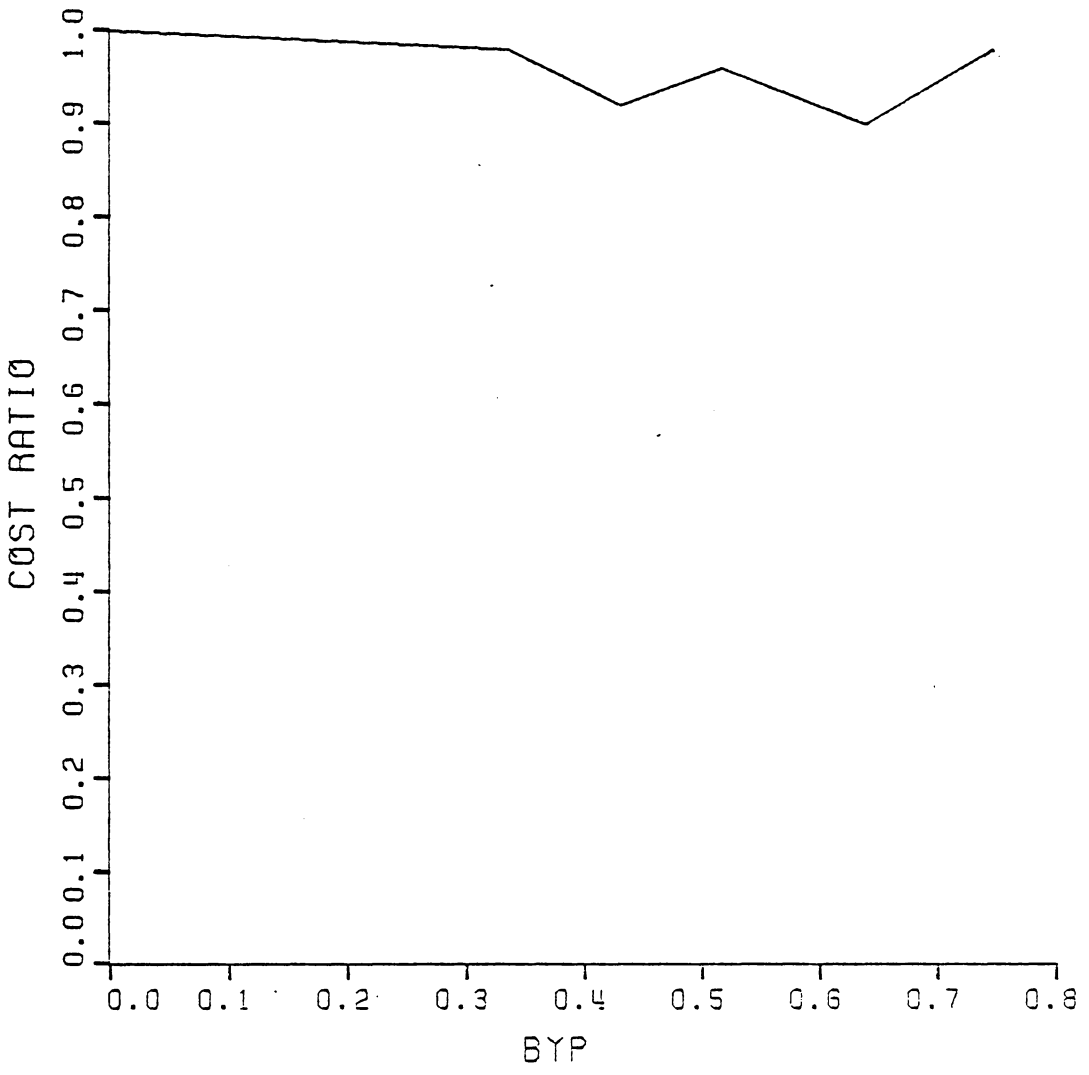

Figure 44. Full Scale System: Cost Ratio

system with bypass, to the conventional 300 kW system cost/kW as a function of the amount of flow bypassed. At zero bypass the system is identical to the conventional system, so the ratio is identically unity. Note that when this ratio drops below unity, the reduction in the system cost is greater than the corresponding reduction in power output, due to the decreased turbine size. The overall flow rate for all cases is the same in this plot. The nominal power output for this case is 300 kW. Figure 45 shows the actual power output as a function of the bypass fraction.

The costs upon which Figure 44 is based are representative costs for a standardized turbular turbine coupled to a generator through a speed increaser [64]. These costs include a turbine with adjustable runner blades and fixed guide vanes, an inlet butterfly valve, a speed increaser, a synchronous generator, a speed regulating governor and the installation cost which is estimated at 15 per cent of the total equipment cost. Cost is taken as a function of effective head and power. The costs given are in January 1982 dollars. Figure 46 shows the estimated costs for the case presented in Figure 44 (i.e. 300 kW, 3 meters of net head). It should be noted that although the cost and the cost/kW are seen to be strong functions of the net head H, the cost ratio which compares the bypass system to the conventional system is almost independent of the net head. This then is a useful parameter in describing systems of this type.

These results show that the use of a smaller turbine with bypass injection will result in a lower cost per kilowatt for the complete

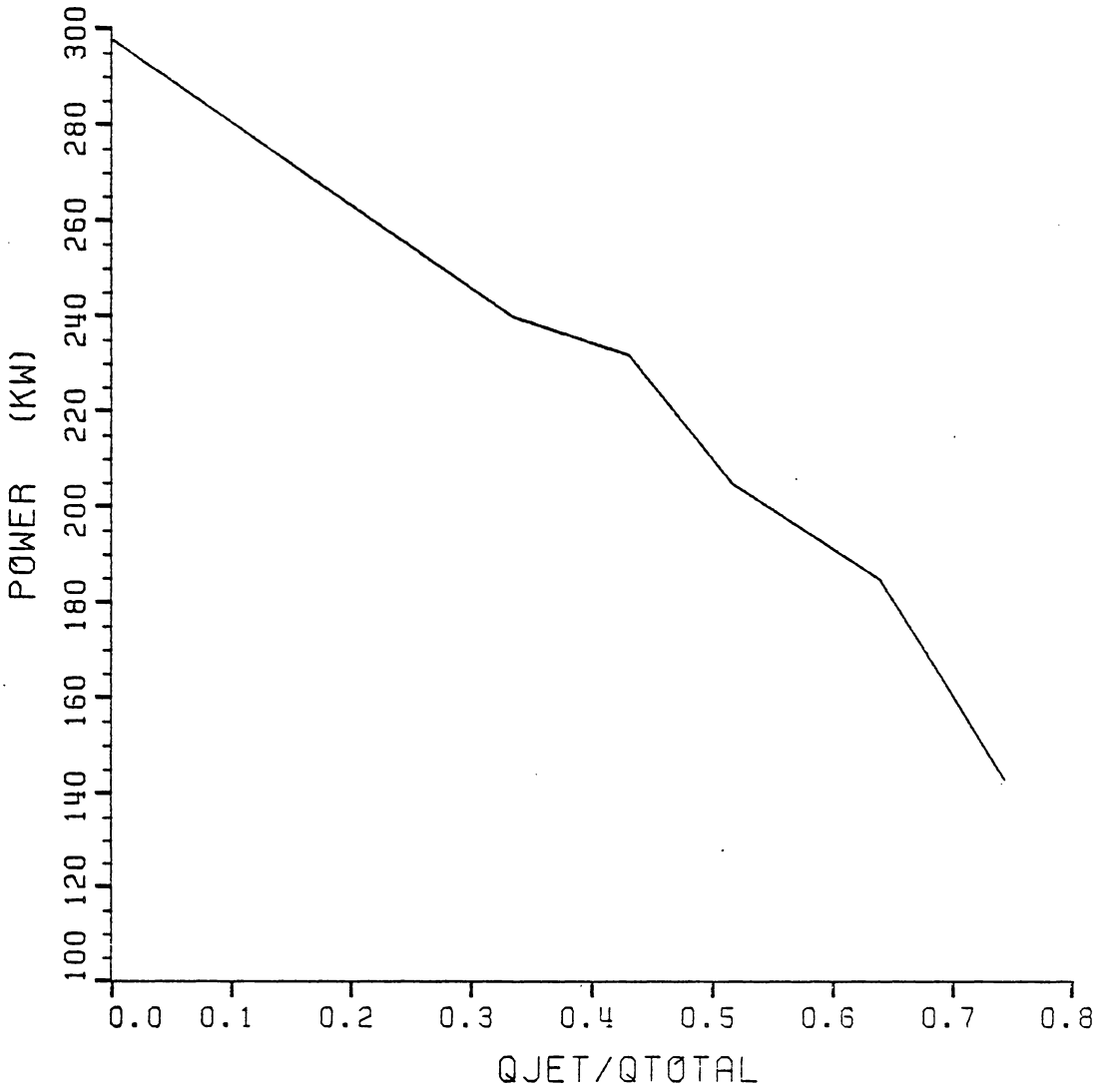

Figure 45. Full Scale System: Power Output

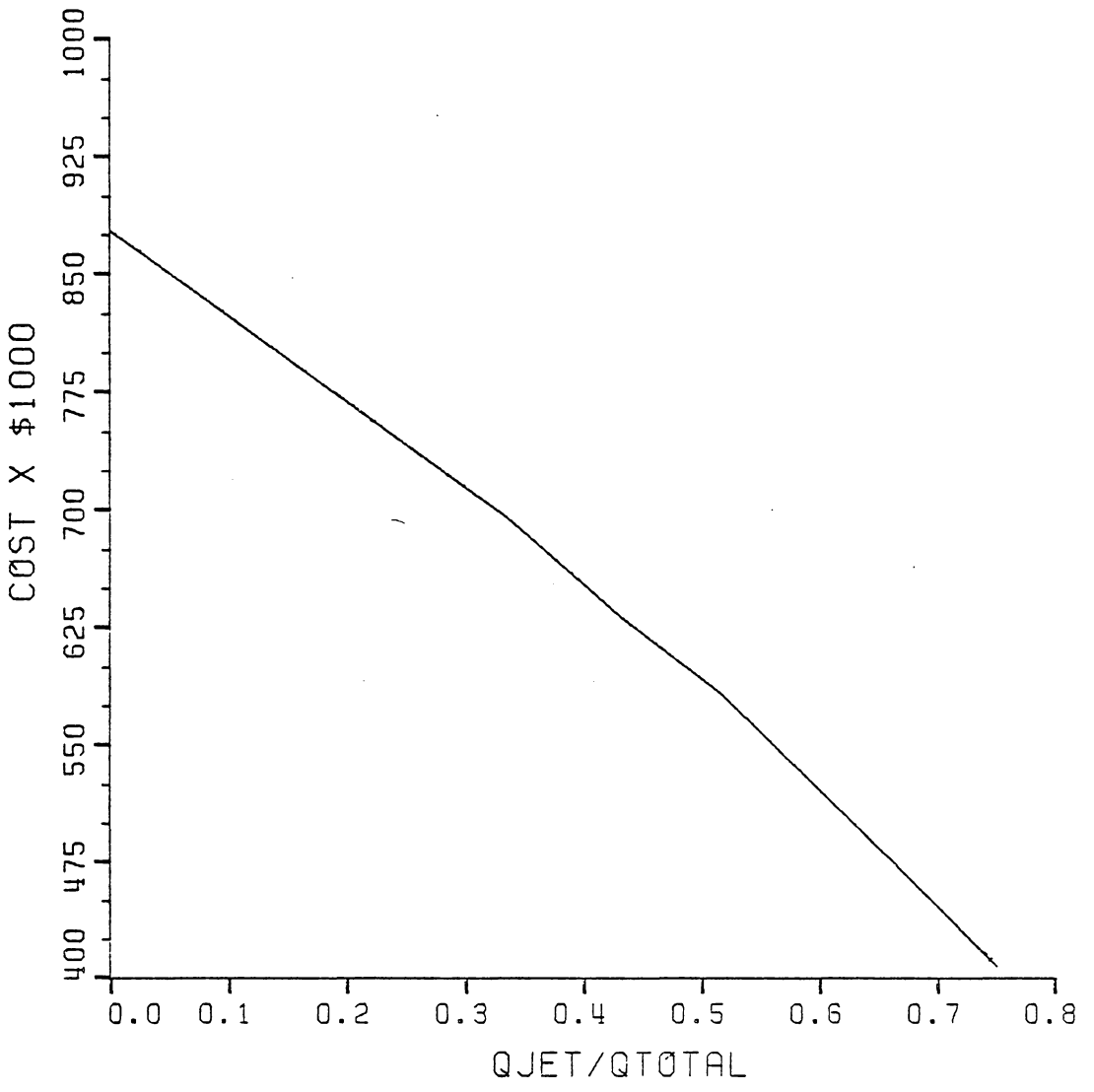

Figure 46. Full Scale System: Cost

system. In some cases the savings are as much as 8-10 per cent of the overall cost. These figures do not include the modifications necessary for the construction of the bypass which has been estimated at approximately 5 per cent of the total system cost. The penstock cost, which has not been included in the analysis, will have no affect on the initial system cost since the total flow rate and therefore the penstock requirements will be the same for each system under a given net head. However, since the bypass systems produce less power, the cost/kW would be affected by the penstock.

It should be pointed out here that although the reduction in cost may not be substantial, the significant point is that the costs are certainly comparable. This means that with the application of a system of this type, a relatively small investment will have as much value in terms of power produced per dollar as a significantly larger investment.

As an example, consider the case illustrated in Table 7 where 3.0 m of net head are available with a flow rate of 13.32 m^3/s. An investment of $878,000 will buy a 1.79 m diameter turbine producing 298 kW of capacity at a cost of $2946/kW. If instead, a 1.49 m turbine were used and 51.7 per cent of the flow bypassed, 205 kW could be produced at a cost of $583,000 or $2844/kW. If 5 per cent were added to cover the cost of the bypass channel, the unit cost would rise to $2986/kW, still within 2 per cent of the conventional system.

Consideration of the seasonal variation in dependable flow illustrates the potential for another significant advantage of the draft tube ejector system for this case. While the conventional turbine is

sized for 13.32 m^3/s at design, the proposed system requires only 6.43 m^3/s through the turbine. If some kind of control gate were installed which allowed the turbine to operate in a conventional manner by closing off the bypass and providing a smooth transition into the draft tube, the turbine would still produce 70 per cent of its power with only 48.3 per cent of its rated flow. This is merely hypothetical at this point but serves to illustrate the potential for further development of this concept.

There is yet another way in which this design can be shown to advantage. Consider a case where flow is abundant but funds are limited. For example, consider 3 m of net head and an available flow of 23 m^3/sec in a run-of-river type site. This represents a potential of 675 kW. However there is only $750,000 to be spent on the turbine and related equipment. For $720,000 a conventional turbine can be purchased which uses 8.88 m^3/s producing 200 kW. Alternatively, the entire flow can be used in a bypass-injection arrangement with a higher effective head rated turbine costing $740,000, 3 per cent more, which will produce 342 kW, or 72 per cent more power. Furthermore, if additional funds should become available the full size turbine can be purchased later to replace the bypass system in the same penstock, to produce 496 kW.

6.5 Cavitation Considerations

An effective draft tube can improve the performance of a hydropower system by lowering the pressure at the turbine discharge. However, discharge pressures below the saturation pressure will cause cavitation

to occur. One possible remedy would be to set the turbine and draft tube low enough so that the absolute pressure at the discharge will never fall below the saturation point. This is not always practical, however, since excavation costs are quite high and maintenance of submerged units can be more difficult. In general, it is desirable to set the turbine as high as possible without risk of cavitation.

The non-dimensional Thoma cavitation factor σ is defined by

$$\sigma = \frac{H_b - H_s}{H_{cr}} . \tag{6.10}$$

where

H_b = [Atmospheric pressure - vapor pressure] (m)

H_s = Static draft head (distance from runner to tailwater)(m)

H_{cr} = Critical head (effective head at which cavitation will occur) (m)

The value of σ is given empirically [7] by

$$\sigma = \frac{(n_s)^{1.64}}{50327} . \tag{6.11}$$

For turbines in the low-head range, H_{cr} is generally 10 to 15 per cent above the effective head [7]. The maximum turbine elevation is defined by

$$Z = H_s + b \tag{6.12}$$

as shown in Fig. 47.

Figure 48 is a plot of the maximum allowable turbine elevation as a function of per cent bypass for various gross heads. Notice that the

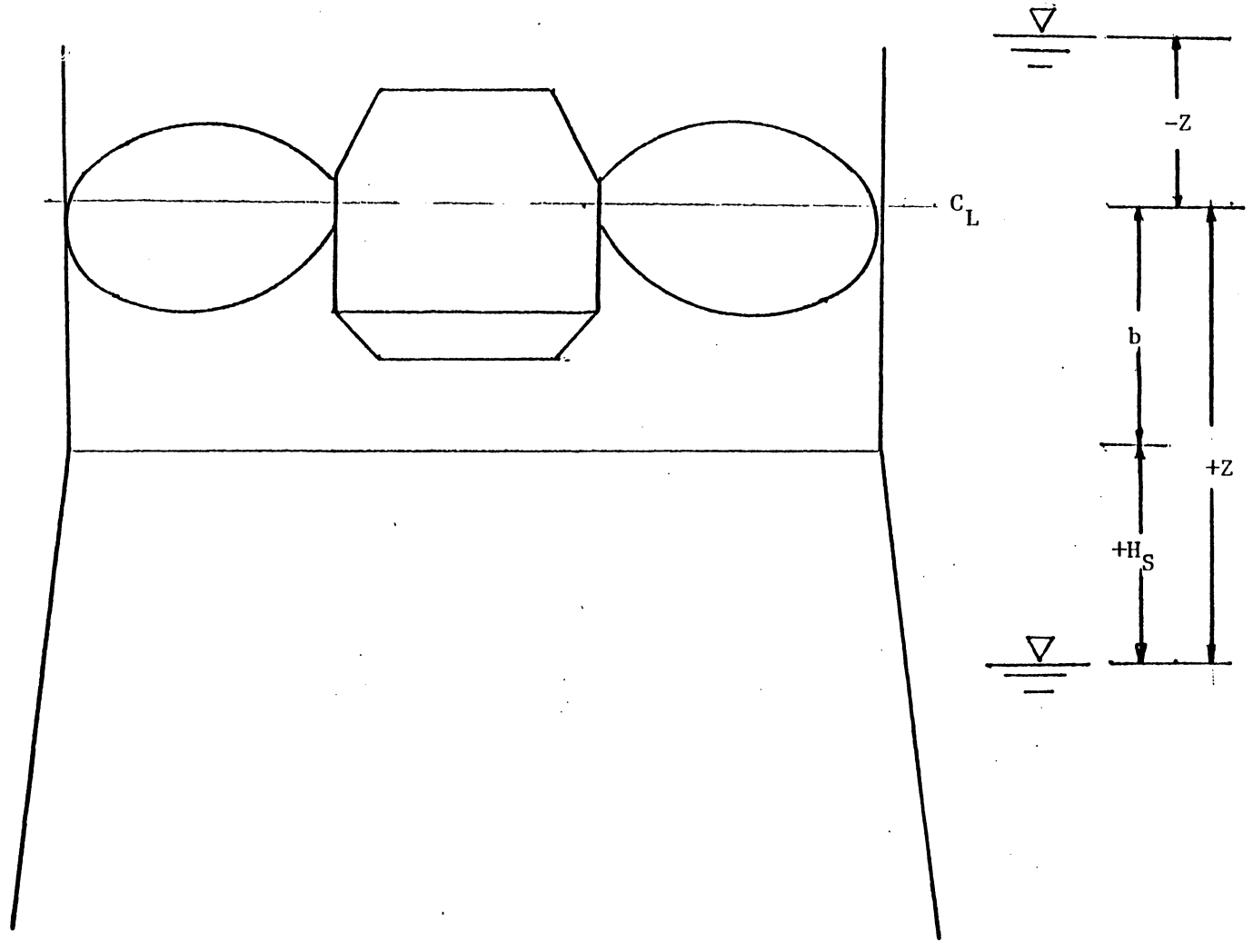

Figure 47. Turbine Elevation Parameters

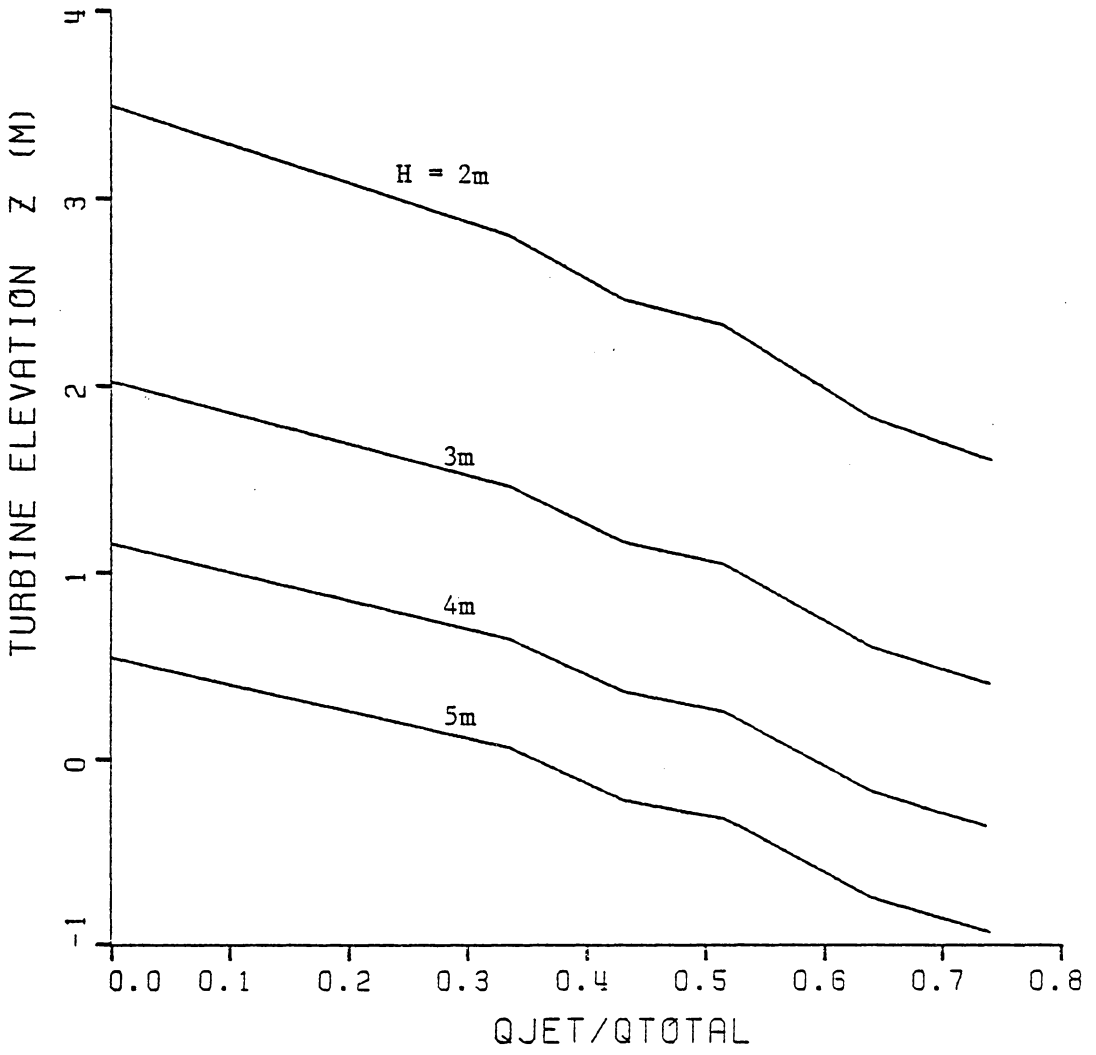

Figure 48. Maximum Allowable Turbine Setting (300 kW Units)

use of bypass increases the likelihood of cavitation, thereby requiring a lower turbine setting. For the higher head cases, it will be necessary to submerge the turbine. This factor would have to enter into the overall system design.

7. CONCLUSIONS AND RECOMMENDATIONS

This thesis describes an investigation of the use of annular jets to enhance pressure recovery in low-head hydraulic turbine draft tubes. An analytical model was developed and refined on the basis of two laboratory test models. The final model was a laboratory scale hydropower system. The analytical model was used to develop performance maps for full size low head systems in the range from 200 to 500 kW. These performance maps were used to evaluate the performance of the complete system from both a technical and economic standpoint.

The results of this analysis show that with the application of annular injection, a small, relatively inexpensive turbine can produce power at the same cost/kW as a larger system, if sufficient flow is available. Furthermore, if capital is the limiting factor, the turbine-bypass system can utilize substantially more flow, resulting in considerably greater capacity for a given investment.

Each hydropower installation is unique which only emphasizes the need for a general analytical model which can optimize each system for the mimimum cost per kilowatt. The system performance presented in this thesis is based on geometry which was selected by the original diffuser analysis. Results of the revised model with increased turbulent viscosity suggest that larger divergence angles could be tolerated without stall. An iterative process is indicated here with each iteration providing new data to help refine the analysis.

Further improvements might include the generalization of the

program to include two-dimensional pressure and velocity distribution in the flow field. This would allow prediction of the system performance in off-design conditions or with swirling discharge flows. In order to make use of this capability, however, more information would be needed on the nature of the flow field in the discharge of low head turbines. There was a noticeable lack of material on this subject in the literature.

Further investigations with the current laboratory model might include detailed velocity profile measurements, variation of the mixing tube and diffuser geometries, and modification of the bypass assembly to allow for baseline (no bypass) measurements of the turbine performance. All of this information would allow further refinement of the computer model, giving more confidence to the type of extrapolations which are presented here.

One final point, Grimshaw et al. [66] in their discussion of hydropower economics have stated that "sacrificing energy income to reduce initial costs in a climate of increasing energy costs can be a misleading temptation". Their point is acknowledged and can be considered relevant to the concept presented here. A conventional type of turbine which utilizes the full available flow will produce the maximum capacity and should be installed if possible. However the system which cannot be afforded will produce no capacity and that too is a sacrifice of energy income.

BIBLIOGRAPHY

1. Brandl, Donald L., "The Economics of Small Hydro," Water Power 81' Proceedings, Vol. II, pp. 947-963, June 22-24, 1981, U.S. Army Corps of Engineers.

2. Hickman, W. W., and McLaughlin, T. B., "DOE Small Hydropower Program," from Small Hydro-Power Fluid Machinery, presented at Winter Annual Meeting, ASME, Chicago, Ill., Nov. 16-21, 1980, ASME, NY, NY.

3. "National Hydroelectric Power Resources Study, Preliminary Inventory of Hydropower Resources," U.S. Army Corps of Engineers, Ft. Belvoir, Va., July 1979.

4. McDonald, Richard J., "Estimate of National Hydroelectric Power Potential at Existing Dams," Institute for Water Resources, U.S. Army Corps of Engineers, July 1977.

5. "Electric Power Supply and Demand 1981-1990," National Electric Reliability Council, Princeton, N.J., July 1981.

6. "11th Annual Review of Overall Reliability and Adequacy of the North American Bulk Power System," North American Electric Reliability Council, August 1981.

7. "Selecting Hydraulic Reaction Turbines," U.S. Dept. of Interior, Bureau of Reclamation, Engineering Monograph No. 20, pp. 24-28, Washington, 1976.

8. Mosonyi, E., Water Power Development, Publishing House of Hungarian Academy of Sciences, Budapest, 1957.

9. Johnstone-Taylor, F., Water-Power Practice, The Technical Press, Ltd., UK, London, 1931.

10. Kolton, A. Y., Etinberg, I. E., Principles of Hydrodynamic Calculation of Water Turbines, Moscow, 1958.

11. Kovalev, N. N., Hydroturbines: Design and Construction, Israel Program for Scientific Translations, pp. 135-150, Jerusalem, 1965.

12. Hunt, Henry J., "Progress in Draft Tube Design and Performance," Civil Engineering, March 1959.

13. Cooper, H. L., "Draft Tube Design Improved by Model Study," Electrical World, Oct. 10, 1936.

14. Falvey, H. T., "Draft Tube Surges - A Review of Present Knowledge and an Annotated Bibliography," Report No. REC-ERC-71-42, U.S. Bureau of Reclamation, Denver, Colorado, Dec. 1971.

15. "Using Excess Flow to Increase Head In Turbines," Power Plant Engineering, March 1, 1927, pp. 314-316.

16. Kerr, S. L., "Moody Ejector Turbine," Transactions of the ASME, Sept. 1921, pp. 7201-7217.

17. Replogle, M. E., "Unique Hydraulic Power Plant at the Henry Ford Farms," Transactions of the ASME, 1915, pp. 1043-1064.

18. Radkey, R. L., Lisseman, P. B. S., and Catherasoo, C. J., "Run of River Ducted Turbines: A Minimum System for the Ultra Low Head River Resource," Hydropower 81, Vol. II.

19. Foreman, K. M., and Gilbert, B. L., "Further Investigations of Diffuser Augmented Wind Turbines," Grumman Aerospace Corporation, Bethpage, N.Y., NTIS Distribution 100-2616-2, 1979.

20. Ghose, S., and Kline, S. J., "The Computation of Optimum Pressure Recovery in Two-Dimensional Diffusers," ASME J. Fluids Engineering, Vol. 100, No. 4, Dec. 1978, pp. 419-426.

21. Embach, H. E., "Calculation of Rotationally Symmetrical Turbulent Flow Through Diffusers," The Brown Boveri Review, Dec. 1964, pp. 789-801.

22. Kline, S. J., Abbott, D. E., and Fox, R. W., "Optimum Design of Straight Walled Diffusers," Trans. ASME Series D, Journal of Basic Engineering, Vol. 81, No. 3, Sept. 1959, pp. 321-331.

23. Reneau, L. R., Johnston, J. P., and Kline, S. J., "Performance and Design of Straight, Two-Dimensional Diffusers, ASME J. Basic Engineering, Vol. 89, No. 1, March 1967, pp. 141-150.

24. Ward-Smith, A. J., "Diffusers and Area Inlargements," Internal Fluid Flow, Oxford University Press, Oxford, 1980, pp. 307-355.

25. Carlson, J. J., Johnston, J. P., and Sagi, C. J., "Effects of Wall Shape of Flow Regimes and Performance in Straight, Two-Dimensional Diffusers," ASME J. Basic Engineering, Vol. 89, No. 1, 1967, pp. 151-160.

26. Sovran, G., and Klomp, E. D., "Experimentally Determined Optimum Geometries of Rectilinear Diffusers with Rectangular, Conical, or Annular Cross Section," Fluid Mechanics of Internal Flow, edited by G. Sovran, Elsevier Publishing Co., Amsterdam, 1967, pp. 270-319.

27. Patterson, G. N., "Modern Diffuser Design," Aircraft Engineering, Vol. 10, p. 267, 1938.

28. McDonald, A. T., and Fox, R. W., "Incompressible Flow in Conical Diffusers," Purdue Research Foundation Project No. 3684, Technical Report No. 1, Sept. 1964.

29. Cockrell, D. J., and Markland, E., "A Review of Incompressible Diffuser Flow," Aircraft Engineering, Vol. 35, No. 10, Oct. 1963, pp. 286-292.

30. Runstadler, P. W., Dolan, F. X., and Dean, R. C., Diffuser Data Book, Creare Inc., TN-186, May 1975.

31. Thompson, R. G., "Performance Correlations for Flat and Conical Diffusers," Airco Cryogenics, ASME Paper No. 79 GT-52, New York, NY, 1979.

32. Kline, S. J., "On the Nature of Stall," J. Basic Engineering, Trans. ASME, Sept. 1959, pp. 305-320.

33. Moses, H. L., and Chappell, J. R., "Turbulent Boundary Layers in Diffusers Exhibiting Partial Stall," ASME J. Basic Engineering, Vol. 89, No. 3, Sept. 1967, pp. 655-665.

34. Woolley, R. L., and Kline, S. J., "A Procedure for Computation of Fully Stalled Flows in Two-Dimensional Passages," ASME J. Fluids Engineering, Vol. 100, June 1978, pp. 180-186.

35. Smith, C. R., and Kline, S. J., "An Experimental Investigation of the Transitory Stall Regime in Two-Dimensional Diffusers," ASME Paper No. 73-WA/FE-11, 1973.

36. Ashjaee, J., Johnston, J. P., and Kline, S. J., "Subsonic Turbulent Flow in Plane-Wall Diffusers: Peak Pressure Recovery and Transitory Stall," Report PD-21, Thermosciences Division, Dept. of Mechanical Engineering, Stanford University, July 1980.

37. Fendrikov, I. A., Fridland, V. Ya., and Yanko, A. K., "Study of Variations in the Characteristics of a Conical Diffuser as a Function of Inlet Conditions," Fluid Mechanics-Soviet Research, Vol. 1, No. 5, 1972, pp. 68-71.

38. Waitman, B. A., Reneau, L. R., and Kline, S. J., "Effects of Inlet Conditions of Performance of Two-Dimensional Diffusers," Report PD-5, Dept. of Mechanical Engineering, Stanford University, March 1960.

39. Wolf, S., and Johnston, J. P., "Effects of Nonuniform Inlet Velocity Profiles on Flow Regimes and Performance in Two-Dimensional Diffusers," ASME Paper No. 68-WA/FE-25.

40. Wirasinghe, N. E. A., "Effect of Swirl on Conical Diffuser Performance," ASME, IAHR Proceedings, Joint Symposium on Design and Operation of Fluid Machinery, Colorado State University, June 1978, pp. 223-233.

41. Lohmann, R. P., Markowski, S. J., and Brookman, E. T., "Swirling Flow Through Annular Diffusers with Conical Walls," United Technology Research Center, Trans ASME Journal of Fluids Eng., Vol. 101, June 1979.

42. Feil, O. G., "Vane Systems for Very-Wide-Angle Subsonic Diffusers," ASME J. Basic Engineering, Vol. 86, No. 4, Dec. 1964, pp. 759-764.

43. Rao, D. M., "Technical Notes: A Method of Flow Stabilisation with High Pressure Recovery in Short, Conical Diffusers," The Aeronautical Journal of the Royal Aeronautical Society, Vol. 75, May 1971, pp. 336-339.

44. Welsh, M. C., "Flow Control in Wide-Angled Conical Diffusers," ASME J. Fluids Engineering, Dec. 1976, pp. 728-735.

45. Senoo, Y., and Nishi, M., "Improvement of the Performance of Conical Diffusers by Vortex Generators," ASME J. Fluids Engineering, March 1974, pp. 4-10.

46. Moon, I. M., "High-Efficiency Flow Diffusion by Means of Suction Boundary-Layer Control," ASME Paper No. 60-AV-13, 1960.

47. Ramaprian, B. R., "Turbulent Wall-Jets in Conical Diffusers," AIAA Journal, Vol. 11, No. 12, Dec. 1973, pp. 1684-1690.

48. Nicoll, W. B., and Ramaprian, B. R., "Performance of Conical Diffusers With Annular Injection at Inlet," ASME J. Basic Engineering, Vol. 92, No. 4, Dec. 1970, pp. 827-835.

49. Fiedler, R. A., and Gessner, F. B., "Influence of Tangential Fluid Injection of the Performance of Two-Dimensional Diffusers," ASME J. Basic Engineering, Vol. 94, Sept. 1972, pp. 666-674.

50. Duggins, R. K., "Research Note: Conical Diffusers with Annular Injection," J. Mechanical Engineering Science, Vol. 17, No. 4, 1975, pp. 237.

51. Frankfurt, M. O., "Efficiency of Tangential Boundary Layer Blowing in Conical Diffusers," Fluid Mechanics-Soviet Research, Vol. 5, No. 1, Jan.-Feb. 1976, pp. 140-145.

52. Mussalli, Y., Larsen, J., Hilke, J., "Performance Characteristics of Peripheral Type Jet Pumps," Proc. Joint Symposium on Design and Operation of Fluid Machinery, Vol. II, June 1978, pp. 123-131.

53. Exley, J. T., and Brighton, J., "Flow Separtion and Reattachment in Confined Jet Mixing," ASME Paper No. 70-FE-B, May 1970.

54. Haynes, W. E., "Conical Diffusers with Peripheral Wall Jets for Low-Head Hydroelectric Applications," Masters of Science Thesis, VPI&SU, Blacksburg, Va., July 1981.

55. Myatt, R. L., "Use of Conical Diffusers With Peripheral Wall Jets in the Optimization of Low-Head Hydro Systems," Masters of Science Thesis, VPI&SU, Blacksburg, Va., August 1981.

56. Patankar, S. V., and Spalding, D. B., Heat and Mass Transfer in Boundary Layers, Intertext, London, 1970.

57. Fox, R. W., and McDonald, A. T., Introduction to Fluid Mechanics, pp. 373, John Wiley & Sons, N.Y., 2nd Ed., 1978.

58. Baumeister, T., Marks' Standard Handbook for Mechanical Engineers, 8th Ed, pp. 3-63, McGraw Hill, NY, 1978.

59. Holman, J. P., Experimental Methods for Engineers, pp. 44-51, McGraw-Hill, Inc., NY, 1978.

60. Mayo, H., and Whippen, W., "Small Scale Hydro (Pumps as Turbines), Allis Chalmers Corporation, Hydro-Turbine Division, 1979.

61. White, F. M., Viscous Fluid Flow, pp. 506-507, McGraw-Hill, Inc., NY, 1974.

62. Moore, J., and J. G. Moore, "Calculation of Five Turbulent Flows Using the Moore Cascade Flow Program," Proc. of the 1980/81 AFOSR-HTTM-Stanford Conference on Complex Turbulent Flows, Sept. 1981, to appear.

63. "Reconaissance Evaluation of Small Low-Head Hydroelectric Installations," Water and Power Resources Service, US Dept. of Interior, Denver, Co., July 1980, Tudor Engineering Co.

64. "Simplified Methodology for Economic Screening of Potential Low-Head Small-Capacity Hydroelectric Sites," EPRI, Palo Alto, Cal., Project 1199-5, Final Report, Jan. 1981, Tudor Engineering Co.

65. Sheldon, L. H., "Cost Analysis of Hydraulic Turbines, "Int. Water Power and Dam Construction, Vol. 33, No. 6, June 1981, pp. 24-28.

66. Grimshaw, P. J., Hartman, D., and Nuessli, W., "Equipment for Small Hydropower in the Light of Long Term Economics," Small Hydro-Power Fluid Machinery, pp. 37-40, ASME, NY, Presented at Winter Annual Meeting, Chicago, Ill., Nov. 16-21, 1980.

APPENDIX A

This appendix contains a listing of the computer program which was used to model the performance of the overall system as described in section 6.3. A condensed list of the major variable names is presented below.

ETA	Turbine Efficiency
ETAGEN	Generator Efficiency
KN	Nozzle Loss Coefficient
PGEN	Generator Rating (kW)
MAXP	Power Available (kW)
QTOTAL	Total Flow Through System (m^3/sec)
HEFF	Effective Head (m)
HCOST	Cost Correlation Based on Effective Head
RATIO	(Conventional System Cost/kW / Ejector System Cost/kW)
BYP	Q_{jet}/Q_{total}
PR	Pressure Recovery Correlation From Diffuser Program
DI	Turbine Diameter (m)
NS	Specific Speed

```
SYS      FORTRAN  A1  04/30/82 15:46 HMOSES      F 80     236 RECS    VA TECH

C$JOB     WATFIV,NOLIST,TIME=60
      REAL ID,KP,KN,MIXLOS,NOZLOS,MAXP,N,NS
C  CONSTANTS
      RHO=997.
      PI=3.14159
      G  =9.806
      CI=3.424
      GAMMA=RHO*G
      IBL=0
C
C  GEOMETRY
      ETA=.90
      ETAGEN=.95
      RVTOL=.001
      TOL=.0001
      KN=.053
      KP=0.026
C
C   PRESSURES
      P0=101000.0
      P4=101000.0
C
C  ELEVATIONS
      Z1=0.0
      Z2=0.0
      Z3=0.0
      Z4=0.0
      AR=4.
C     THETA=3.08
      THETA=4.5
C
C  BEGIN
C
      K=9
      DO 76 II=4,5
      DO 76 JJ=20,50,5
      PGEN=100.*II
      H=JJ/10.
      IF(H.NE.5.) GO TO 300
      WRITE (6,299)
  299 FORMAT ('1')
      Z0=H
      WRITE(6,280)
  280 FORMAT (//,3X,'PGEN',2X,'HEAD',2X,' RA',3X,'RV',3X,'QCORE',
     $3X,'POWER',3X,'COST',4X,'HEFF',4X,'CP',3X,'BYP',4X,'DIAM',
     $' RATIO',3X,'TVR',5X,'NS',5X,'RPM',4X,'Z')
C   SELECT TURBINE DIAMETER
      CALL DIAM (II,H,DI)
      DO 76 I=1,K
      IF (I.GT.1) GO TO 77
      GO TO 44
   77 IF (I.LT.5) GO TO 76
   44 CONTINUE
C     IF(I.EQ.6) GO TO 76
C     IF(I.EQ.8) GO TO 76

      RA=(I-1)/20.
      MAXP=(PGEN/0.768)*1000.
      QTOTAL=MAXP/(GAMMA*H)
      ATOT=PI*DI**2/4.
      ACORE=(1.0-RA)*ATOT
      DI2=SQRT(4.*ACORE/PI)
```

```
  400 EXECUTE SEARCH
C
      P1=(   P0/GAMMA +(Z0-Z1) -(1.+KP)*VC**2/(2.*G)   )*GAMMA
      P2=(   P4/GAMMA +(Z4-Z2) -(CP)*(VC)**2/(2.*G)   )*GAMMA
      HEFF=((P0-P2)/GAMMA+(Z0-Z2)-(1.+KP)*VC**2/(2.*G))
C   TAKE CARE OF NEGATIVE HEAD
      IF(HEFF.LT.0.)GO TO 555
      TVR=VC/SQRT(2.*G*HEFF)
  555 ET=HEFF*ETA*ETAGEN
C
  406 POWER=QCORE*ET*GAMMA/1000.
      IF (PGEN .LE.100.) GO TO 417
      P=POWER-100.
C  DETERMINE COST OF MECHANICAL EQUIPMENT
      CALL HCOST (HEFF,C1,P,COST)
      COST1=COST
      P=P+100.
      CALL HCOST (HEFF,C1,P,COST)
      P1=POWER/100.
      L=P1
      Q=L
      PFRAC=P1-Q
C  INTERPOLATE
      COST=PFRAC*(COST-COST1)+COST1
      GO TO 418
  417 COST=100.
  418 CALL DRAFT (HEFF,POWER,D12,NS,N,Z)
C
      IF (RA.NE.0.0) GO TO 407
      CREF=COST
      WREF=POWER
  407 CONTINUE
      CKW1=COST/POWER
      RATIO=CKW1/(CREF/WREF)
      WRITE(6,600)PGEN,H,RA,RV,QCORE,POWER,COST,HEFF,CP,FRACMJ,D12,RATIO
     S,TVR,NS,N,Z
  600 FORMAT(1X,F6.1,2F6.2,F5.2,F7.2,2F8.0,2F7.2,F7.3,F6.2,2F7.3,2F7.0,F
     $6.2)
   75 CONTINUE
   76 CONTINUE
      GO TO 30
C
      REMOTE BLOCK SEARCH
C
C  SEARCH FOR RV
C
      IF(RA.EQ.0.) GO TO 540


  500 DELRV=1.
      RV=0.0
      EXECUTE SOLVE
      E1=ERROR
  510 RV=RV+DELRV
      EXECUTE SOLVE
      E2=ERROR
      IF((E2*E1).GT.0.) GO TO 520
      IF(DELRV.LT.RVTOL) GO TO 530
      RV=RV-DELRV
      DELRV=DELRV/2.
      GO TO 510
  520 E1=E2
      GO TO 510
  540 RV=0.
      EXECUTE SOLVE
  530 CONTINUE
      END BLOCK
```

```
      REMOTE BLOCK SOLVE
      V3=QTOTAL/ATOT
      VC=V3/(RV*RA+1.-RA)
      QCORE=VC*ACORE
      VJ=VC*RV
      FRACMJ=(QTOTAL-QCORE)/QTOTAL
      CP=PR(FRACMJ,RA,AR,THETA)
C     IF(CP.GT.1.99)CP=1.99
C     IF(CP.LT..5)CP=.5
      ERROR=((Z0-Z4)+VC **2 *(CP)/(2.*G)-(1.+KN)* (VJ)**2/(2.*G))
     &*GAMMA
      END BLOCK
   30 STOP
      END
C
      FUNCTION PR(FRACMJ,RA,AR,THETA)
      PR1(A,B,C,D,E,FRC)=A+B*FRC+C*FRC**2+D*FRC**3+E*FRC**4
      IF(RA.GT..01)GO TO 120
      PR=.80
      GO TO 250
  120 IF(RA.GT..21) GO TO 125
      PR=PR1(0.52845,-5.16179,56.6231,-181.596,233.537,FRACMJ)
      GO TO 250
  125 IF (RA.GT..26) GO TO 126
      PR=PR1(11.60656,-111.0552,425.8853,-736.979,520.8332,FRACMJ)
      GO TO 250
  126 IF(RA.GT..31)GO TO 130
      PR=PR1(21.5213,-205.505,753.386,-1225.36,768.225,FRACMJ)
      GO TO 250
  130 IF(RA.GT..36)GO TO 131
      PR=PR1(51.5652,-416.419,1289.463,-1799.81,973.077,FRACMJ)
      GO TO 250
  131 IF(RA.GT..41)GO TO 140
      PR=PR1(89.5973,-687.267,1993.21,-2581.55,1273.5,FRACMJ)
      GO TO 250


  140 IF(RA.GT..46)GO TO 145
      PR=PR1(-39.0989,187.049,-244.594,-20.0096,161.325,FRACMJ)
      GO TO 250
  145 IF (RA.GT..56)GO TO 150
      PR=PR1(586.7137,-3722.34,8870.73,-9417.34,3770.14,FRACMJ)
      GO TO 250
  150 PR=PR1(-172.653,766.884,-1140.19,570.384,FRACMJ)
  250 RETURN
      END
C
      SUBROUTINE DIAM (II,H,DI)
C  THIS SUBROUTINE FINDS THE APPROPRIATE TUBULAR TURBINE
C  FOR THE GIVEN HEAD AND POWER REQUIREMENT
      IF (II.GT.1) GO TO 1
      DI=2.4922*H**(-0.8109)
      GO TO 11
    1 IF (II.GT.2) GO TO 2
      DI=3.4224*H**(-0.7735)
      GO TO 11
    2 IF (II.GT.3) GO TO 3
      DI=4.0675*H**(-0.7491)
      GO TO 11
    3 IF (II.GT.4) GO TO 4
      DI=4.7269*H**(-0.7541)
      GO TO 11
    4 CONTINUE
      DI=5.2718*H**(-0.7549)
   11 CONTINUE
      RETURN
      END
```

```
      SUBROUTINE HCOST (HEFF,CI,P,COST)
C THIS COMPUTES COST AS A FUNCTION OF HEAD & POWER
C FOR TUBULAR TURBINES
C USE EFFECTIVE HEAD
      H=HEFF*3.2808
      IF (P.GT.100) GO TO 1
      COST=1760.743*H**(-0.68368)
      GO TO 7
    1 IF (P.GT.200.) GO TO 2
      COST=2079.401*H**(-0.63489)
      GO TO 7
    2 IF (P.GT.300.) GO TO 3
      COST=2564.506*H**(-0.64003)
      GO TO 7
    3 IF (P.GT.400.) GO TO 4
      COST=3096.657*H**(-0.66933)
      GO TO 7
    4 CONTINUE
      COST=3402.572*H**(-0.67543)
    7 CONTINUE
      COST=(CI/2.48)*COST
      RETURN
      END
C
      SUBROUTINE DRAFT (HEFF,POWER,DI2,NS,N,Z)

C  THIS COMPUTES THE SPECIFIC SPEED AND THE
C  MINIMUM TAILWATER SETTING ALLOWED WITHOUT CAVITATION
      REAL N,NS
      HB=9.808
      NS=2334./SQRT(HEFF)
      HCR=1.15*HEFF
      SIGMA=(NS**1.64)/50327.
      FACTOR=0.08806+0.0004605*NS
      B=FACTOR*DI2
      HS=HB-SIGMA*HCR
      Z=HS+B
      HPMET=1.36*POWER
      N=(NS*HEFF**1.25)/SQRT(HPMET)
      RETURN
      END
CSENTRY
```

The vita has been removed from the scanned document

HEAD AUGMENTATION IN HYDRAULIC TURBINES BY MEANS OF DRAFT TUBE EJECTORS

by

Robert P. Siegel

(ABSTRACT)

The use of draft tubes with annular injection was investigated with respect to low-head applications. A numerical model was developed and refined to fit the data from two laboratory test models. The latter model was a laboratory scale hydropower system which demonstrated 20-31 per cent head augmentation under various conditions. The numerical model was used to generate performance maps of full scale, low-head systems in the range from 200 to 500 kW. The performance maps were then used in a system modeling program to evaluate the system performance, cost and cavitation characteristics. The draft tube ejector system was found to reduce the system cost/kW by 2-10 per cent when compared to a conventional system with the same gross head and total flow rate. This was accomplished by using smaller, less expensive turbines which utilize excess flow in draft tube ejectors to increase the effective head across the turbine. The resulting reduction in system cost was found to exceed the corresponding reduction in capacity. The use of draft tube ejectors was found to require slightly lower turbine settings due to increased cavitation risk.